© 2010

ŞÌMAL ÖZEN

ALL RIGHTS RESERVED

BIASING NEURAL ACTIVITY: ENTRAINMENT OF CORTICAL NEURONS BY

APPLIED ELECTRIC FIELDS

by

ŞÌMAL ÖZEN

A Dissertation submitted to the

Graduate School – Newark

Rutgers, The State University of New Jersey

In partial fulfillment of requirements

for the degree of

Doctor of Philosophy

in Integrative Neuroscience Program

Written under the direction of

Professor György Buzsàki

and approved by

Professor Bart Krekelberg

Professor David McCormick

Professor Denis Paré

Professor Làszlò Zàborszky

Newark, New Jersey

October, 2010

Biasing neural activity: Entrainment of cortical neurons by applied electric fields

Low intensity electric fields have been suggested to affect ongoing neuronal activity in both *in vitro* studies and in human studies. However, the physiological mechanism of how weak electrical fields affect and interact with intact brain activity is not well understood. I performed in vivo extracellular and intracellular recordings from the neocortex of anesthetized rats and extracellular recordings in behaving rats. Electric fields were generated by sinusoid patterns at slow frequency (0.7, 0.8, 1.25 or 1.7 Hz) via electrodes placed on the surface of the skull or the dura. Transcranial electric stimulation (TES) reliably entrained neurons directly in widespread cortical areas, including the hippocampus. The percentage of TES phase-locked neurons increased with stimulus intensity and depended on the behavioral state of the animal. TES-induced voltage gradient, as low as 1 mV/mm at the recording site, was sufficient to phase-bias neuronal spiking. TES-induced effects were rapid to evolve and disappeared quickly after TES-offset. Intracellular recordings showed that both subthreshold and spiking activity of neurons were under the combined influence of TES forced fields and network activity. Our findings suggest that TES in chronic preparations may be used for experimental and therapeutic control of brain activity.

Acknowledgement

To the divine scientific inquiry within each of us…

Table of Contents

List of Tables

List of Illustrations

Chapter 4

List of abbreviations

AC	alternating current	10
ACG	autocorrelogram	40
CCG	crosscorrelogram	40
DC	direct current	10
EEG	electroencephalogram	22
EMG	electromyogram	22
EOG	electrocorticogram	22
LFP	local field potential	1
mPFC	medial prefrontal cortex	31
NREM	non-rapid eye movement	22
pF	peak frequency	50
pN	peak-to-peak *noise* amplitude	42
p2p	peak-to-peak spike amplitude	41
REM	rapid eye movement	22
SD	standard deviation	41
SNR	signal-to-noise ratio	41
snrN	signal-to-noise ratio of the *noise*	42
SWS	slow wave sleep	2
tDCS	transcranial direct current stimulation	17
TES	transcranial electric stimulation	2
TMS	transcranial magnetic stimulation	18
V_i	intracellular potential	51

Chapter 1: Introduction

The presence of extracellular electric fields is an integral part of neural electro-transmission. Extracellular fluid is highly conductive; thus the presence of electric charge(s) creates electric fields of various magnitudes. These electric fields, in return, affect the excitability of the nerve cells in the vicinity (Bishop and O'Leary, 1950; Jefferys, 1981; Chan and Nicholson, 1986).

The potential impact of extracellular electric fields on neuronal excitability raises two important issues. The first one, rather a chicken-and-egg problem, is related to intrinsic brain activity. Normal and pathological activities of neuronal assemblies generate electric fields that are commonly manifested in local field potential (LFP) recordings. *To which extent LFP modulates the activity of the very same neurons that contributed to the generation of the field* is a critical question, yet to be answered (Jefferys and Haas, 1982; Jefferys, 1995; Anastassiou et al., 2010).

The second issue is whether the effects of electric fields on neural activity can be exploited for the treatment of certain neurological and psychiatric disorders (Rosenthal and Wulfsohn, 1970; Webster et al., 2006; Nitsche et al., 2009). The external manipulation of brain activity using electric field stimulation offers a variety of opportunities that can be utilized for clinical and experimental purposes. However, current therapeutic usage of electric stimulation is limited to severe cases and small patient groups. Meanwhile, experimental application of electric fields has been confined to in vitro or in silica preparations or behavioral studies conducted in humans, leaving a fundamental question unanswered: *how*

do externally applied electric fields affect neuronal activity in the intact brain?

As an attempt to understand the effects of intrinsically induced fields, and to investigate the possibility of manipulating brain activity using a non-invasive method, I aimed to elucidate the mechanisms by which applied electric fields interact with ongoing brain activity. I used electric fields oscillating at a slow frequency (0.7-1.7 Hz) to mimic intrinsic neocortical slow oscillation. I hypothesized that the activity of cortical neurons could be modulated by field stimulation and that the extent of the induced effects would depend on the stimulation intensity and background neural activity. In order to test these hypotheses, I performed multi-site extracellular recordings from various neocortical and hippocampal regions in both anesthetized and naturally sleeping animals, and investigated the effects of applied fields on single and multi-unit activity. Overall, our findings suggest that transcranial electric stimulation (TES) is a reliable and effective method to modulate cortical unit activity.

In Chapter 1, I provide an overview of the extracellular electric fields and the characteristics of the environment, in which these fields are created. This introduction is followed by experimental and clinical evidence demonstrating physiological, therapeutic, and behavioral effects of electric fields. Background neuronal activity is critical in shaping cortical responses to field stimulation. Thus, in the following sections, characteristic neocortical and hippocampal activities observed during different behavioral states are reviewed with particular emphasis on neocortical slow oscillations and slow wave sleep (SWS) state.

Chapter 2 is dedicated to a detailed description of the methods I applied in my experiments. Surgical and recording methods specific to experiments on anesthetized and behaving rats are explained separately. Analytical procedures that were common to both types of experiments are described together.

Chapters 3 and 4 describe the results obtained from the two experimental studies. In the first study (discussed in Chapter 3), I investigated the effects of applied electric fields on neural activity in anesthetized animals. This study revealed that unit activity could be reliably entrained in an intensity-dependent manner by electric field stimulation. In the second study (discussed in Chapter 4), I extended the experiments to naturally sleeping and behaving animals and investigated how ongoing neuronal activity could be affected by and interact with TES. Results of these experiments suggested that transcranial stimulation, in conjunction with ongoing network states, could be used to phase-modulate unit activity across widespread cortical regions.

The final chapter, Chapter 5, is dedicated to the summary of our findings and discussions about the characteristics of our TES application, the implementation of TES in humans and the potential directions for future studies.

1.1. Electric fields in the brain

The presence of an electric charge either inside or outside of the brain creates an extracellular electric field that exerts force on all electrically charged structures, including glial and nerve cells (Eq. 1.1; cf., Crowell, 2007). This force on electric charge(s) creates polarization of the cell membrane and thus

modulates the physiological activity of neurons (Bishop and O'leary, 1950;

Bindman et al., 1964b; Chan and Nicholson, 1986). Hence, extracellular electric

fields, whether brain-generated or externally-induced, affect neuronal activity

(Jefferys, 1995).

$$E = \lim_{q \to 0} F/q \qquad \textbf{Equation 1.1}$$

Equation 1.1. Definition of the electric field. *E*, electric field. *F*, force experienced by the test particle. *q*, unit charge of the test particle with the smallest charge possible. Note that an electric field (mV/mm) is defined by the magnitude, which is the force exerted on a positive charge of 1 Coulomb, and the direction of that force (cf., Crowell, 2007).

Electric fields of various magnitudes are generated by intrinsic neuronal

activity. Such *endogenous extracellular fields* exist in the intact brain; but they

are also present during special conditions, particularly when the extracellular

space is altered such that the extracellular resistivity is increased as observed in

wounded tissue, in certain pathologies or during development (Hotary and

Robinson, 1990; Jefferys, 1995; Bragin et al., 1997). Epileptic tissue is the most

common example where the tissue resistivity is high and extracellular fields of up

to tens of mV/mm are generated (Haas and Jefferys, 1984; Snow and Dudek,

1984; Ghai et al., 2000).

Endogenous electric fields can be categorized by their magnitude and the

number of neurons that contribute to the creation of the field.

Spiking activity, including antidromic activation of cells, creates electric fields

that can affect neurons in the vicinity (30-40 µm) of the active cell (Taylor and

Dudek, 1984; Holt and Koch, 1999; Gold et al., 2006). In the synaptic cleft

electric fields can reach up to 10^4 mV/mm in magnitude (Sylantyev et al., 2008)

and these fields can affect the electro-diffusion within the cleft, altering the timing

of synaptic transmission. However, spiking activity-induced fields are unlikely to

exert a strong effect on the membrane potential of the neighboring neurons (Holt

and Koch, 1999). This is due to two reasons: 1) the spatial extent of the induced

effects are minute; 2) these events are transient (~1 msec); they last much

shorter than the time required to charge the cell membrane.

Another way in which a charged neural element can polarize its adjacent

neighbors is through *ephaptic coupling* (Taylor and Dudek, 1982; Jefferys, 1995;

Holt and Koch, 1999). Such polarization is commonly observed between nearby

axons and within dendritic bundles of pyramidal cells. Similar to spiking-induced

fields, ephaptic coupling-induced fields are also confined to a small area, the

immediate vicinity of the active cell or cellular elements.

Despite the considerably large magnitude within the focal area, the impact of

spatially confined fields substantially diminishes at a distance of tens of microns

from the source. The magnitude of the field is strictly (negatively) correlated with

the distance from the source(s) creating the field (Coulomb's Law: Eq. 1.2; cf.,

Nunez and Srinivasan, 2006). Thus, the spatial extent of the field is critical to

define field-induced effects.

$$E(r) = (q.a) / (4\pi.\epsilon_0. R^2) \qquad \textbf{Equation 1.2}$$

Equation 1.2. Coulomb's Law. *E(r),* electric field at the observation location r (vector-location). *q,* the positive charge creating the electric field. *a,* unit vector pointing from the source to the observation location. $\epsilon_0,$ the permittivity of the empty space. *R,* scalar distance between the source and the observation location. Note that the exerted force falls off proportional to the distance from the source (cf., Nunez and Srinivasan, 2006).

The impact of fields induced by spiking activity is dramatically different when discharging of many nearby neurons synchronizes within a few milliseconds, generating a population spike. Such synchronous firing happens either sporadically or at regularly spaced intervals (Destexhe et al., 1999; Buzsaki and Draguhn, 2004; Ray et al., 2008). The latter is commonly referred as *oscillation*. These population spikes can exceed several millivolts and generate large voltage gradients across the somata of neurons and affect their physiology (Jefferys, 1995; Park et al., 2005; Anastassiou et al., 2010). A prominent example of this phenomenon is hippocampal sharp-waves (Buzsaki et al., 1983; Buzsaki, 1986; Suzuki and Smith, 1988) which create one of the largest voltage gradients in the brain (15 mV/mm; Ylinen et al., 1995). The impact of these endogenously generated fields is often high enough to synchronize the spiking activity of many cells (Purpura and Malliani, 1966; Taylor and Dudek, 1982; Jefferys and Haas, 1982).

Fields induced by oscillatory activity have unique characteristics that vary depending on the particular background neural activity and the anatomical location that they are associated with. Fields observed in dentate gyrus, for instance, have a much smaller magnitude during SWS than that of the ones observed during running (0.5-4 mV/mm vs. 4-8 mV/mm; Winson, 1974; Buzsaki et al., 1986). In contrast, in the CA1 region of the hippocampus, the voltage gradient during sharp-waves, during SWS, may exceed 10 mV/mm.

1.2. Neuronal interactions with electric fields

The presence of electric fields affects both spontaneous and evoked neural activity (Bindman et al., 1964a; Purpura and McMurtry, 1965). All of the effects manifested arise from a common underlying mechanism: field-induced polarization of the cell membrane (Jefferys and Haas, 1982; Chan et al., 1988; Radman et al., 2007). Depending on the physiological and morphological characteristics of the neuron (Chan and Nicholson, 1986; Radman et al., 2007; 2009), the induced polarization may change the timing or the discharge frequency of the spontaneous activity, or the amplitude of the evoked potentials (Ranck, 1975; Jefferys, 1981).

1.2.1. Field effects on membrane potential

The membrane potential of a given neuron is defined by two parameters: 1) the current flow induced by synaptic activity and 2) the current flow induced by the extracellular field (Cable Equation: Eq. 1.3; cf., Koch, 1999).

Despite the common (but incorrect) assumption, the extracellular potential is not uniform, spatially-invariant or constant in time (Sanchez-Vives and McCormick, 2000; McCormick et al., 2003; Anastassiou et al., 2010). Accordingly, there is always an electric field and an associated extracellular current flow outside of the cells. Some of this current passes the cell membrane and flows intracellularly. However, the presence of the cell membrane introduces a '*boundary condition*' and interrupts the current flow at the compartments where the current enters and leaves the cell. The accumulation of charges at these

boundaries leads to the hyper- or de-polarization of the cell depending on the relative distance of the current entry and exit locations to the soma.

$$c_m \cdot (\partial V_m / \partial t) = -V_m / r_m + (1/r_i) \cdot (\partial^2 V_m / \partial x^2) + (1/r_i) \cdot (\partial^2 V_e / \partial x^2) \quad \textbf{Equation 1.3}$$

Equation 1.3. Cable equation. c_m, membrane capacitance. r_i, axial resistance. r_m, membrane resistance. t, time. x, space. V_e, extracellular potential. V_m, transmembrane potential. Note that V_m is defined by the current passing across the membrane and the current passively flowing along the fiber (cf., Koch, 1999).

1.2.2. Field effects on unit firing

Field-induced membrane polarization can be high enough to alter spike timing (Francis et al., 2003; Radman et al., 2007), the discharge frequency (Bindman et al., 1964b), the amplitude of evoked potentials (Jefferys, 1981), or any combination of these properties.

Modulation of firing rate requires high intensity. Extremely high intensity fields (~100 mV/mm) can even introduce epileptic discharges (Lian et al., 2003). In contrast, low intensity fields polarize the cell membrane only by 0.1-1 mV (Francis et al., 2003; Radman et al., 2007). This level of polarization would not be high enough to suppress or drive the cell directly, but it may be sufficient to alter the spike timing and modulate the ongoing activity (Fig. 1.1; Radman et al., 2007).

$$\Delta\varphi = 2\pi \, (v_m - v_{rest}) / (\Delta v_{thresh} - \Delta v_\pm) \quad \textbf{Equation 1.4}$$

$$\Delta v_{thresh} = v_{thresh} - v_{rest} \quad \textbf{Equation 1.5}$$

$$\Delta v_\pm = v_\pm - v_{rest} \quad \textbf{Equation 1.6}$$

Equation 1.4-6. Modulation of spike timing. $\Delta\varphi$, change in spike timing. Δv_{thresh}, voltage change required to reach threshold. $\Delta v_\pm$, voltage change due to background synaptic input. v_m, transmembrane potential. V_{rest}, resting membrane potential. Note that the change in spiking timing is a function of field-induced and synaptic activity-induced membrane polarizations and the action potential threshold (Radman et al., 2007).

Radman et al (Eq. 1.4-6; Radman et al., 2007) demonstrated that field-induced modulation of spike timing is closely correlated with ongoing spiking activity and the action potential threshold. In the presence of abundant synaptic inputs, the cell is closer to the threshold and the impact of the field-induced polarization is more pronounced (Radman et al., 2007; Anastassiou et al., 2010).
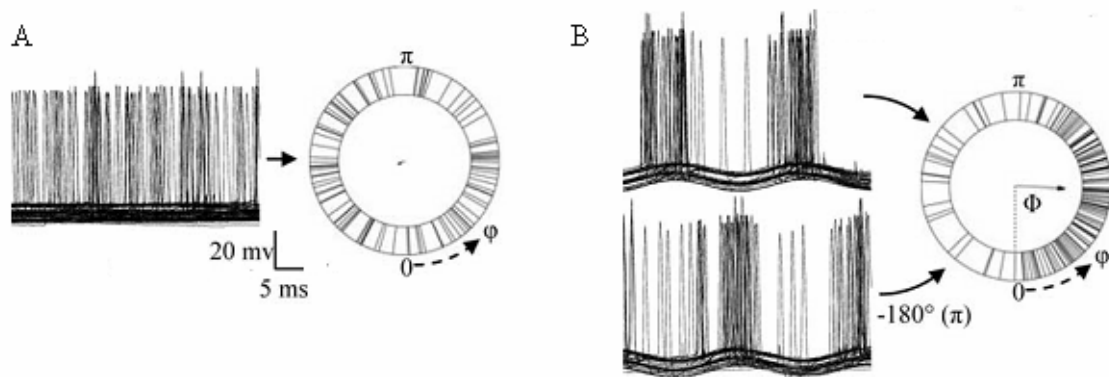
Figure 1.1. **Effects of alternating current (AC) electric fields on spike timing.** A,B. Activity from a CA1 pyramidal neuron in response to an intracellular depolarizing ramp current injection and exposure to an alternating current field. In vitro recording. Left, Overdrawn intracellular spikes. Right, circular scatter plots, showing spikes with respect to the phase of the field. Insets, direction of the mean angle. A. Activity in the absence of the electric field. B. Activity in the presence of the uniform AC field (10 mV/mm, 30 Hz; top left) and in the presence of the same field phase shifted by 180° (bottom, left). Right, Circular spike-phase distribution. Note that in the absence of the field, spikes had no temporal pattern; the field biased spiking to the rising phase of the stimulation (Adopted from Radman et al., 2007).

1.3. Factors that determine the impact of the field

A variety of factors are critical in shaping field-induced effects on sub- and suprathreshold neural activity. Most of these factors are related to the induced-field (Holt and Koch, 1999; Anastassiou et al., 2010); and some highly depend on the active and passive properties and the morphological characteristics of the

neuron (Chan and Nicholson, 1986; Chan et al., 1988; Lopez et al., 1991). The rest is due to anatomical and physiological properties of the particular region in which the field is created.

1.3.1. Properties of the field

i. Spatial characteristics of the field

If neurons were simple passive cables, the *spatial homogeneity* of the field would be the most critical criterion to determine the amount of membrane polarization. Spatially inhomogeneous fields create larger potential differences along the neuron. Hence, they induce differential entrainment of different compartments of the same cell, and thus a higher amount of overall polarization (Holt and Koch, 1999; Anastassiou et al., 2010). A prominent example of such fields is hippocampal theta oscillations (Vanderwolf, 1969; Buzsaki, 2002). According to realistic models, due to their depth profile (Bullock et al., 1990; Bragin et al., 1995), theta oscillations induce substantially different polarization across soma and distal apical dendrites (0.2 mV vs. -0.5 mV, respectively; Anastassiou et al., 2010). Thus, theta oscillations have a high impact on cellular activity.

ii. Temporal characteristics of the field

A pyramidal cell membrane takes about 20 msec to respond to a time-invariant, direct current (DC) field (Bikson et al., 2004; Deans et al., 2007). On the other hand, when exposed to a time-variant, alternating current (AC) field, the

membrane response develops at the same time course as of the field (Deans et al., 2007). This temporal difference in response results from the properties of the bilipid cell membrane, which functions as a low-pass filter. Thus, the modulation of the cell membrane is frequency-dependent. For fields fluctuating at a rate slower than the membrane time constant (≤ 20-30 Hz), the low-pass filtering capacity of the membrane becomes negligible and field-effects are not attenuated (Anastassiou et al., 2010). Accordingly, if the frequency is slower than 10 Hz, AC fields are almost as effective as DC fields. However, fields fluctuating at a high frequency may not be able to affect membrane potential. As the field frequency increases, the effectiveness of the field substantially decreases; a 100 Hz field is 5 times less effective than a 10 Hz field (Deans et al., 2007).

iii. Magnitude of the field

Field intensity has, seemingly, clear effects on neural modulation. As the magnitude of the field increases, more cells are entrained. The entrainment becomes so robust that it can be observed at the population level through LFP recordings (Deans et al., 2007). Fluctuations of the membrane potential are linearly correlated with field strength (Deans et al., 2007). However, the relationship between the field-intensity and unit entrainment is not straightforward as manifested by the lack of a clear intensity-threshold (Bikson et al., 2004). This is mostly due to the composite effects of background neural activity, the network state, on field-induced effects.

iv. Magnetic properties of the field

A related concept to the electric field is the *magnetic field,* which arises from the motion of (an) electric charge(s) (Crowell, 2007). However, electric fields oscillating at a low frequency are 'uncoupled' from their magnetic fields for which the magnetic field induction can be assumed negligible. All electrical activity measured from the surface or inside of the brain is at a frequency 'slow' enough to fall under this category (Nunez and Srinivasan, 2006).

Our stimulation consisted of AC fields fluctuating at a frequency of 1.25 Hz, which were slow enough to induce membrane polarization while avoiding magnetic coupling. The intensity was weak (~ 1mV/mm) but effective and the spatial properties of the field were presumably inhomogeneous considering that the stimulation was applied through transcranial electrodes.

1.3.2. Properties of the neurons

i. Length characteristics

Electrotonic length and the actual length of the neuron are critical to determine how much current will flow within the cell. A large electrotonic length would enable more compartments of the cell to become polarized through the field-induced current flow (Eq. 1.7; cf., Dayan and Abbott, 2001).

$$\text{Electrotonic length} = \sqrt{R_m / R_a}. \quad \textbf{Equation 1.7}$$

Equation 1.7. Electrotonic length. The defining feature of the passive voltage spread along the neuron. R_a, axial resistance. R_m, membrane resistance (cf., Dayan and Abbott, 2001).

Overall, neurons with large diameters, high membrane resistivity or low intracellular resistivity are affected the most. Similarly, longer neurons are presumed to be effectively modulated by the field since they are, theoretically, exposed to more spatial inhomogeneity of the field (Anastassiou et al., 2010).

ii. Dendritic layout and the geometry of the field

The relationship between the geometry of the field and the dendritic geometry of neurons affects the impact of the electric field (Chan and Nicholson, 1986; Deans et al., 2007; Radman et al., 2007). The optimal alignment is achieved when the current flow, i.e., the field, is parallel to the layout of the dendritic extensions (Jefferys, 1981; Chan and Nicholson, 1986: Fig. 1.2). Any deviation from parallel alignment requires higher intensities to elicit the same neural response (Ghai et al., 2000). Accordingly, fields vertical to the dendrites rarely elicit any effects.

Another critical factor is the direction of the current flow which determines the entry and exit locations for the current to flow in and out of the cell. These locations are relatively hyperpolarized and depolarized as a result of the current accumulation at cell boundaries. The resultant transmembrane potential reflects the interactions between the magnitude of these polarizations, the relative proximity of these compartments to the soma, and the physiological properties of the cell. For most cell types, the depolarization of the compartments near the soma, e.g., proximal distal dendrites, increases the excitability (Jefferys, 1981; Fig. 1.2; Chan and Nicholson, 1986).
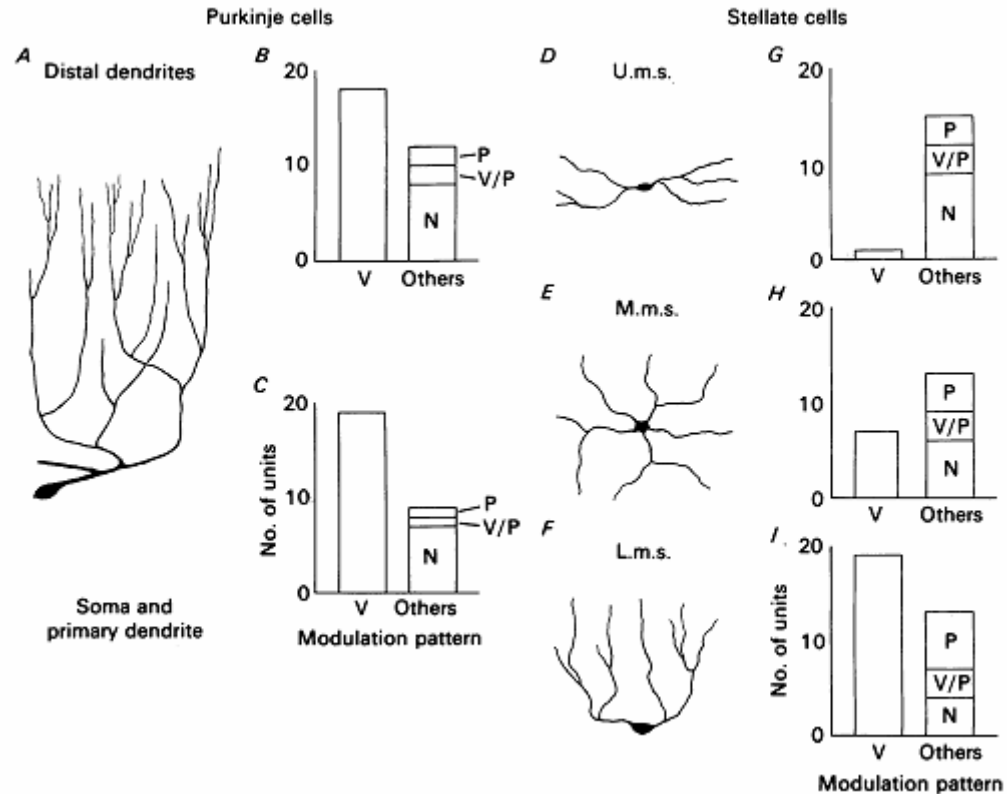
Figure 1.2**. The dendritic layout with respect to the geometry of the field is critical for unit modulation**. Modulation of cerebellar neurons by electric fields with the current flow was directed either towards (*V*) or away from (*P*) the purkinje cell soma. Field was applied through silver plates placed parallel to the dorsa-ventral axis of the cerebellum. Constant current stimulation. A,D,E,F. Layout of the dendritic orientations of purkinje cells (*A*) and upper (*Ums*), middle (*Mms*) and lower (*Lms*) molecular layer stellate cells (*D,E,F*; respectively). B,C,G,H,I. Distribution of unit-modulation for purkinje cell soma/proximal dendrites, and distal dendrites (*B,C;* respectively) and upper, middle and lower molecular layer stellate cells (*G,H,I*; respectively). *V,* significantly modulated cells when the current was directed towards purkinje cell soma. *P,* significantly modulated cells when the current was directed away from purkinje cell soma. *V/P,* significantly modulated cells regardless of the direction of the current flow. *N*, cells that were not modulated by any configuration (Adopted from Chan and Nicholson, 1986).

Morphological complexity of the dendritic arbor (Gold et al., 2006) is another factor defining extracellular field effects (Chan and Nicholson, 1986; Radman et al., 2009). The dendritic tree rarely stays in one plane or in one orientation. Hence, field-induced polarization differs among individual dendritic branches according to their alignment with the field (Anastassiou et al., 2010).

Our experimental conditions were different from the conditions in slice preparations, where the field geometry can be well organized and different cellular properties can be probed for comparison. Nevertheless, by simultaneously recording from multiple cells across wide-spread cortical regions and layers, we were able to obtain a diverse pool of data that allowed us to compare field-effects across different cell populations.

1.3.3. Properties of the medium

i. Anatomical location

The magnitude of the field is shaped by the characteristics of the anatomical locus in which the field is created. The laminar organization, the cell density and the properties of the extracellular space (and thus the extracellular resistance) are critical factors that can either amplify or attenuate the impact of the field (Jefferys, 1995; Ghai et al., 2000; Francis et al., 2003). The hippocampal circuitry with a densely packed organization of cells is one of the regions where robust field-effects can be observed (Jefferys, 1981). Whereas, in loosely organized regions, e.g., basal ganglia, field effects may not be strong.

ii. Background neural activity and the physiological noise

A canonical excitatory cell needs almost 15 mV of depolarization to elicit an action potential (Henze and Buzsaki, 2001). Field-induced polarizations are often on the order of hundreds of microvolts, far below this level. However, background neural activity (Jacobson et al., 2005) can facilitate a suprathreshold response to

an otherwise subthreshold signal (Gluckman et al., 1998). Once added to the biological noise, even the smallest fields might be effective to modify spike timing (Bikson et al., 2004; Radman et al., 2007). Hippocampal ripples that induce 1 mV of membrane polarization can delay spiking activity almost 40 degrees (Anastassiou et al., 2010) when coupled with Schaffer collateral inputs (Ylinen et al., 1995). Physiological noise can also explain the heightened sensitivity to the field-stimulation, in vivo (Jefferys, 1995; Saunders and Jefferys, 2007).

Ongoing neural activity does not necessarily have an additive contribution to field-effects. Background network activity can modify the impact of the field intensity (Francis et al., 2003; Fujisawa et al., 2004), and can elicit different neural responses to the same field-stimulation (Marshall et al., 2006; Frohlich et al., 2008; Vyazovskiy et al., 2009). In other words, field-effects, particularly in vivo, are shaped by the network activity.

By recording in vivo from neatly organized structures, the neocortex and the hippocampus, we had a higher probability of observing field-effects in the presence of different background activities.

1.4. Characteristics of field effects

Field induced-effects have two important characteristics: 1) the degree of persistence, and 2) the mediation of the observed effects.

Field-effects can last from seconds up to hours (Bindman et al., 1964a; Purpura and McMurtry, 1965; Nitsche and Paulus, 2000; Nitsche et al., 2003b)

depending on the occurrence of the molecular changes required for synaptic plasticity (Hattori et al., 1990; Liebetanz et al., 2002; Nitsche et al., 2003a).

Neurons, close to the extracellular sources that create the field, are directly polarized by the induced current flow, while neurons in distant regions are not. However, field-induced effects are not limited to the 'directly' modulated cells, and can reach beyond of its region of spatial efficacy. The effects are transmitted to the other neurons in distant regions through synaptic connections (Sanchez-Vives and McCormick, 2000; Lang et al., 2005; Haider et al., 2007). Thus, at the point of observation (recording location), induced effects can either be directly introduced by the field, or be mediated from regions 'directly' affected by the field.

Our study was novel in the sense that for the first time, both the time-course and the spatial extent of TES-effects were investigated in vivo.

1.5. Therapeutic application of electric fields

Intentional exposure to external electric sources has effects similar to the ones induced by endogenous electric fields. This is the reason why a variety of electric stimulation techniques are applied for diagnostic and therapeutic purposes. Among those, weak-to-moderate intensity (1 - 2 mA) TES is the closest one to the electric fields that are the subject of my dissertation.

Experimental and clinical applications of low intensity TES have been traditionally confined to *transcranial direct current stimulation* (tDCS), which creates a constant current flow across electrodes placed on the skull or scalp (Nitsche et al., 2003c).

Effects of tDCS are strictly correlated with the direction of the induced current flow (Lippold et al., 1961; Lippold and Redfearn, 1964; Bindman et al., 1964b; Nitsche et al., 2005). Anodal stimulation (applied through a positively charged electrode) elicits excitation of the underlying cortex; whereas cathodal stimulation suppresses the activity (Purpura and McMurtry, 1965; Nitsche and Paulus, 2000; Nitsche et al., 2005; Boggio et al., 2008). These stimulations provide an opportunity to maintain interhemispheric balance and tune up or down the abnormal level of activity (Baker, 1970; Fregni et al., 2005a; Boggio et al., 2008; Nitsche et al., 2009).

When TES is combined with behavioral tasks, the induction of changes in the excitability can be confined to the active circuitry and can work as an enhancer to the ongoing cognitive process (Hummel et al., 2005; Boggio et al., 2006; Galea and Celnik, 2009). Similarly, TES-applied during sleep can enhance intrinsically induced sleep-associated brain rhythms (Huber et al., 2000; 2002; Gilula and Barach, 2004; Marshall et al., 2006).

TES is often confused *with transcranial magnetic stimulation* (TMS), which relies on creating an electromagnetic field through the charging and discharging of a coil held above the head of the subject. The induced-magnetic field creates an electric field in the underlying cortex, thus producing effects similar to TES (Barker et al., 1985; Walsh and Cowey, 2000; Hallett, 2000; Fitzgerald et al., 2006). Considering, the simple electronics required, and the similar effects produced, TES has a clear advantage over the expensive and complicated TMS (Brocke et al., 2005).

TES can elicit experience of pain and contractions of neck and facial muscles (Rossini et al., 1985). The muscle contraction is generated through direct and/or transsynaptic activation of the cells of the pyramidal tract (Hakkinen et al., 1995). Pain is induced by the activation of nociceptors in the local area under and around the stimulating electrodes. Both of these effects occur in rare occasions and they can be avoided by careful arrangement of stimulating electrodes and/or using low intensities (Marshall et al., 2006). If high intensity stimulation is required, the application of local anesthetics could help to increase the nociceptor activation threshold (Hakkinen et al., 1995). Placement of the stimulating electrodes under the pericranium can also be a convenient solution to completely avoid the activation of pain receptors (Hakkinen et al., 1995).

Other, relatively minor side effects include tingling and light itching of the area under the electrodes, feeling of fatigue, headache, nausea, or post-stimulation insomnia. Tingling is the most common one, whereas others are reported less frequently (Poreisz et al., 2007). Apart from these, measurements of neuron specific enolase concentration (Nitsche et al., 2003b), behavioral assessments (Nitsche and Paulus, 2000), MRI-based histological evaluations (Nitsche and Paulus, 2000), measures of psychomotor processing or measurement of emotional states (Iyer et al., 2005) have not revealed any disruptive effects of TES.

Overall, TES is safe and it could be utilized for various purposes ranging from abolishing epileptic activity (Nakagawa and Durand, 1991; Ghai et al., 2000), to the modulation of cognitive functions (Kirsch, 2002; Kincses et al., 2004; Fregni

et al., 2005b; Marshall et al., 2006; Fecteau et al., 2007), even to the modulation of sleep (Rosenthal and Wulfsohn, 1970; Rosenthal and Calvert, 1972; Rosenthal, 1972a; 1972b). Despite the vast amount of clinical and experimental evidence that suggests multiple potential benefits of TES application, its current usage is limited since the underlying mechanism of how electric fields affect intact neural activity is still not known.

1.6. Implementation of field-stimulation in vivo

In an 'ideal' medium, the current flow is direction-independent and the current distribution is homogeneous (Nunez and Srinivasan, 2006). In contrast, current distribution in the head/brain is non-uniform. Not only does the resistivity vary across different components of the head, e.g., skin, skull, cerebral cortex, etc.; but it is also direction specific in certain parts of the brain. For example, the resistivity of the white matter is lower in the plane parallel to the layout of the axons. This together with the presence of gyri complicates the efforts to estimate field-effects on human neural tissue.

In vitro studies where homogeneous electric fields are induced across the whole slice / brain deviate substantially from the human case. Only, in vivo studies are amenable to determine the optimal electrode configuration(s) to effectively alter the membrane properties of neurons in the target structure(s) while inducing minimal effects on the rest of the population. The goal of my research was to establish the methods required for chronic application of TES to modulate the firing patterns of neurons in neocortical and hippocampal areas.

1.7. Overview of target regions

The neocortex constitutes the cortical mass at the dorsal surface of the brain and is associated with various cognitive functions, including but not limited to the processing of sensory information, the initiation of motor commands and the storage of long-term memories. Its accessibility simplifies the efforts to manipulate its activity through TES. Moreover, the morphology of the neocortex is grossly uniform throughout the entire brain; albeit the cell densities and cell types might differ across regions (cf., Kandel et al., 1991; cf., Squire et al., 1999). The neatly organized layer formation provides an advantage to induce and amplify electric fields and to observe the field-effects on different types of neurons across different layers.

The hippocampus allocated in the medial temporal lobe, is critically involved in mnemonic functions (Scoville and Milner, 1957; Squire, 1992; 2004). Hippocampal circuitry has also a well defined laminar organization with specific inputs and outputs (Amaral and Witter, 1989; Tamamaki and Nojyo, 1993; Dolorfo and Amaral, 1998). Similar to the neocortex, the hippocampus is prone to experience large magnitude of extracellular fields due to its structured laminar formation.

The neocortex and the hippocampus vary in their anatomical layout and local processing. They have different and unique background activities associated with different behavioral states (Vanderwolf, 1969; Buzsaki, 1986; Steriade et al., 1993c; McCormick and Bal, 1997; Buzsaki, 2002). Yet, these two networks constitute a functional entity for certain cognitive processes, e.g., declarative

memory formation (Buzsaki, 1996; Siapas and Wilson, 1998; Sirota et al., 2003).

Investigations on the activity of these structures provided the opportunity of

comparing field stimulation in two functionally inter-connected but anatomically

and physiologically different regions.

1.8. Behavioral states and associated physiological activities

Behavioral state is tightly regulated by the nuclei in the brain stem, the

hypothalamus and the basal forebrain (McCormick and Bal, 1997; Pace-Schott

and Hobson, 2002). A regular night-sleep is composed of 90 minutes of cycles

going through *non-rapid eye movement* (NREM) and *rapid eye movement* (REM)

sleep states that differ vastly in terms of muscle activity, eye movement and

neural activity (Fig. 1.3;Hobson, 2005).
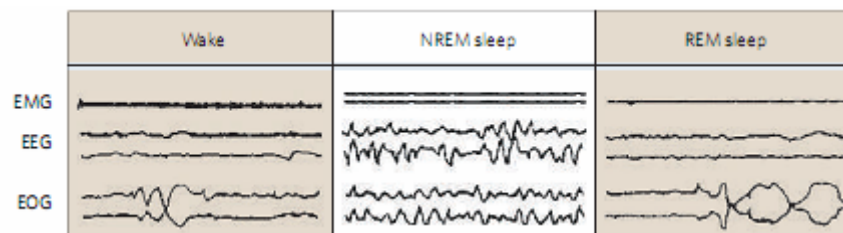
Figure 1.3. **Behavioral states.** Left, waking state. Middle, NREM sleep. Right, REM sleep. *EEG*, electroencephalogram. *EMG*, electromyogram. *EOG*, electrocorticogram. Note 1) the highest muscle activity during waking; moderate during NREM sleep and none for REM sleep; 2) the eye movement during waking and REM sleep; but not during NREM sleep; 3) the low amplitude, fast EEG activities during waking and REM sleep; and large amplitude slow activities during NREM sleep (Adopted from Hobson, 2005).

Behavioral states associated with sleep-wake cycle can be grouped into 2

categories based on the major activity observed in the largest cortical volume: 1)

neocortical desynchronized state, including wake, REM sleep, and shallow

anesthesia, and 2) neocortical synchronized state including SWS, behavioral

immobility and deep anesthesia (Fig. 1.4).
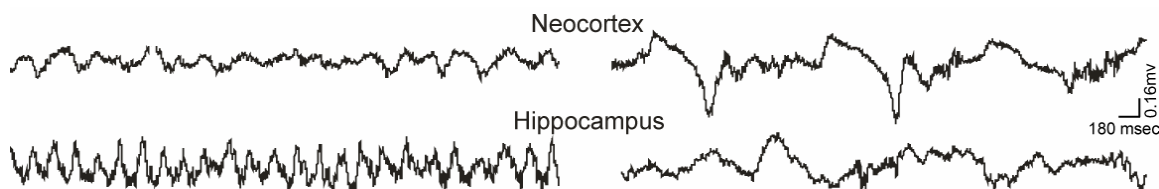
Figure 1.4. **Major activity states across neocortical-hippocampal networks.** Left. Neocortical desynchronized state. Top, neocortical LFP trace (<1,250 Hz) showing fast, desynchronous neocortical activity. Bottom, hippocampal LFP trace showing theta oscillations. Right. Neocortical synchronized state. Top, neocortical LFP trace showing slow oscillations. Bottom, hippocampal LFP trace showing sharp-wave and ripple.

1.8.1. Neocortical desynchronized state

During REM sleep (Aserinsky and Kleitman, 1953) and wake, especially

during cognitive engagement, the neocortex is desynchronized with low

amplitude, fast activities, including bursts of gamma oscillations (Gray and

Singer, 1989; Engel and Singer, 2001). The hippocampal activity, on the other

hand, is highly synchronized at 4-8 Hz theta oscillations (Vanderwolf, 1969;

Huerta and Lisman, 1995; Buzsaki, 2002).

1.8.2. Neocortical synchronized state

As drowsiness turns to sleep, the neocortical activity slows down and

increases in amplitude. NREM sleep gradually progresses from early to deep

sleep in 4 stages. At stage 2, bursts of fast activity, *sleep spindles*, and high

amplitude deep positive waves, *K-complexes*, emerge (Steriade et al., 1993b;

Amzica and Steriade, 1997; Steriade and Amzica, 1998). As sleep deepens (SWS, stage 3 and 4), neocortical and thalamic structures become robustly synchronized into large amplitude *slow oscillations* at 0.8-2 Hz frequency (Steriade et al., 1993b; 1993c; McCormick and Bal, 1997; Steriade et al., 2001), meanwhile hippocampal activity is governed by irregular high amplitude events, *sharp waves*, and bursts of fast oscillations, *ripples,* observed at the cell body layer (Buzsaki, 1986; Buzsaki et al., 1992; Ylinen et al., 1995).

1.9. Neocortical slow oscillation

Characteristic oscillations observed during these two behavioral states, network states, create powerful electric fields. The neocortical slow oscillation (0.5-1.5 Hz) is one of these oscillations.

Slow oscillation is the major cortical activity (Steriade et al., 1993a; 1993b; 1993c) observed in both animals and humans (Achermann and Borbely, 1997). During SWS and under anesthesia, even in isolated cortical preparations, large areas of the neocortex, along with various subcortical structures, are synchronized into cyclical periods of global excitation followed by widespread silence (Steriade et al., 1993c; Timofeev et al., 2000; Sanchez-Vives and McCormick, 2000). All neocortical cells discharge during negative field potentials and remain silent during positive field potentials recorded from deep layers of the cortex. These periodically occurring and overtly synchronized active and silent periods are called *UP* and *DOWN states* (Fig. 1.5).

UP and DOWN states are associated with decreased and increased input

resistances, respectively (Steriade et al., 2001; Shu et al., 2003). Certain channel

inactivations (Luthi and McCormick, 1998), decreased extracellular Ca^{+2} and thus

decreased synaptic transmission (Massimini and Amzica, 2001) mark the

transitions from UP to DOWN state. Various thalamic, neocortical and even

hippocampal cells have resonance properties predisposing them to oscillate in a

slow frequency range (0.6-1 Hz).
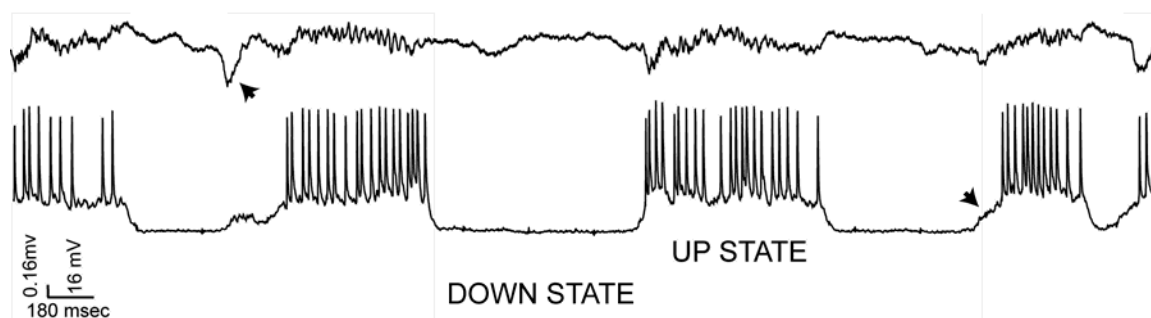
Figure 1.5. **Neocortical slow oscillation**. Recording was performed under urethane and ketamine xylazine anesthesia. Top, low pass filtered LFP trace (<1250 Hz) from a neocortical recording site. Bottom, the intracellular trace. Gray shade, UP states. Note that UP states are associated with somatic spikes, membrane depolarization (lower arrowhead) and extracellular negativity (upper arrowhead).

Slow oscillations promote synaptic changes (Sejnowski and Destexhe, 2000;

Massimini and Amzica, 2001; Rosanova and Ulrich, 2005) through the

modulation of spindle activity (Steriade et al., 1993b; Steriade and Amzica,

1998). Faster activities in beta and gamma oscillations frequency range were

also modulated by slow oscillations (Mukovski et al., 2007). Furthermore, unit

activity in various subcortical structures (Timofeev and Steriade, 1996; Stern et

al., 1997) and paleocortical and hippocampal networks (Sirota et al., 2003; Sirota and Buzsaki, 2005; Isomura et al., 2006) are affected by this slow oscillation.

Based on these interactions, it was suggested that UP and DOWN *states* bind neocortical and hippocampal networks to facilitate spatial and declarative memory formation (Buzsaki, 1998; Steriade and Timofeev, 2003; Molle et al., 2004). Thus, external manipulation in this frequency range would a) create an alteration very close to the natural activity, b) have great potential to affect the activity of large populations of neurons, and c) have particular implications for experimental and therapeutic applications aiming to target the declarative memory system. Therefore, I designed my experiments to test the effects of slow oscillation frequency stimulation.

1.10. Rationale

Various clinical and experimental studies highlight the great potential of TES to modulate brain activity through the creation of extracellular electric fields. Despite studies demonstrating the complexity of the underlying mechanism (Jefferys, 1995; Francis et al., 2003; Radman et al., 2007) and a multitude of early studies in humans (Redfearn et al., 1964; Rosenthal, 1972a; Rossini et al., 1985), surprisingly few electrophysiological experiments on TES have been carried out in vivo and none in chronic behaving animals.

In recent studies on humans, significant enhancement of certain cognitive processes was achieved by TES (Marshall et al., 2006; Terney et al., 2008). However, the physiological effects of the stimulation could not be investigated.

Marshall and colleagues (2006) asked healthy subjects to learn a list of word pairs. Learning was followed by the evaluation of subjects' pre and post-sleep memory performance using a cued-recall test. During SWS sleep, the experimental group received bilateral TES through electrodes placed on the frontal cortices. Trapezoid-shaped DC electric fields oscillating at 0.75 Hz frequency were applied 5 times for the duration of 5 minutes, interrupted by 1 minute long stimulation free periods. TES did not induce any effect on blood concentrations of cortisol, growth hormone or norepinephrine. Neither, the overall sleep duration was altered. Not surprisingly, post-sleep recall performance of both experimental and control groups was improved compared to their pre-sleep performance. However, the improvement in experimental group's performance was significantly better than that of the control group. The higher improvement was specific to hippocampus-dependent memories, and it was only observed when TES was applied at the night of the consolidation (Marshall et al., 2006). Moreover, the effect was only present when slow oscillation-matching TES was applied during SWS; but not when it was applied during REM sleep or wake-state, implying that electric fields with matching characteristics to the intrinsic activity have a higher chance to modulate neuronal activity (Frohlich et al., 2008; Vyazovskiy et al., 2009).

Physiological aspects of these exciting behavioral results could, unfortunately, not be studied due to a) stimulation-induced artifacts and b) the non-invasive nature of the study. The only physiological evidence for the stimulation-induced effects was an increase in the spectral power in the frequency ranges of

neocortical slow oscillation (0.5-1 Hz) and spindles (8-12 Hz) during three of the 1-minute long stimulation-free periods. Thus, how TES facilitated the recall of declarative memories remained unclear. This exciting finding further emphasizes the need for a thorough physiological understanding of TES-induced effects on neuronal activity.

The increased power in an oscillatory activity might be explained by an increase in the firing rate of neurons, an increase in burstiness of the neurons or an overall increase in synchrony. Thus, it can be assumed that TES applied in Marshall's study (2006) increased the synchrony in the slow oscillation by, at least, temporally biasing the firing of multiples of cells; but how?

The results of Marshall et al (2006) should be interpreted in light of the findings reviewed so far. The stimulation created surface-positive electric fields on bilateral frontal areas. The induced-current flow led to depolarization of somata and proximal dendrites and therefore an increase in neuronal excitability for certain phases of the trapezoid shape stimulation. Such a time bound polarization of many cells, probably, induced synchronization within and across affected cortical regions. Most likely, the regions closest to the stimulation sites were directly affected and thus more strongly synchronized. The prefrontal cortex was probably among those areas since the stimulating electrodes (anodes) were placed on F3 and F4. This region, like all other neocortical regions, is already endowed with an intrinsic ability to generate slow oscillations (Massimini et al., 2004). Thus, it is most likely that prefrontal neurons were preferentially entrained and then they transmitted these effects to the distant regions through their

synaptic connections (Sanchez-Vives and McCormick, 2000). The synchrony might have been enhanced as additional locations were progressively recruited (Timofeev et al., 2000). Hippocampal regions might have been entrained either by direct stimulation-induced effects or through synaptic links. Increased synchrony in neocortical-hippocampal networks might have led to an improvement in memory consolidation (Siapas and Wilson, 1998; Sirota et al., 2003; Battaglia et al., 2004).

Testing the physiological part of this hypothesis and understanding how neocortical and hippocampal unit activities behave under the influence of slowly oscillating electric fields were the main goals of my dissertation research. In order to address this issue, I investigated the neurophysiological effects of TES in anesthetized and chronically implanted animals. I particularly focused on slow oscillation frequency stimulation due to the physiological and functional significance of intrinsic slow oscillation. First, I investigated the possibility of modulating neocortical unit activity by field stimulation in anesthetized animals (Chapter 3). Then, I extended my experiments to chronically implanted, naturally sleeping animals in order to evaluate the interactions between network and TES-induced effects (Chapter 4). Results of both studies provided compelling evidence to conclude that chronic in vivo application of TES can be utilized for external manipulation of neural activity in widespread cortical areas.

Chapter 2: General Methods

2. 1. Surgery and recording

All procedures followed the rules and regulations of the National Institute of Health as detailed in the Guide for the Care and the Use of Laboratory Animals and were approved by the Institutional Animal Care and Use Committee at Rutgers University.

2.1.1. Surgery and recording from anesthetized animals

For acute experiments, male Sprague-Dawley rats (n=16; 100-400 g; Hilltop Laboratories, NJ) were initially anesthetized with urethane (1.25 g/kg, i.p.) followed by hourly supplements of ketamine/xylazine mixture (18 and 1.8 mg/kg, i.m.). Atropine-sulphate (0.03 mg/kg) was subcutaneously administered to aid breathing. Body temperature was kept constant at 37°C using a heating pad. Paw-withdrawal reflex was periodically checked.

Surgeries and recordings were all performed while the head of the animal was fixed to the stereotaxic frame. Depending on the experiment, a number of small holes of 1-2 mm in diameter were drilled in the skull at pre-determined coordinates. Bone fragments were cleaned, and the dura was opened. Small walls of dental cement were constructed around the holes. Recording electrodes were slowly lowered down to the desired depth. Holes were covered with hot liquid wax during recording to enhance mechanical stability and to diminish pulsations.

High-density two-dimensional silicon probes were used to record unit and LFP activity. The use of high-density silicon probes (Csicsvari et al., 2003) enabled a thorough observation of local interactions by sampling the activity of a large number of neurons across multiple recording sites, while causing minimal tissue damage.

For neocortical recordings, three different types of high-density silicon probes were used. The first probe, used in 5 acute experiments, had 4 shanks spaced at 200 μm, each with 8 recording sites staggered at 20 μm vertical spacing (Acreo, Sweden). The second probe, used in 5 acute experiments, had 5 shanks spaced at 200 μm, each with 12 recording sites staggered at 15 μm vertical spacing; the middle shank had 4 additional recording sites at 250 μm spacing, above the highest electrode site (Acreo, Sweden). For these experiments (Fig. 2.1Aa), extracellular recordings were performed in the left medial prefrontal cortex (mPFC); with the tip of the rightmost shank targeted at AP 2.8 mm, ML 0.5 mm, and 1.5 – 3.0 mm from the dura. For most of the experiments, the probe was placed such that the recording sites were facing the medio-lateral axis. In that configuration, simultaneous recordings across different layers of mPFC could be recorded through multiple shanks of the probe. In a subset of experiments, the probe was placed facing the midline in order to record from the same layer across different subregions of mPFC (in the antero-posterior axis, <0.5 mm apart). These probes were used for the voltage gradient measurements along the mediolateral axis for postmortem recordings.

The third probe used in the remaining acute experiments (n=5, Fig. 2.1Ab) had 32 recording sites spaced 50 µm apart along the vertical axis of one shank (NeuroNexus, Ann Arbor, MI) and was placed in the somatosensory area / hippocampus at AP -3.5 mm and ML 2.5 mm from bregma and 2.4 – 3.5 mm from the dura. Recordings included sub-granular layers of the somatosensory cortex and CA1 subregion of the hippocampus. The same single-shank linear probe was used to map the volume-conducted current of TES in postmortem recordings. Stainless steel screws for reference and ground electrodes were implanted above the cerebellum.

In three of the experiments, a borosilicate glass micropipette (30-70 MΩ) filled with 2% Biocytin in 1 M K-Acetate (pH: 7.4) was vertically inserted into somatosensory cortex at AP –3.3 mm, ML 2.0 mm from bregma for intracellular recording. A silver/silver-chloride wire was placed in the neck muscle tissue and served as the reference electrode. Intracellular recordings were only performed if healthy and stable condition of the cell was maintained over 10 minutes after impaling. 'Healthy' recording implied an input resistance >20 MΩ, resting membrane potential <-55 mV, and overshooting action potentials. Recordings that did not meet these criteria were discarded. The sub-threshold activity of the cell under different network states was recorded along with frequent sets of evoked responses to hyperpolarizing and depolarizing current pulses of 0.1-0.6 nA lasting for 500 msec. The recorded cells were loaded with Biocytin through iontophoresis (0.5-0.8 nA current injections for 0.2-3 hours).
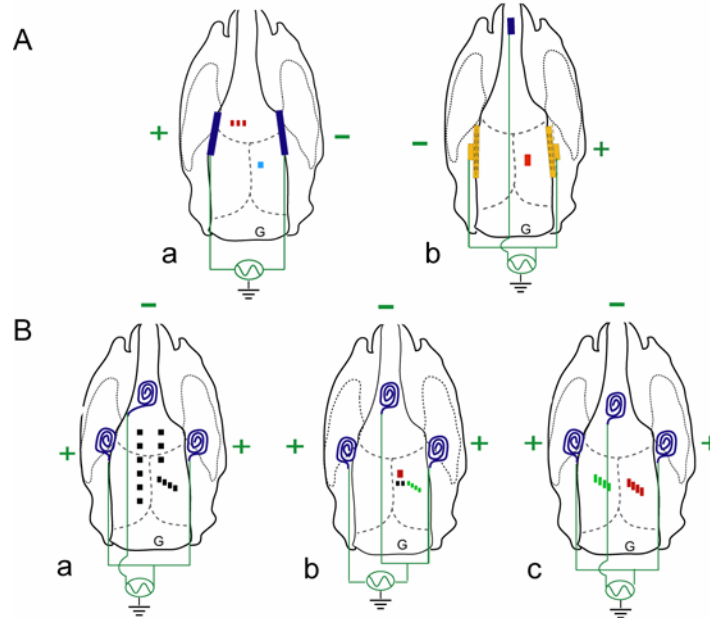
Figure 2.1. **Placement of recording electrodes.** Aa-b. Acute experiments from anesthetized animals. *Red*, shanks of the silicon probe. *Cyan*, intracellular pipette. *Blue*, stimulating electrodes (silver wires). *Yellow*, stimulating electrodes (flexible cables). Ba-c. Experiments in chronically implanted animals. From left to right: rat #1, rat #2, rat #3. *Red*, shanks of the silicon probe. *Green*, tetrodes. *Black*, single wires. *Blue spirals*, stimulating electrodes (bifilar wires). *G,* ground.

2. 1. 2. Surgery and recording from chronically implanted animals

For chronic experiments, three male Long-Evans rats (250-350 g from Charles River Laboratories) were implanted with stimulating and recording electrodes.

Rat #1 had 13 single wires (20 µm in diameter) implanted in various cortical sites either at fixed depths from the surface of the cortex or attached to a movable drive (Fig. 2.1Ba). Six single wires were implanted in the left hemisphere (deep layers of prefrontal and somatosensory cortices) at 2 mm anteroposterior spacing from 3.2 mm to -6.8 mm relative to bregma and 1.5 mm from the midline. Three wires were implanted in the right hemisphere (deep

layers of prefrontal and somatosensory cortices) at 2 mm anteroposterior spacing from 3.2 mm to -0.8 relative to bregma and 1.5 mm from the midline. In addition, four single wires, attached to a movable microdrive, were placed in the right somatosensory cortex above the hippocampus at AP -3.5 mm, ML 1.2 mm.

In rat #2, a 32-site single-shank silicon probe (staggered at 20 µm spacing), 4 tetrodes and 2 single wires (20 µm in diameter) were used (Fig. 2.1Bb). The silicon probe, affixed to a movable microdrive, was implanted in the right hemisphere at AP -3.7 mm and ML 1.2 mm. Four tetrodes, affixed to a movable drive, were implanted such that the tip of the 2nd tetrode was targeting at AP -4.9 mm, ML 3.0 mm from bregma. Two wire electrodes were implanted in the right somatosensory cortex; one was at AP -4.9 mm, ML 1.0 mm from bregma and 1.2 mm from the surface of the cortex, the other, attached to a movable drive, was implanted at AP -4.9 mm, ML 1.5 mm from bregma.

Rat #3 had a 4-shank silicon probe (600 µm inter-shank intervals; 16 recording sites with 50 µm spacing on each shank; Acreo, Sweden) and 4 tetrodes implanted bilaterally above the hippocampus (Fig. 2.1Bc). The silicon probe attached to a movable drive was implanted in the right hemisphere parallel with the long axis of the hippocampus with the tips at AP -3.6 mm, ML 0.5 mm and AP -4.5 mm, ML 2.1 mm from bregma. In addition, four tetrodes affixed to separately movable drives were implanted in the left hemisphere at the same antero-posterior position and with the same orientation.

Chronic recordings were performed while the animal was sleeping or resting in its home-cage, except for experiments designed to compare field-induced

effects across different behavioral states. For those experiments, recordings were performed while the animal was exploring a novel environment (circular track or open field) while receiving random food rewards. For all experiments, the spontaneous activity was recorded for at least an hour prior to and post stimulation sessions.

2.2. Electric field stimulation

A sinusoidal waveform TES stimulation was applied multiple times (minimum of 5 trials) for a given stimulation protocol that varied in intensity, frequency (0.7-1.7 Hz) and duration (10-60 cycles, or 1 min long trials for a subset of acute experiments). Each stimulation trial was followed by a stimulation-free period (>40 sec, or 10 sec for short stimulation trials). In most sessions, the stimulation was applied through 3 stimulating electrodes (3-poles), such that the same polarity was applied to side electrodes while the center (frontal) electrode received the opposite polarity (Fig. 2.2Ad,e). This configuration yielded synchronous electric fields applied in both hemispheres. In a few acute experiments, bipolar stimulation was used (Fig. 2.2Aa-c). Trials using the same stimulation protocol were combined for the statistical analysis.

2.2.1. Stimulation electrodes and their placement

The placement of the stimulating electrodes was arranged depending on the proximity to the target area and the technical constraints regarding the shape and the size of the electrodes used for stimulation.

i. Extracranial / extracerebral stimulation electrodes and their placement

In acute experiments, stimulation was provided by a pair of silver wires placed into grooves in the bone prepared by drilling parallel to the lateral ridge of the skull or by screws driven halfway into the skull bone (Fig. 2.2Aa,b). Placement of screws and wires was secured using dental cement. In some acute experiments, capton-based epidural grids with 32 equidistant sites (2.5 mm x 4 mm) were placed between the bone and dura (Fig. 2.2Ac). Grids were placed so that the active sites were facing the bone in order to avoid the direct focal stimulation. For a subset of experiments, bilateral epidural grids were accompanied by a silver wire placed in the oral cavity of the animal (Fig. 2.2.Ad).
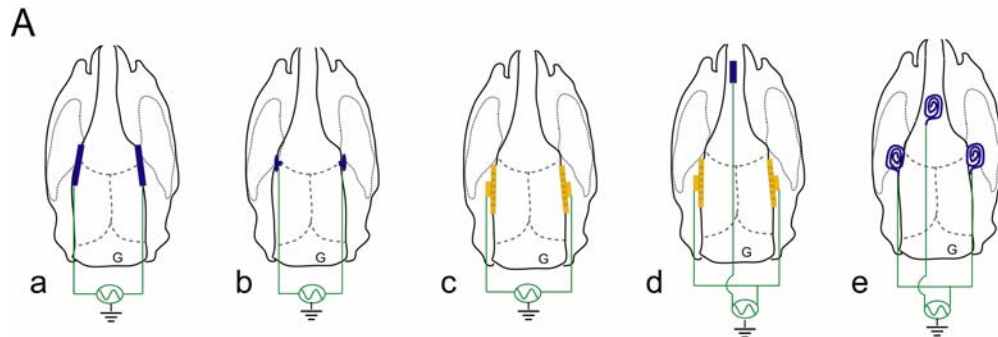
Figure 2.2. **Stimulation configurations**. Placement of stimulating electrodes in acute (*Aa-d*) and chronic (*Ae*) experiments. Aa. Silver wires placed on the skull. Ab. Screws driven halfway into the skull. Ac. Flexible cables placed epidurally. Ad. Flexible cables placed epidurally in addition to a silver wire placed in the oral cavity of the animal. Ae. Wire coils placed on the skull for chronic stimulation. The coils on the left and right sides of the skull had the same virtual polarity against the third electrode placed above the frontal cortex, unless stated otherwise. Note the closest form to human transcranial application is the configuration shown in (*Ae); thus this configuration is referred as *TES* throughout the text. *G,* ground.

ii. Transcranial stimulation electrodes and their placement

A spiral was formed from 200-µm stainless steel wire (approximately 3 mm in diameter). One such electrode was implanted on each temporal bone and one on the calvarium midline above the olfactory bulb during the surgery (Fig. 2.2Ae). The temporal bone electrodes were approximately 6 mm posterior from the midline electrode. The surface facing the muscle and skin was kept insulated, whereas the insulation of the surface facing the skull was removed.

2.2.2. Stimulation protocol

Constant current stimulation was used in 7 acute experiments and constant voltage stimulation was used for the remaining experiments (n=9 for acute and n=17 for chronic experiments). The stimulation signal was recorded directly from the stimulator (STG1008 Stimulus Generator; Multi Channel Systems, Germany) using one of the external recording channels. This signal was used as reference TES signal in the analysis and figure displays. Note that, depending on the recording location and configuration, the actual stimulation signal observed at a given location in the brain might have differed from this signal. However, having the same reference-stimulation signal enabled a valid comparison within and across experiments. Throughout the text, the peak-to-peak amplitude of the stimulator output is referred to as stimulus intensity.

Each stimulation session was assigned a certain frequency, in the range of 0.7-1.7 Hz and a peak-to-peak amplitude, in the range of 0.1-5.4 V or 0.1-0.16 mA. Each session involved multiple trials (minimum 5, mostly more than 10),

during which the continuous sine wave signal with the assigned frequency and intensity was applied (Fig. 2.3). The trial duration varied depending on the experiment (minimum 10, maximum 100 cycles of sine wave signal); but for most experiments, a trial lasted for 50 cycles. Each trial was interrupted by a stimulation-free period that typically lasted more than 40 sec. For measuring cycle by cycle evolution of the TES-induced effects, short trials (10-15 cycles long) with short stimulation-free periods (~10 sec) were used.
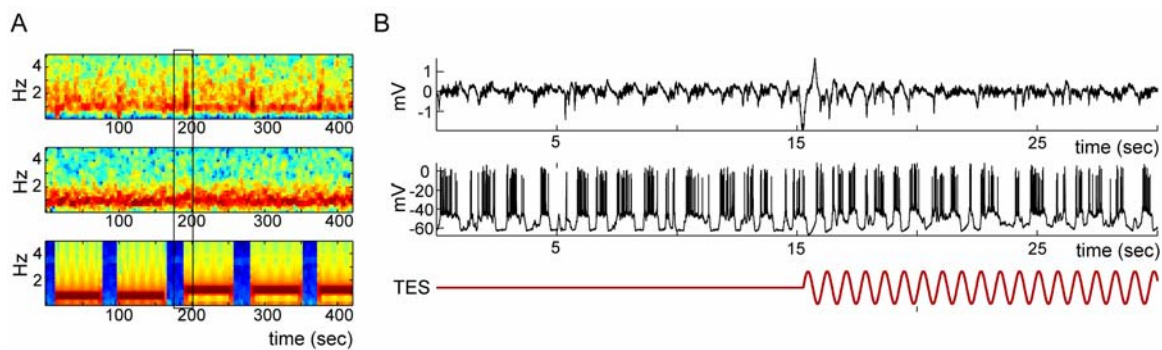
Figure 2.3. **Stimulation trials.** A. Short recording segment (> 6 min) during TES. Top, the spectrogram of the neocortical LFP (<1250 Hz) after removing the volume conducted current. Middle, the spectrogram of the intracellularly recorded membrane potential. Bottom, the spectrogram of TES. The highlighted region in the inset is expanded in (*B*). Note that first 2 and last 3 trials belonged to different stimulation protocols that varied in frequency. B. Zoomed in epoch shown in (*A*). Top, neocortical LFP after removing the volume conducted TES. Note the artifact due to cleaning of the volume conducted current at the onset of the stimulation. Middle, intracellular trace. Bottom, TES.

Figure 2.3 shows a short recording segment during stimulation. Spectrograms show 5 stimulation trials interrupted by stimulation-free periods. Note the change in the stimulation protocols (Fig. 2.3A) between the first two and the last three sessions shown (frequency increase from 0.8 to 1.7 Hz).

The stimulation was applied at a frequency very similar to that of intrinsic slow oscillation which was the major background activity in the experiments. In order

to avoid a possible Type 1 error through coupling of intrinsic slow oscillation and TES signal by chance, the stimulation was applied in multiple trials of short duration (≤1 min) and interrupted by stimulation-free periods (≥10 sec). Trials that belonged to different stimulation sessions were separated by longer duration of stimulation-free periods (>10 minutes) to avoid spillover effects that could be introduced by the previous trial.

Obtaining recordings in chronic animals during stable sleep epochs was very time-intensive; it required several hours of experiments per day that yielded only a few hours of good recording. The number of different stimulation protocols that could be applied in each animal was limited by this time constraint. Therefore, in order to have a full-spectrum of intensities, I deployed a rather segregated experimental design for the three chronically implanted animals. I used the first animal to probe a wide range of intensities. For the second and the third animals, I focused on the low and high ends of the intensity range, respectively.

There was an intended variability across experiments in terms of recording locations, stimulating electrodes, induced-field geometry, and stimulation parameters. One reason was the requirement for methodological developments in the absence of prior studies using field-stimulation in vivo. The other reason was to compare the impact of multiple variables, such as the geometry of the field, intensity, etc., on the field-induced effects. However, chronic recordings enabled repeated testing of similar experimental conditions in the same animal, decreasing the impact of confounding factors.

Various intensities were used within and across recording sessions in order to measure the intensity-dependence of the exerted effects. At all times, I kept the stimulation intensity at a level far below that required to cause pathological events. In none of the experiments presented here did I observe any kind of disturbance in physiological or behavioral activity of the animals.

2.3. Data acquisition and processing

Extracellular signals were amplified (x1000) and wide-band pass filtered (1 Hz-5 kHz). Intracellular signals were buffered (x1) and amplified by a DC amplifier (Axoprobe 1A; Axon Instruments). Signals were continuously acquired at 20 kHz on one or two synchronized 64 channel DataMax systems (16 bit resolution; RC Electronics, Santa Barbara, CA). All analyses were conducted off-line.

For the analysis of the intracellular signal (<1250 Hz, low-pass), the signal was band-pass filtered at 0.5-10 Hz using a Butterworth Filter (a Matlab-based function) in order to eliminate the high frequency component of action potentials (Isomura et al., 2006).

Unit activity was detected from the high-pass filtered (>0.8 kHz) trace and single units were semi-automatically isolated using Klusta-Kwik© (Harris et al., 2000), followed by a manual refinement using a custom-made software (Fig. 2.4; Hazan et al., 2006), which utilized spike waveforms, autocorrelograms (ACG) and crosscorrelograms (CCG). Using this method, single units could reliably be clustered (Bartho et al., 2004; Fujisawa et al., 2008).
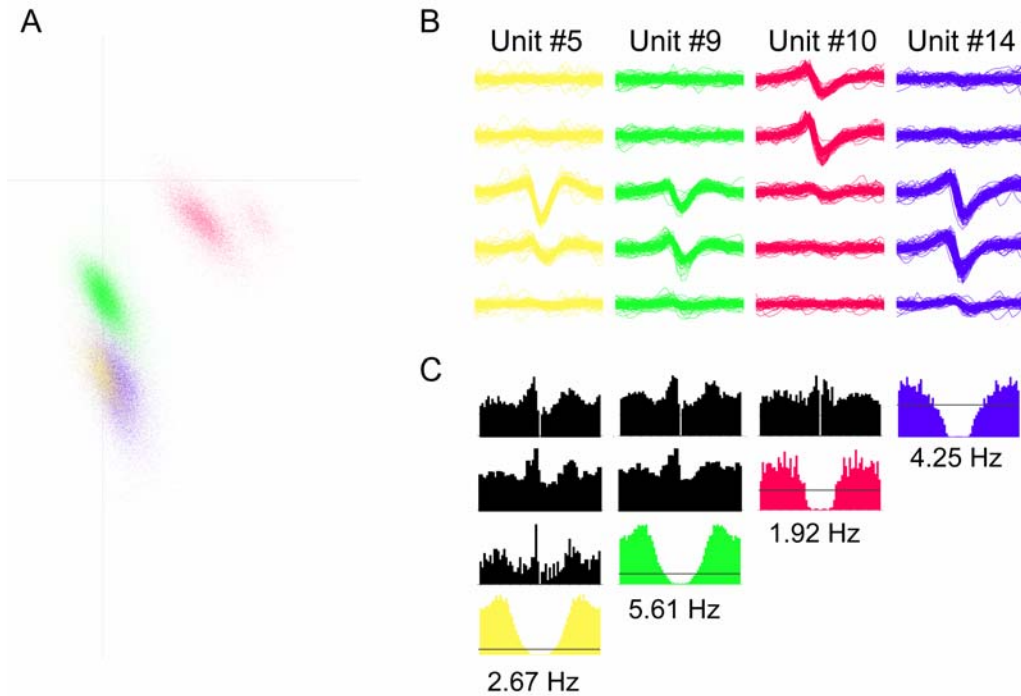
Figure 2.4. **Spike clustering.** Clustering of 4 cells recorded simultaneously. A. Spike clusters projected on the first principal components of the second and third channels from the top, shown in (*B*). B. Spike waveforms (1.6 msec trace) of four isolated cells. C. Autocorrelograms (ACG) and crosscorrelograms (CCG) of the cells given in (*B*). *Colored histograms*, ACGs of specified cells. *Black lines* in ACGs indicate the asymptotic value. Firing rates are given below. *Black*, CCGs of cell pairs (the intersection of ACGs). Reference cell is at the bottom. Each bin, 1 msec. Duration, 30 msec.

To ensure that only high quality units were used in the analyses, I set two criteria for spike inclusion: 1) The peak-to-peak spike amplitude (p2p) had to be >60 μV. 2)The peak-to-peak spike amplitude had to exceed 3.6 times the temporally-local background noise, determined according to the standard deviation of the signal in the immediate vicinity of each spike (between 0.8-0.4 msec before and 0.4-0.8 msec after the extracellular trough), and scaled by the natural logarithm (lan) of the number of samples across which the standard deviation (SD) was computed (Fig. 2.5).

This definition of spike signal-to-noise ratio (SNR) = p2p / SD(noise) / lan(n), is independent of the number of samples used to compute the noise and is asymptotically 1 for band pass-filtered white noise.

These values were determined based on the properties of spike-frequency *noise* events extracted from postmortem recordings of the second chronically implanted animal. From each electrode (2 wires and 4 tetrodes), the peak noise amplitude (pN) and the signal-to-noise ratio of the noise (snrN) were computed (snrN= pN/ SD(noise)/lan(n)). The amplitude threshold was determined as the mean and twice the standard deviation of the mean pN across each electrode (mean(mean(pN))+ 2*SD(mean(pN))). The derived value, 60 µV, was in line with our previous observations that smaller amplitude spikes result in clusters bordered closely by other clusters (Henze et al., 2000). The SNR threshold was determined as the mean of the 99th percentile snrN values across electrode. High-frequency noise events detected from other postmortem recordings (from the 1st chronically implanted animal and from few experiments done in acute recordings) had similar properties.

Each spike was screened according to these criteria; failure to pass either of the criteria resulted in elimination of that spike from the analysis. Although these strict criteria eliminated numerous true spikes, it reduced the likelihood of obtaining false positive results (Fig 2.5B-D).

Since the neuron type was not a defining characteristic for the unit entrainment, multiunits were also incorporated into the analysis. Spikes of poorly isolated cells recorded from the same electrode (e.g., the shank of the probe,

etc.) were merged. A cluster was classified as '*multiunit*' if the autocorrelogram

lacked a clear refractory period.
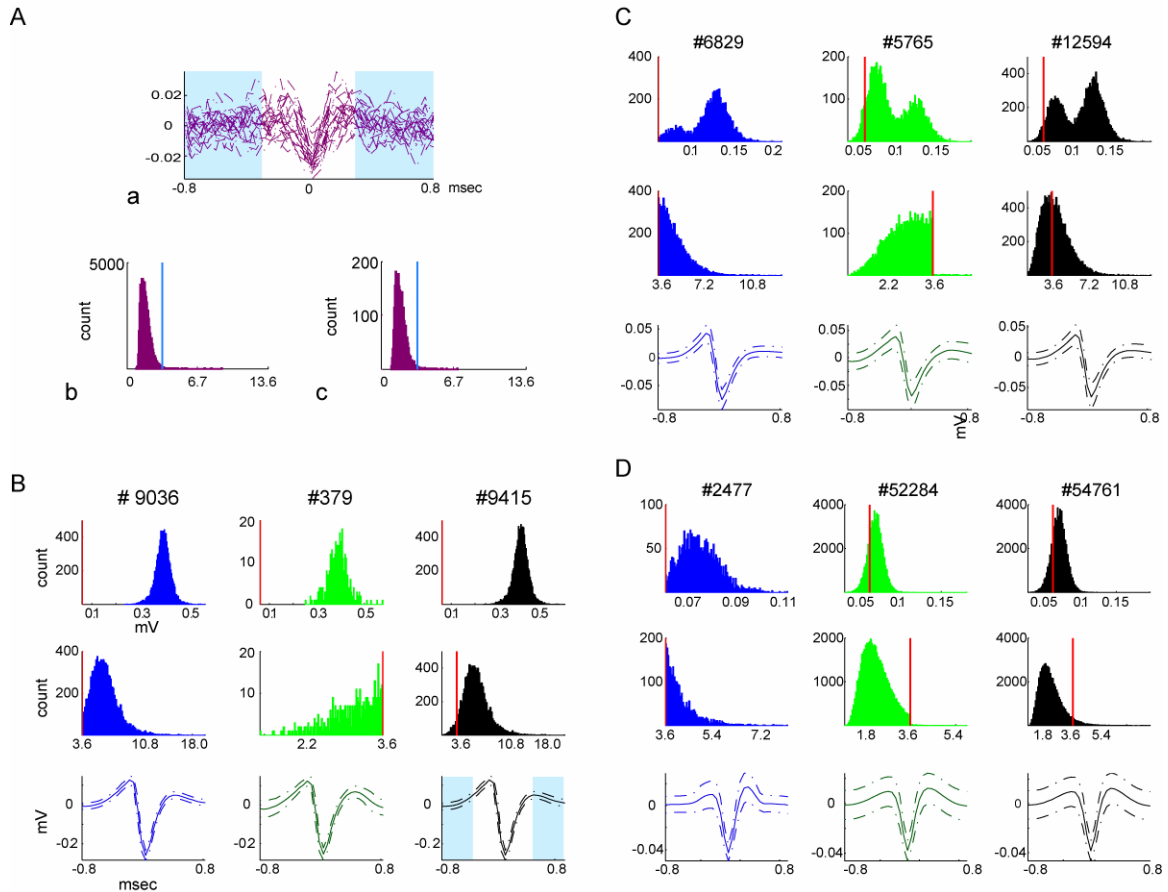
Figure 2.5. **Elimination of low-quality spikes**. A. Deriving SNR threshold. Spike-frequency noise events extracted from the dead animal. Aa. Overlaid traces of noise-waveform during TES. Ab. Noise- SNR distribution during stimulation free period. Ac. Noise-SNR distribution during TES. All from the most lateral tetrode in (*Fig 2.1Bb).* Based on all measurements across all electrodes (excluding silicon probe), SNR threshold was determined as 3.60. *Light blue shade*, period across which the SD-background noise was computed. *Cyan*, SNR threshold. B,C,D. Spike-quality checks for three cells. Cell in (*B*) was recorded under anesthesia as shown in (*Fig 2.1Aa)*. Cells in D and E were recorded simultaneously during sleep as shown in (*Fig 2.1Bc)*. Right column (*black*), before noise-elimination. Middle column (*green*), eliminated events. Left (*blue*), after noise-elimination. The number of events under each category is given on the top row. Top, peak-to-peak spike amplitude distribution. Middle row, SNR distribution. Bottom row, mean waveform of spikes under each category. Dashed lines, ±1 standard deviation. *Light blue shade*, period across which the SD-background noise was computed. Note that the spike quality check, and so the noise-elimination, was performed for the whole duration of recording, and prior to the analysis. Note that spike-ality decreases from (*B*) to (*D*); and so more events are discarded.

2.4. Histology

At the end of the experiments, the animals were deeply anesthetized with urethane (2.5 g/kg, i.p.) and transcardially perfused with ~50 ml of cold saline (0.9 %) followed by ~400 ml of buffered fixative (4 % paraformaldehyde with glutaraldehyde 0.5 % in 0.1 M phosphate buffered saline, pH: 7.4). Brains were post-fixed at 4°C overnight, and kept in 0.1M phosphate buffered saline until sectioning. Coronal sections of (50 - 100 µm) thickness were sliced. For the single cell verification, sections were embedded in 20% sucrose in 0.1M phosphate buffer for cryoprotection, which was followed by freezing and thawing three times. During washing, sections were processed with a detergent (0.5% Triton-X) to facilitate the antibody penetration into the cell. After pre-incubation with the Avidin-Biotin-HRP complex (VectorLabs); the labeled neurons were revealed by using diaminobenzidine and nickel complex (DAB-Ni). The laminar organization of recorded regions was revealed by NeuN or Nissl staining.

2.5. Data analysis

2.5.1. Cell classification

Short-latency temporal interactions (< 5 msec) with other neurons can be used to categorize neurons as putative inhibitory or excitatory cells (Bartho et al., 2004; Isomura et al., 2006; Sirota et al., 2008; Fujisawa et al., 2008). The significance of monosynaptic connections was evaluated according to the global and point-wise significance values obtained by jittering (n=500) the cross-correlograms between single unit pairs. Neuron pairs that had CCGs with

significant peaks or dips within 5 milliseconds from the spikes generated by the reference neuron, were regarded as monosynaptically connected (Fujisawa et al., 2008). The significant peaks and dips were interpreted as evidence that reference cells were putative excitatory or inhibitory cells, respectively (Fig. 2.6).
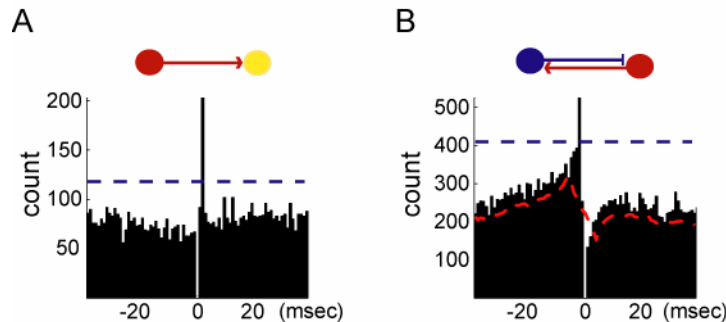
Figure 2.6. **Cell classification**. A,B. Example cross-correlograms between neuron pairs recorded in the somatosensory cortex. A. The reference neuron (*red*) excites the postsynaptic target neuron (*yellow*), as revealed by the short-latency large single bin. B. Bidirectional connectivity between a putative excitatory cell (*red*) and an inhibitory interneuron (*blue*; the reference cell in the CCG). Note the large peak before and transient suppression in the activity after the firing of the reference putative inhibitory neuron. *Blue* and *red dashed lines*, global maximum and point-wise minimum significance levels obtained by jittering (n=500) the CCG (Fujisawa et al., 2008).

2.5.2. Evaluation of phase-modulation

Unit activity was investigated for a TES-induced temporal pattern by evaluating the distribution of spikes with respect to the stimulation phase. The null hypothesis was that *there was no temporal relation between the applied field and the unit firing* (Fig 2.7)*.* In cases with uniform spike-phase distributions, the null hypothesis could not be rejected (Fig. 2.7A). Rejection of the null hypothesis implied that *there was a TES-dependent temporal bias on spiking activity;* in other words *TES entrained unit firing* (Fig. 2.7B)*.*
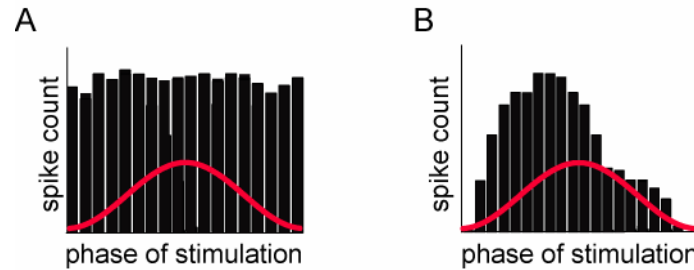
Figure 2.7. **Assessment of phase-modulation.** Hypothetical spike phase histograms. A. Uniform distribution. The null hypothesis is not rejected. B. Non-uniform distribution (unimodal distribution). The null hypothesis is rejected.

i. Phase-modulation of unit activity by TES

Phase of the reference TES signal was obtained using Hilbert transformation, a built in Matlab function. Each spike was assigned to the instantaneous phase of the TES-signal. Observation of the spike-phase histograms revealed bimodal phase distributions for some units. In such cases, depending on how much the preferred phases were opposing each other; the net effect could be canceled out, leading to a Type 2 error (false negative). Hence, conventional uniformity tests, such as commonly used Rayleigh test, were inappropriate. Instead, Kuiper's test of random deviation from uniformity on circular data (Fisher, 1993) was used to evaluate the significance of the phase-modulations. This omnibus test was preferred since it did not require any predefined assumption regarding the modality of the distribution. A P-value (Kuiper's test) less than 0.01, was considered to reflect *significant phase-modulation.*

Since omnibus tests require a sufficiently large sample of data, 2 sets of criteria were applied: 1) the number of spikes had to be ≥ 250 per stimulation session, 2) the number of trials had to be ≥ 5 for a given stimulation session. Because both multi- and single units had different number of spikes and both

were evaluated using the same test, I examined whether the number of spikes biased our results. A fixed number of spikes (n=600, n=1000) was randomly chosen from a given TES session and tested against uniformity. Such sub-sampling generally yielded the same results as when all spikes were included.

The caveat of omnibus tests is the inability to define the modality of non-uniform distributions. Hence, preferred phase(s) of unit modulation could not be computed. Nevertheless, for high intensity stimulation protocols, the common preferred phase(s) could be deduced from the population level displays. On the contrary, for weak intensity stimulation, preferred phase(s) as well as the strength of the entrainment varied substantially across units. For these situations, the added value of knowing the preferred phase(s) for any given cell was minimal. Thus, for the purpose of demonstrating TES-induced temporal bias, not knowing the exact phase(s) did not introduce a vital limitation.

For the color-coded population displays, the spike count of each cell was normalized by subtracting the mean from the count of each bin and dividing by the standard deviation. In some figures, simultaneously recorded units were ordered according to the strength of their phase-modulation (P-values, Kuiper's test) for visual clarity. The unit with the smallest P-value was presented in the top row, and the unit with the biggest P-value was presented at the bottom. The range of observed P-values correlated with the stimulation protocol, particularly with its intensity. In most of the figures, units with P-values < 0.01 were separated by a black line from the units with P-values ≥ 0.01 in order to present the distribution of significance values.

ii. Statistical evaluation of phase-modulation across sessions

For each stimulation session, the fraction of significantly entrained units (P<0.01, Kuiper's test) was computed. Sessions, where the activity from at least 6 units was recorded, were included into further analysis. These sessions were categorized into groups (either 2 or more) according to the stimulation intensity. The mean and standard deviations were computed for each group.

Statistical comparison across groups required one additional step. In most cases, the same neuronal population was included more than once within an intensity group; e.g., 0.4 V and 0.8 V TES performed in the same recording session would go into the same <1.2 V intensity group. When this was the case, the data from these sessions was re-sampled and the percent of significantly modulated units was recomputed, for 1000 iterations. The median value was used instead of those separate sessions. Statistical evaluation between groups was then performed by either using an unpaired T-test or a one-way ANOVA. For chronically implanted animals, one recording session with unexpectedly no unit entrainment regardless of the TES intensity, was a clear outlier; so it was excluded from statistical testing.

iii. Detection and evaluation of bimodal phase-modulation

Spike-phase histograms of significantly modulated neurons (P< 0.01, Kuiper's test) were semi-automatically inspected for the modality of their phase preference, e.g., unimodal vs. bimodal. Using a spike-count threshold ((mean firing + peak firing)*0.5), additional peaks in the histograms were detected. The

fraction of bimodally entrained neurons was compared across intensity groups (2 or 3 groups, with sessions >5 units) either using an unpaired T-test or a one-way ANOVA. If needed, re-sampling was performed as previously explained.

iv. Detection and evaluation of phase-modulation of multiunits

Multiunits were identified based on the investigation of the refractory period and the waveform of units for the duration of entire recording. For the comparison of multiunit and single unit entrainment, the fraction of significant entrainment (P<0.01, Kuiper's test) was computed within each unit-type (e.g., [the number of modulated multiunits] / [the number of multiunits]). The effect of the combination of two factors, the unit-type and the TES intensity were evaluated using a 2-way ANOVA test. If re-sampling was needed, it was performed as described above.

v. Comparison of state dependence of phase-modulation

To evaluate the behavioral state-dependence of TES-induced effects, the Chi-square test was performed, comparing the counts of phase-modulation P-values (Kuiper's test) calculated for each single- and multi-unit. Two or three P-value categories were considered as not-significant (nS, P>.01), significant (S, .001<P≤ .01), and highly significant (hS, P≤.001) and the counts of these categories across conditions (behavioral states) were evaluated by the Chi-square statistics.

vi. Phase-modulation of unit activity by the neocortical slow oscillation

The peak spectral power of LFP within the 0.4-10 Hz frequency range was computed in 3.2 seconds windows in order to examine the relationship between spikes and the neocortical slow oscillation. The signal was bandpass filtered around the peak frequency (peakF) between [0.75*peakF 1.25*peakF] Hz using a 2nd order Butterworth filter (a built-in Matlab function). The phase of the band-pass filtered signal was then derived using Hilbert Transformation (a built-in Matlab function).

Since intrinsic brain oscillations are not pure sine waves, it is critical to assess that all phases were uniformly distributed over the range of 0°- 360° and that no bias was introduced into the analysis. Thus, the phase distribution of the slow oscillation signal was screened for uniformity (Fig. 2.8).
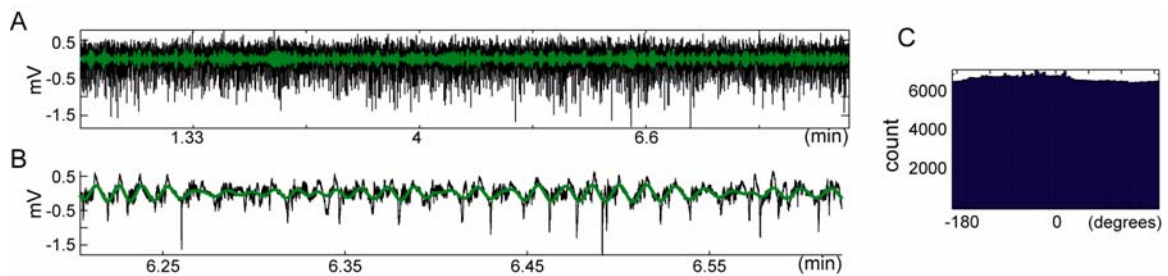
Figure 2.8. **Obtaining the phase of the slow oscillation.** A,B. LFP traces from one neocortical recording site. *Black*, raw signal (<1250 Hz). *Green*, signal band-pass filtered around the peak frequency. B. Zoomed in epoch from (*A*). C. Phase distribution of the intrinsic slow oscillation. Note that each phase bin is almost equally represented.

After establishing that the intrinsic signal had no bias in phase distribution (i.e., all phases were equally represented in the signal; Fig. 2.8C), the instantaneous phase of each spike was derived. The significance of the phase-modulation was evaluated using Rayleigh circular statistics, since the unimodal

phase-modulation by the intrinsic slow oscillation could safely be assumed from prior experimental evidence (Steriade et al., 1993c). The Rayleigh test is a circular test that checks for a unimodal deviation from uniformity in a circular data set (Fisher, 1993). Using the Rayleigh test, the mean preferred phase and its significance for each unit could be calculated.

2.5.3. Modulation of firing rates by TES

For the display of cycle-by-cycle unit firing, peri-event time histograms of spike times around the first and last troughs of the reference TES signal were constructed. For the evaluation of TES-induced effects on firing rate, mean spike counts for each cycle (one period: peak to peak sine wave) were normalized by the peak firing rate of each unit (single or multiunit) during the entire pre-stimulation-post trial sessions. Units that fired < 1Hz for the duration of pre and post stimulation sessions were excluded from the figure and analysis. Only, the stimulation sessions that were repeated > 5 times were used.

2.5.4. Subthreshold entrainment by TES

Intracellular potential values were computed for each instantaneous phase of the stimulation signal. The relationship between the filtered intracellular potential (V_i) and the TES-phase was assessed using a joint probability density function. This measure allowed the assessment of the correlation between TES-effects and V_i at various phases (Isomura et al., 2006). The joint probability density plot (Fig. 2.9Ba) presents the probability (c-axis) of the subthreshold potential of the

neuron to be at a certain value (y-axis) for a given stimulation phase (x-axis) in a

3-D histogram. The same analysis was performed to investigate the correlation

between V_i and the intrinsic slow oscillation.

2.5.5. Removal of the volume conducted TES-artifact from intracellular potential

For one intracellularly recorded cell, V_i was corrected for the added effect of

the induced field (Fig. 2.9).
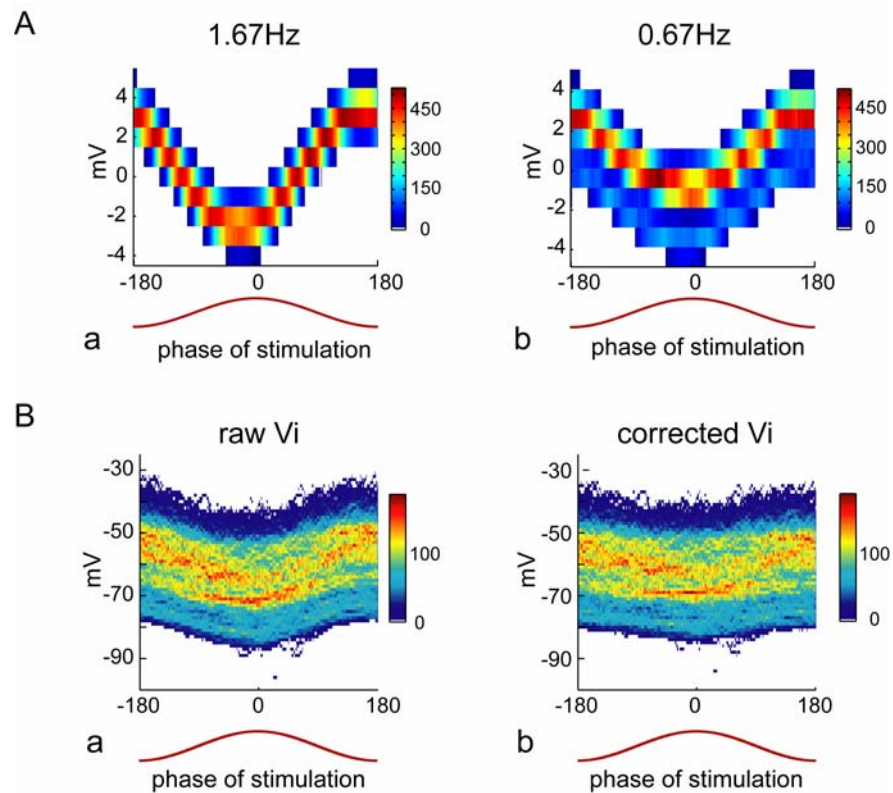
Figure 2.9. **Removal of the volume conducted TES-artifact from V_i.** A. Joint probability density counts of the volume conducted TES (1.2 V) applied at 1.67 Hz (*Aa*) and 0.67 Hz (*Ab*). Recordings were performed using the intracellular pipette after losing the cell. B. Joint probability density counts of the V_i with respect to the TES-phase before (*Ba*) and after (*Bb*) correcting for the volume conducted current. *Red line*, TES-phase. *Warm colors*, high numbers of occurrence. *White color*, 0 occurrence.

TES was repeated after the pipette was withdrawn from the neuron and the extracellular potential was recorded for 1.2 V (peak-to-peak) stimulation applied at 2 different frequencies (Fig. 2.9Aa,b). For each phase bin, the average extracellular polarization was calculated, and subtracted from V_i to obtain a field-corrected joint density (Fig. 2.9Bb).

2.5.6. Removal of the volume conducted TES-artifact from LFP

For LFP display and analysis, the volume-conducted TES-artifact was removed as follows. The TES-related component of the LFP was estimated using the least-square fit between the TES-signal and the LFP. Both the time delay parameter and the scaling factor of the fit were adjusted dynamically in 10 second windows, sliding in 7-second steps. By subtracting the best-fit component from the LFP, a continuous artifact-free signal was constructed (Fig. 2.10).

Although this method worked reliably for the low-to-medium intensity stimulations; it is difficult to claim that the resultant signal was completely artifact-free. Hence, the investigation of stimulation-induced effects on LFP was excluded from current analysis. The only exception is the spectral power presented in Chapter 4 to display EEG correlates of different behavioral states of the animal. This was used only for display purposes, and the signal was in complete agreement with the activity state of the animal, supporting that the cleaning algorithm did not introduce any artificial patterns.
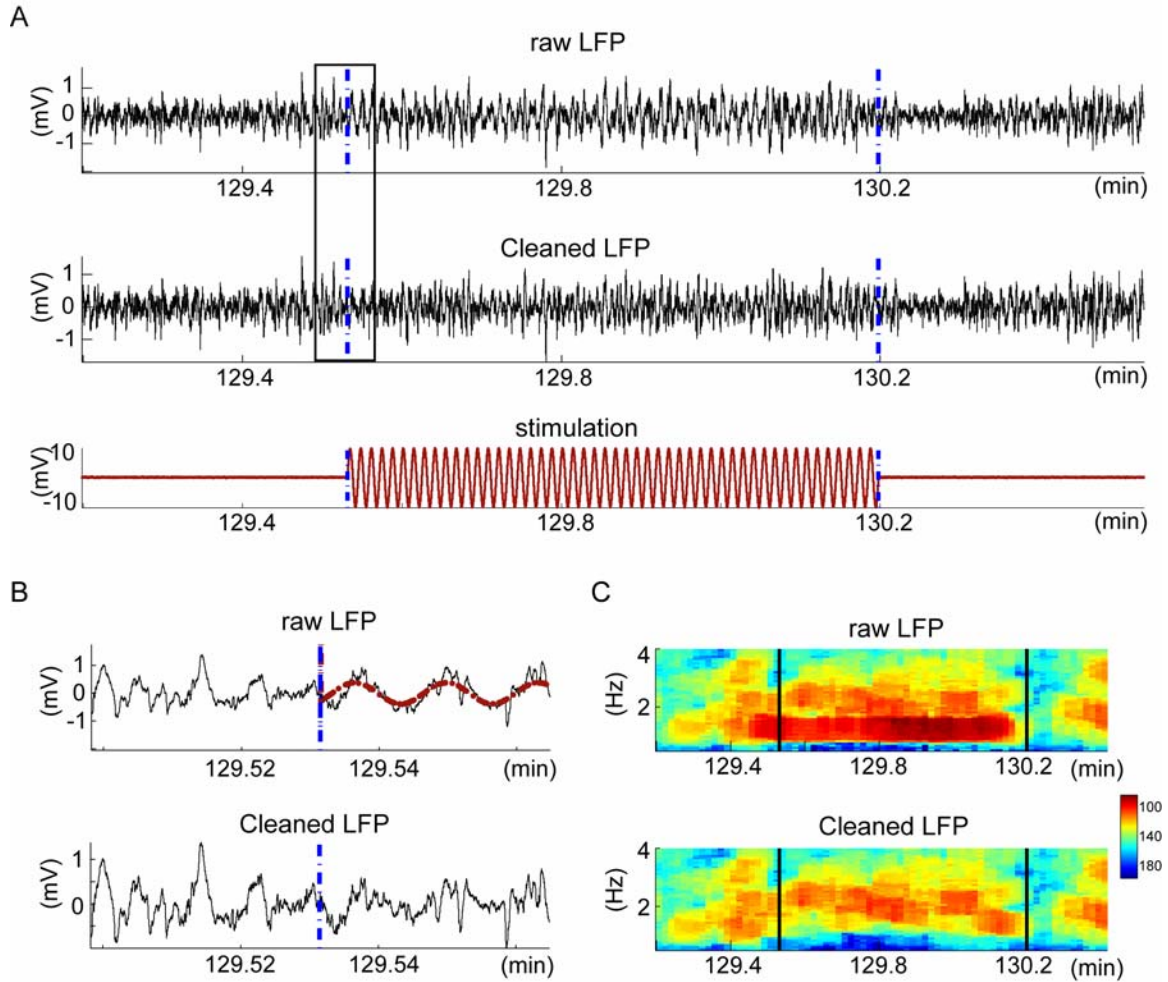
Figure 2.10. **Removal of the volume conducted TES-artifact from LFP.** A. LFP (<1250 Hz) before, during and after TES. Top, raw LFP as recorded. Note the volume-conducted sinusoid pattern (added stimulation artifact). Middle, LFP after removing the additive field artifact (Cleaned LFP). Bottom, TES. B. Zoomed-in segment from (*A*). Top, raw LFP (*black*) with the volume-conducted signal (*red*). Bottom, after removal of the artifact from raw LFP. C. Time-resolved spectrograms of LFP before and after removal of the stimulation artifact. Same episode as in (*A*).

2.5.7. Spectral analysis of LFP

Spectrograms of the LFP trace were computed using sliding windows of 4 second lengths with 1 second overlap. For stimulation periods, the corrected LFP signal was used.

Chapter 3: Effects of electric field stimulation on neuronal activity in vivo

3.1. Summary

Low intensity electric fields have been suggested to affect cellular physiology in various in vitro studies. However, how such electric fields affect neural activity in the intact brain has not been shown. Motivated by this intriguing question, I investigated whether neocortical activity, at the single neuron level, can be entrained by a slowly oscillating (0.7-1.7 Hz) electric field stimulation.

In the absence of established work combining in vivo recording with electric field stimulation, the foremost requirement was to develop an effective stimulation technique. Using extracranially or epidurally placed stimulating electrodes, I could induce weak electric fields (~1 mV/mm) in anesthetized animals. The induced-field modulated unit activity in wide-spread neocortical regions in an intensity-dependent manner. The effects were variable across units; not all units were entrained and the phase preference of units was not necessarily the same. As the field intensity increased, the entrainment became more robust and similar across neurons. The field-induced entrainment coexisted with the network induced, UP-DOWN states related membrane polarizations. In short, our findings demonstrated that the activity of neocortical neurons in anesthetized animal could be biased by slowly oscillating electric fields.

3.2. Background and significance

In vitro studies have demonstrated that electric fields affect unit activity by modulating the firing rate (Bindman et al., 1964b), the timing of action potentials (Francis et al., 2003; Radman et al., 2007), and/or the amplitude of evoked potentials (Creutzfeldt et al., 1962; Ranck, 1975; Jefferys, 1981). It has also been shown that the extent of the induced effects depends on the morphological and biophysical properties of the neurons (Chan and Nicholson, 1986; Chan et al., 1988; Radman et al., 2009) and on the properties of the extracellular space (Jefferys, 1995; Francis et al., 2003). At the other end of the spectrum, studies in humans have demonstrated behavioral effects brought about by transcranial electrical stimulation (Marshall et al., 2006; Kirov et al., 2009). To bridge these different levels of inquiry, it was critical to understand how applied electric fields affect neuronal activity in the intact brain.

The use of a combination of urethane and ketamine-xylazine anesthesia creates a brain state that fluctuates between periods of neocortical desynchronization and prolonged periods of robust neocortical synchrony in the frequency range of 0.7-2 Hz (Steriade et al., 1993b; 1993c; Contreras et al., 1996; Volgushev et al., 2006). Therefore, this preparation provided a network state, in which the endogenous oscillation pattern could be matched with slowly oscillating field stimulation.

3.3. Methods

Surgery and recordings were performed in urethane and ketamine-xylazine anesthetized animals (n=11) as described in Chapter 2 (Fig 2.1Aa-b). Slowly oscillating electric field stimulation (07-1.7 Hz) was applied in multiple configurations as shown in Figure 2.2Aa-d. In most of the experiments (n=9 animals), stimulation was applied through 2 stimulating electrodes (2-pole configuration) receiving alternating polarity stimulation (Fig. 2.1Aa-c). This configuration created anti-phase electric fields in two hemispheres. In two rats, 3-pole stimulation was used (Fig. 2.1Ad). All other procedures were performed as described in Chapter 2.

3.4. Results

Results presented in this section were obtained from 11 animals across 69 stimulation sessions. Spiking activity was studied in 215 units (n=183 in mPFC; n=29 in somatosensory cortex; n=3 in hippocampus). Intracellular recordings were performed in three layer 5 neurons in the somatosensory cortex (n=2 experiments with simultaneous intracellular and extracellular recordings; n=1 experiment with intracellular recording only).

In a subset of experiments (n=4 in mPFC; n=1 in somatosensory cortex), 23 of 113 extracellularly recorded units could be classified as putative excitatory (n=17) or inhibitory cells (n=6) on the basis of their monosynaptic connections (see Methods in Chapter 2, Fig. 2.6).

3.4.1. Influence of background activity on unit firing

As expected, the intrinsic slow oscillation exerted a powerful effect on both the membrane potential and the discharge probability of most neurons (Steriade et al., 1993c; Isomura et al., 2006). UP and DOWN states were visible from the raw LFP data. Downward (negative) deflections of the LFP traces, *troughs*, were in phase across different recording sites and coincided with the depolarized states of the intracellularly recorded cells (Fig. 3.1B).
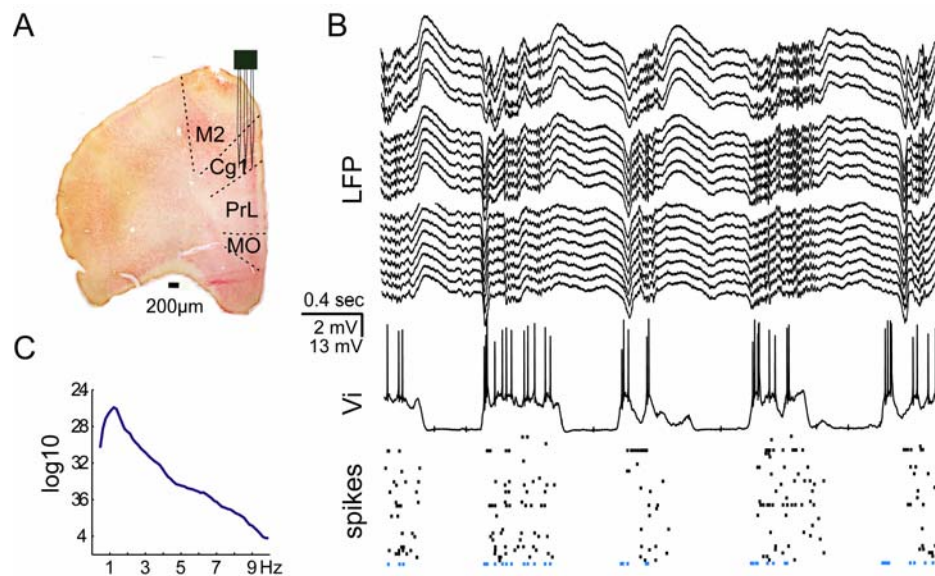
Figure 3.1. **Spontaneous slow oscillation was the dominant background activity.** A. Histological section showing the placement of 3 shanks of a 4-shank silicon probe in mPFC. B. Background activity. Top, multiple-site recording of unit and LFP from mPFC (activity from 3 shanks is shown; faulty sites are excluded). Middle, simultaneous intracellular recording from a layer 5 pyramidal cell in the somatosensory cortex. Bottom, spikes of extracellularly recorded putative single neurons. *Cyan*, spikes of intracellularly recorded cell. C. Power spectrum density from one of the neocortical recording sites. Note the peak frequency at 1.22 Hz.

The dominant power of LFP during stimulation free periods was in the slow oscillation frequency band (1 - 1.5 Hz range across animals). Power spectrum

density from an example recording is shown in Figure 3.1C. The clear peak in the

spectrogram shows the highest power at 1.22 Hz.

The relationship between spikes and the intrinsic slow oscillation was

examined in a subset of experiments (n=5 experiments; n=64 units in mPFC;

n=27 units in somatosensory cortex; n=1 unit in hippocampus). The distribution

of the spike phase histograms revealed a similar phase preference across all

neocortical units, indicating a global increase in firing during UP states and a

global silence during DOWN states (Fig. 3.2).
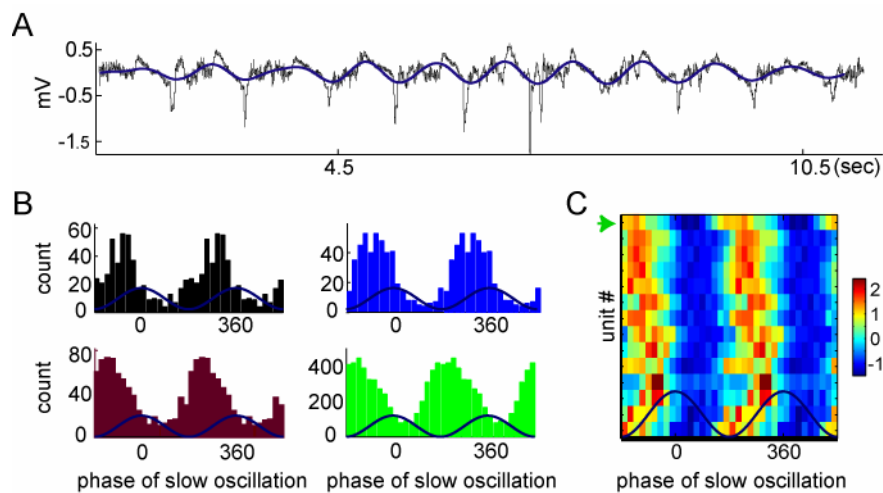
Figure 3.2. **Unit activity was entrained by the intrinsic slow oscillation**. A. LFP trace, showing slow oscillation. *Black*, raw LFP (<1250 Hz). *Blue*, band pass filtered LFP (0.9-1.5 Hz). Recorded in left mPFC (AP 2.8 mm, ML 0.5 mm from bregma, 1.6 mm from the cortical surface). B,C. Synchronized network activity during slow oscillations (9-minute long epoch). Peak frequency, 1.2 Hz. B. Spike phase histograms of 4 simultaneously recorded neurons. *Black*, unidentified single unit. *Blue*, putative excitatory cell. *Dark brown*, unidentified multiunit. *Green*, intracellularly recorded pyramidal cell from Layer 5 in right somatosensory cortex (AP -3.3 mm, ML 2.0 mm from bregma). C. Summary plot showing spike phase histograms of all simultaneously recorded units (n=13 units in mPFC; n=1 in somatosensory cortex). Each row corresponds to a unit, color-coded for standardized firing rate (mean subtracted from the rate of the entire cycle and divided by the standard deviation). Hot colors indicate higher occurrence. *Green arrow head*, intracellularly recorded cell in *B*. *Black line* (at the bottom edge of the plot), separates significantly phase modulated units (P<0.01, Rayleigh test) from non-modulated ones. Note that all units were significantly modulated; the black line is below all neurons.

UP and DOWN states were also visible in the membrane potential (V_i) of the

intracellularly recorded cell from Layer 5 of the somatosensory cortex (Fig. 3.3).

The joint probability distribution of the membrane potential indicates that the

beginning of the DOWN state, slightly after 0° degree in the figure, was

associated with a higher probability of membrane hyperpolarization, and vice

versa.
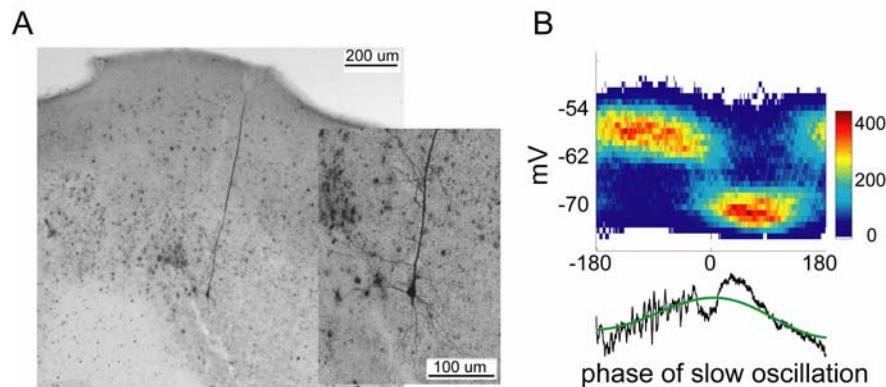
Figure 3.3. **UP and DOWN states were visible from the subthreshold membrane potential.** A. Histological reconstruction of the biocytin-labeled neuron. Right, higher magnification of the neuron in right somatosensory cortex (AP -3.3 mm, ML 2.0 mm from bregma). B. Illustration of UP-DOWN states observed at the subthreshold level. Top, joint probability counts of V_i with respect to the phase of the slow oscillation. Warm colors indicate high number of occurrence. Bottom, illustration of the slow oscillation. *Black*, representative LFP trace for one cycle of slow oscillation, showing strong gamma activity on the ascending phase (UP state). *Green*, one cycle of filtered slow oscillation. LFP was recorded from the left mPFC (AP 2.8 mm, ML 0.5 mm from bregma, 1.6 mm from the cortical surface).

3.4.2. Phase-modulation of unit activity

Figure 3.4A illustrates a short segment of LFP traces and unit activity during

1.25 Hz stimulation applied through 2 stimulating electrodes. Visual observation

suggests the coexistence of both network-induced slow oscillation and the

applied field.
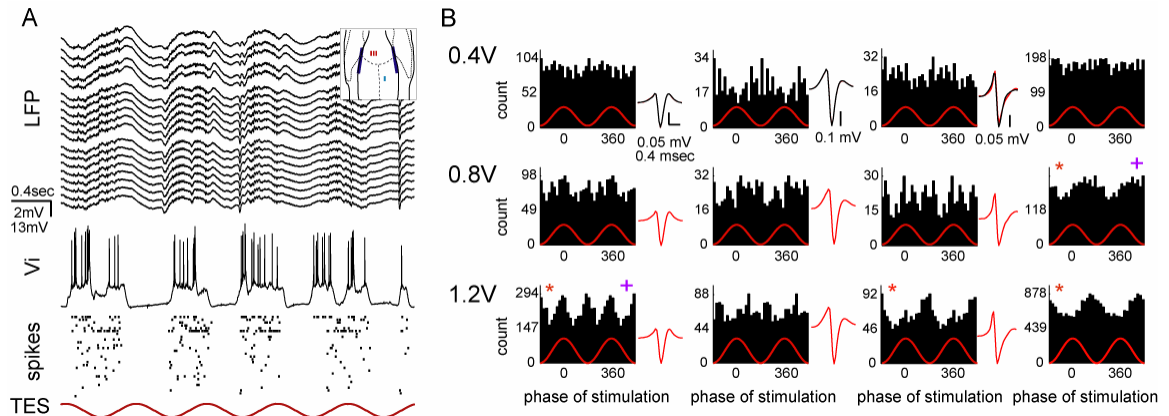
Figure 3.4. **Entrainment of suprathreshold neuronal activity by applied fields.** A. Top, multiple-site recording of unit and LFP with a 4-shank silicon probe from left mPFC (AP 2.8 mm, ML 0.5 mm from bregma, 1.6 mm from the cortical surface). The activity from 3 shanks is shown; faulty sites are excluded. Inset, locations of the stimulating and recording electrodes. *Cyan,* intracellular electrode. *Red,* shanks of the silicon probe. Middle, simultaneous intracellular recording from a layer 5 pyramidal cell in the somatosensory area (same cell as in *Fig. 3.3*). Bottom, spikes of the clustered units. Red sinusoid line, applied field at 1.25 Hz. B. Four simultaneously recorded cells (columns) during stimulation at 3 different intensities (rows). Averages of >300 stimulation cycles. Average filtered unit waveforms, recorded from the probe site with the largest amplitude unit, are shown for each stimulation session separately (red). Waveforms during stimulation-free epochs are shown in the top row (black). Note that the two waveforms (stimulation-free and the smallest intensity stimulation) overlap almost completely. Unit at right is the intracellularly recorded neuron. *Purple plus,* bimodal phase preference. *Red star*, significant phase-modulation (P < 0.01, Kuiper's test).

Stimulation-induced artifacts could have contaminated the spike detection leading to a Type 2 error, and, consequently, a false rejection of the null hypothesis. Indeed such stimulation-artifacts with a high frequency component were present in some of our recordings. A noise-elimination process, based on spike amplitude and signal-to-noise ratio, was used to eliminate the contamination of results by such artifacts. In addition to noise elimination, spike-quality was further assured by comparing the average (and randomly selected) spike waveforms during stimulation and no-stimulation epochs. Overall, waveforms of 218 units (n=190 single units and n=28 multiunits) were uniform

during both spontaneous activity and stimulation epochs (e.g., Fig. 3.4B). All analysis was performed on these units.

A few units displayed bimodal phase preference (see the purple plus in Fig. 3.4B), discrediting the validity of significance tests on the basis of single phase preference. Therefore, the effect of stimulation on unit activity was investigated using an omnibus test, Kuiper's test against uniformity (Fisher, 1993) at 0.01 significance level.

In all acute experiments (n=3, epidural flex cable electrodes; n=5, screw electrodes; n=3, wire electrodes; Figure 2.2Aa-d), at least a few of the clustered units were entrained by the stimulation (0.7-1.7 Hz). The fraction of entrained neurons depended on the stimulation intensity. Figure 3.4B illustrates that against the strong intrinsic slow oscillation, weak stimulation (0.4 V peak to peak) did not have a profound effect on the neuronal population (only 6% of the units (n=16) were entrained). However, at higher intensities (0.8, 1.2 V), a larger fraction of the units (15% and 69%; n=13 and n=26 units, respectively) was significantly ($P<0.01$) phase-locked to the forced field.

i. Intensity dependence of phase-modulation

It should be noted that low to medium intensity stimulation elicited variable entrainment profiles (Fig. 3.5). The level of phase-modulation and the preferred phases varied across simultaneously recorded neurons. Moreover, some neurons displayed different entrainment profiles across different intensity stimulations (e.g., Unit #24, Fig. 3.5).
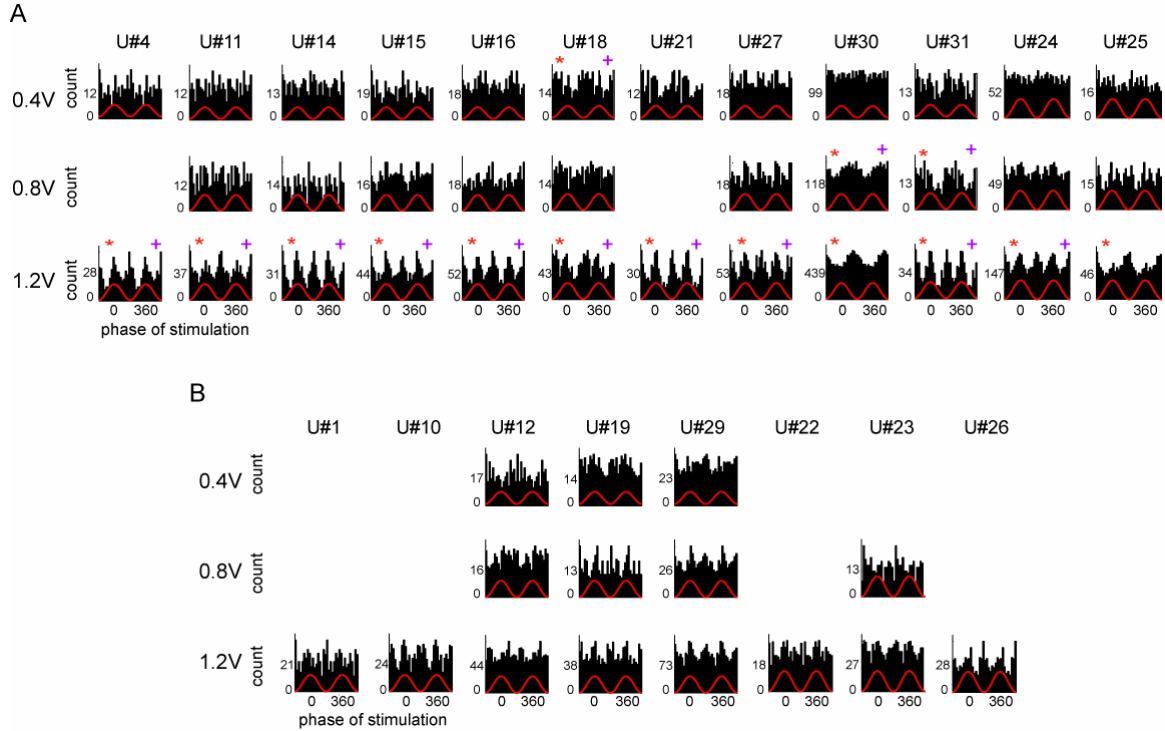
Figure 3.5. **Variable unit entrainment**. Each histogram in A and B represents the activity of one unit (single or multiunit) recorded simultaneously at 3 stimulus intensities (weak 0.4 V, medium 0.8 V, and strong 1.2 V). Same experiment as in (*Fig. 3.4*). Empty sites correspond to units excluded due to insufficient number of spikes (<250) for the duration of that stimulation session. A. Units, significantly modulated (P<0.01, Kuiper's test) by at least one of the stimulation protocols. *Purple plus,* bimodal phase preference. *Red star,* significant phase-modulation (P<0.01, Kuiper's test). B. Non-modulated neurons regardless of the stimulation intensity.

It is critical to note that not all neurons were entrained by the weak intensity stimulation (Fig. 3.5B). Although the higher intensity stimulations drove many more cells, even with the highest intensity used in these experiments, the entrainment was confined to a subset of units (Fig. 3.6A).

Overall, the strength of the entrainment and the number of modulated units increased as the stimulation intensity increased (Fig 3.6A). The mean percentage of significantly entrained units across experiments increased from 3% for low intensity stimulation (<0.3 V, n=8 experiments) to 33% for medium intensity

stimulation (≥1.2 and <2 V, n=8 experiments; Fig 3.6B). However, comparison of

mean percentage of significantly entrained units across two groups did not reveal

a significant difference (Rank Sum test across two groups; Group #1: <1 V

stimulation, n=5 experiments, n=62 units; Group #2: >1 V stimulation, n=6

experiments, m=103 units).
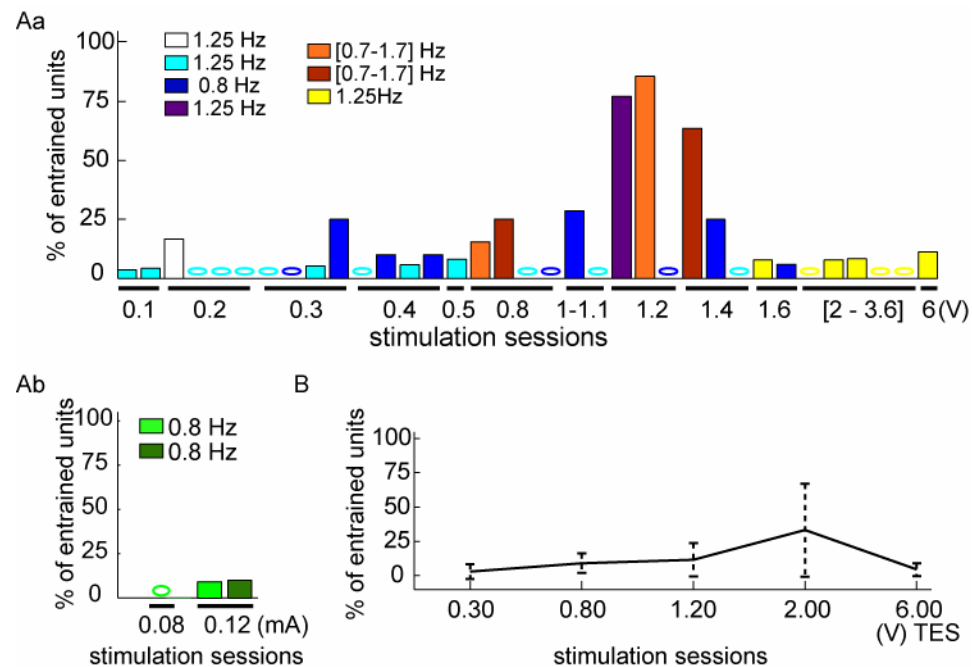
Figure 3.6. **Stimulation-intensity dependent unit modulation**. A. Percentage of significantly modulated units (P<0.01, Kuiper's test). Aa, Constant voltage stimulation. Ab, Constant current stimulation. Stimulation sessions were categorized into intensity groups (x-axis). Colors indicate different animals. *White, cyan, blue, purple*, experiments with 2-pole stimulation configuration (screws as stimulating electrodes; Chapter 2, Fig. 2.2Ab). *Yellow, orange, red,* experiments with 2-pole stimulation configuration (wires as stimulating electrodes; Fig 2.2Aa). *Light* and *dark green,* experiments with 3-pole stimulation configuration (epidural grids and a silver wire as stimulating electrodes; Fig. 2.2Ad). Frequency of each protocol is indicated. Only sessions during which the activity from ≥ 5 units was recorded are shown. B. Statistics of unit entrainment across animals. Stimulation sessions were divided into 5 categories based on intensity. The upper boundaries of the categories are shown in x-axis. The lower boundary of 0.3 V stimulation was 0.1 V. The mean ± 1 standard deviation across experiments. Note i) the positive relationship between stimulation intensity and the level of unit entrainment, 2) the variability across experiments.

It should be noted that the main goal of these acute experiments was to identify the most optimal electrode configuration for affecting neurons in large areas of the neocortex. Therefore, the experimental conditions varied across animals. Thus, the most accurate comparison regarding the effects of stimulus intensity can be evaluated only within the same experiment (color coded bars in Fig. 3.6A).

ii. Phase-modulation of subthreshold activity

The spontaneous, network-induced slow oscillation was coupled with a strong bimodality of V_i of the intracellularly recorded neurons (Fig. 3.3B; Steriade et al., 1993b; UP and DOWN states; Sanchez-Vives and McCormick, 2000). During stimulation, the slow oscillation-related V_i bimodality was preserved (Fig. 3.7).
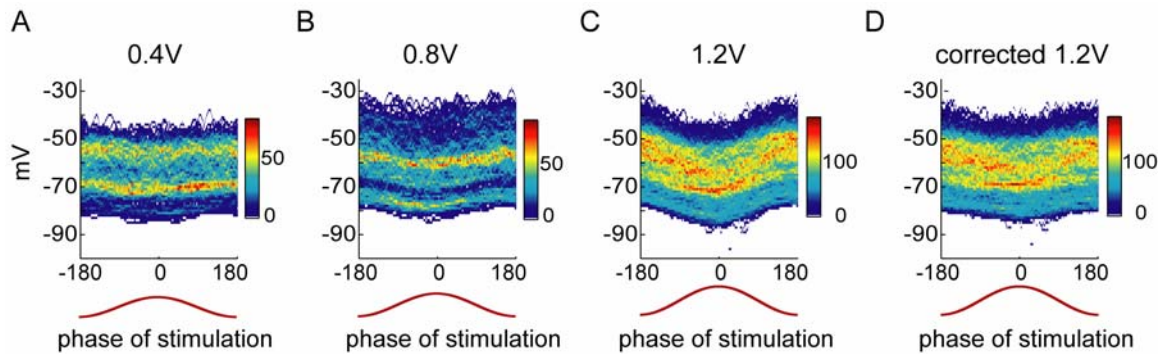
Figure 3.7. **Entrainment of subthreshold neuronal activity by applied fields.** Illustration of intrinsic network- and extrinsic field-control of neural activity. The same cell as in Figure 3.3A and the right column in Figure 3.4B. A,B,C,D. Joint probability density counts of V_i with respect to the phase of the stimulation signal are shown for weak (*A*), moderate (*B*) and strong (*C*) intensity stimulation sessions (0.4 V, 0.8 V, and 1.2 V respectively). D. V_i-corrected by subtracting the volume-conducted current, recorded extracellularly after withdrawing the pipette from the neuron. *Red line*, phase of stimulation. *Warm colors*, high occurrence. Note the co-existence of network-induced V_i bimodality (hot color bands at two Vi levels) and increasing phase-locking of V_i to the applied field as field strength increases. Note also the increasing differences between DOWN state probabilities for $0°$ and $180°$ of stimulation signal from (*A*) to (*C*).

However, the probability of the UP and DOWN states of the membrane was biased by the field stimulation, indicating a combined effect of the network-activated and stimulation-induced forces (note differences in DOWN state probability between 0° and 180° of stimulation in Fig. 3.7). The effect was dependent on the stimulation intensity. Similar observations were made in two other intracellularly recorded cells (Fig. 3.8; note the different phase preference in Fig. 3.8A-C).
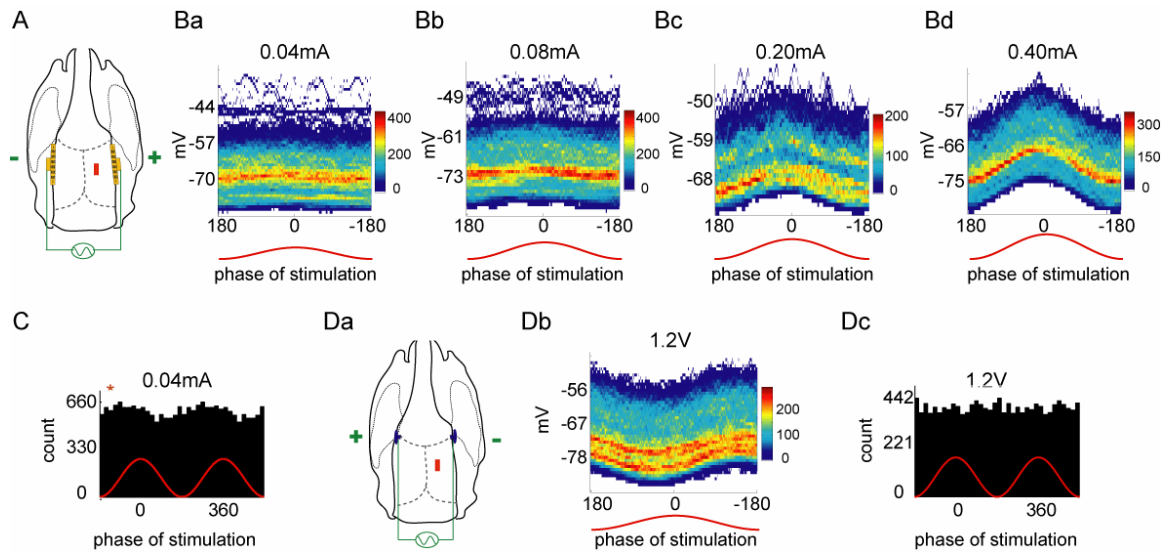
Figure 3.8. **Entrainment of sub- and suprathreshold neuronal activity by applied fields**. A,B. Identical display as in (Figure 3.7) for another intracellularly recorded layer 5 neuron in the somatosensory cortex (~980 μm). Aa. Stimulation configuration. Note that stimulation polarity was reversed compared to (*D*) and (Figure 3.7). *Red rectangle*, recording site. Ba-d. Joint probability density of the V_i with respect to the phase of the stimulation signal for different intensities of stimulation (0.04 mA, 0.08 mA, 0.20 mA and 0.40 mA peak-to-peak). Constant current stimulation. *Red line*, phase of stimulation. C. Histogram shows phase-modulation of action potentials by 0.04 mA stimulation. *Red star,* significant phase-modulation (P<0.01, Kuiper's test). D. Same display for another intracellulary recorded neuron from the somatosensory area. Da. Stimulation configuration. *Red rectangle*, recording site. Db. Joint probability density of the V_i with respect to the phase of the stimulation signal. *Red line,* phase of stimulation. Dc. Histogram shows the lack of phase-modulation of action potentials by the stimulation.

In one experiment, stimulation was repeated after the pipette was withdrawn from the cell, and the extracellular field in the immediate vicinity of the neuron was recorded to estimate the stimulation-induced true intracellular potential. The phase-modulation of V_i signal was corrected by subtracting the mean of the stimulation-induced extracellular potential from Vi at each phase bin (20°). Stimulation intensities that effectively phase biased unit spikes induced 2-3 mV of intracellular polarization (Fig. 3.7D).

iii. Phase-modulation across cell types

Observation of spike-phase histograms demonstrated that field-induced effects (presence and absence of phase-modulation) did not differ among putative excitatory and inhibitory neurons (Fig. 3.9).
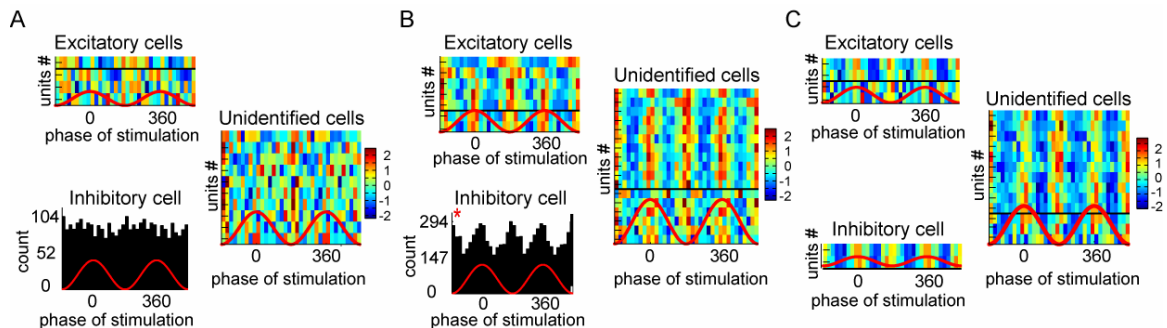
Figure 3.9. **Similar entrainment of excitatory and inhibitory neurons by applied fields.** A,B. Phase-modulation by weak (0.4 V, n=15 units) and strong (1.2 V, n=25 units) intensity stimulations (1.25 Hz) recorded in the same animal. 2-pole configuration (Chapter 2, Fig 2.2Aa). *Black,* spike-phase histogram of the putative inhibitory cell. In summary plots, each row corresponds to a unit color-coded for standardized firing rate. Units are ordered depending on their significance of phase-modulation. The unit with the smallest P-value is at the top. *Black lines,* separate significantly modulated units (P<0.01, Kuiper's test). Same color scale applies for all summary plots within subfigures. A. n=1 inhibitory, n=4 excitatory, and n=10 unidentified cells. B. n=1 inhibitory, n=7 excitatory, and n=17 unidentified cells. C. Phase-modulation from another experiment. n=2 inhibitory, n=4 excitatory, and n=13 unidentified cells. Stimulation, 1.2 V, 1.25 Hz, 2-pole configuration (Fig 2.2Ab). Note the similarity of phase-modulation across cell types.

However, due to insufficient number of data points for identified cell populations, this claim could not be supported by statistical assessment.

iv. Phase-modulation across neocortical regions

Region-specificity of field-entrainment was investigated by comparing unit responses recorded in prefrontal and somatosensory cortices (n=2 animals with simultaneous recording in mPFC and somatosensory cortex; n=1 animal with simultaneous recording in somatosensory cortex and the CA1 region of the hippocampus; n=3 animals with recording in somatosensory cortex, only; and n=6 animals with recording in mPFC, only).
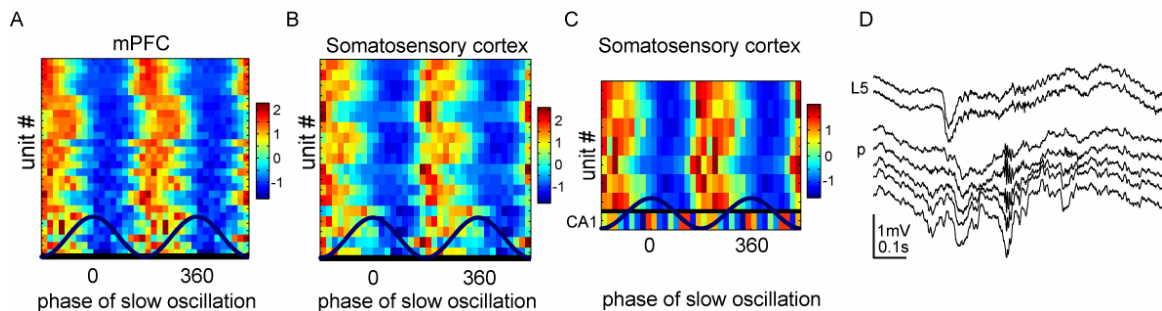
Figure 3.10. **Slow oscillation strongly entrained neocortical neurons.** A,B,C. Summary plots from 3 experiments. A. Prefrontal recording, 33 minutes long (AP 2.8 mm, ML 0.5 mm from bregma, 2.1 mm from the cortical surface). 1.4 Hz, peak frequency. All units (n=27) were significantly entrained by intrinsic slow oscillation. B. Recording in somatosensory cortex, 10 minutes long (AP -3.5 mm, ML 2.5 mm from bregma, 2.1 mm from the cortical surface). 1.5 Hz, peak frequency. All units (n=19) were significantly entrained by intrinsic slow oscillation. C. Recording from the deep layers of the somatosensory cortex and CA1 subregion of the hippocampus, 10 minutes long (AP -3.5 mm, ML 2.5 mm from bregma, 2.4 mm from the dura). 1.2 Hz, peak frequency. All somatosensory units (n=7) were modulated by intrinsic slow oscillation whereas hippocampal (CA1) multiunit was not affected. D. Sharp wave-ripple event in the hippocampus. Upper two traces, neocortical LFP (<1250 Hz), recorded from the top two electrode sites of a 32 site linear silicon probe with 50 μm spacing. Bottom five traces, hippocampal LFP (<1250 Hz) recorded from the channels at the tip of the same silicon probe. The second neocortical trace and the first hippocampal trace were approximately 1.1 mm apart. *L5*, somatosensory cortex Layer 5. *p*, CA1 pyramidal cell layer. Note fast hippocampal ripple in traces 3 to 6 (from top).

In line with previous studies (Steriade et al., 1993b; 1993c; McCormick and Bal, 1997; Steriade et al., 2001), during stimulation-free periods the major activity in the somatosensory neocortex was the slow oscillation. Spikes of all somatosensory cortical cells were phase-locked to the UP states (%100, n=32 units, Fig. 3.10B,C; Fig. 3.2; Fig. 3.3B). In contrast, only a small percentage of hippocampal units was entrained by neocortical slow oscillations, as reported earlier (Isomura et al., 2006). Instead, hippocampal units were strongly active during sharp-wave associated ripples (Fig. 3.10), which occurred largely independent of the neocortical slow oscillations (Sirota et al., 2003; Isomura et al., 2006).
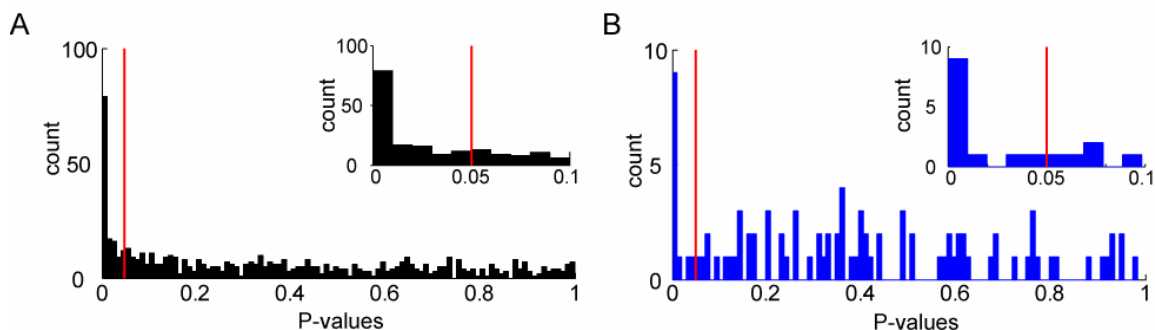
Figure 3.11. **Unit entrainment across neocortical regions was similar.** Region-specific distribution of P-values across experiments. A,B. Distribution of phase-modulation statistics (P-values, Kuiper's test) of units recorded in mPFC (*A)* and in somatosensory cortex (*B*). *Red line*, 0.05 significance level. Right insets, zoomed-in display for the distribution of P-values <0.1. Note that a given unit may appear more than once for different intensity stimulation sessions. A. Units recorded in left mPFC (n=59 experiments, n=183 units, AP [2.8 - 3.00] mm, ML 0.5 mm from bregma, 1.6 to 3.1 mm from the cortical surface). B. Units recorded in somatosensory cortex (n=32 units, AP -[3.5 - 2.8] mm, ML [1- 2.5] mm from bregma, [1- 2.8] mm from the cortical surface).

Neurons in the somatosensory cortex were phase-modulated by applied fields in an intensity dependent manner (20% - 52% of entrainment across n=35 units

in total; Fig. 3.11). Not all units were entrained; nor did all entrained units have the same phase preference. Also, a few units had different phase preferences across different intensity stimulations. Despite these differences, the overall phase entrainment profiles for the majority of neurons in mPFC and somatosensory cortex were similar.

3.4.3. Effects of stimulation-features on unit entrainment

Frequency dependency of field-effects has been demonstrated before (Deans et al., 2007). In our experiments, the frequencies applied, 0.7-1.7 Hz, were within the slow oscillation frequency range and they elicited a comparable level of phase-modulation 69% vs. 70% of unit modulation for 1.2 V stimulation applied at 1.25 Hz and 1.67 Hz , with n=26, n=10 units; respectively). Figure 3.12A,B,C demonstrate that many of the cells modulated by one frequency were likely to be modulated by other slow oscillation frequencies (percent of modulation: 57%, 33%, 43%; n=7, n=6, n=8 units, respectively). Despite the overall similarity in the fraction of phase-modulated neurons, individual cells occasionally had particular frequency preferences (Fig. 3.12D,E,F).

As expected from previous work, the modulation of unit activity depended highly on the geometry of the induced field. Reversing the polarity of the stimulation did change the preferred phases for unit modulation (Fig 3.7 and Fig. 3.8D versus Fig 3.8A,B,C).

All types of stimulation electrodes, e.g., silver wires, stainless steel screws or epidural grids, were effective in eliciting unit entrainment (Fig 3.6 vs. Fig 3.7).

Nevertheless, electric fields introduced by different types of electrodes had different spatial properties since the physical size and the surface area of the electrodes were different. However, a systematic calculation of how such properties affected unit modulation could not be done due to other uncontrolled variables in the experiments.
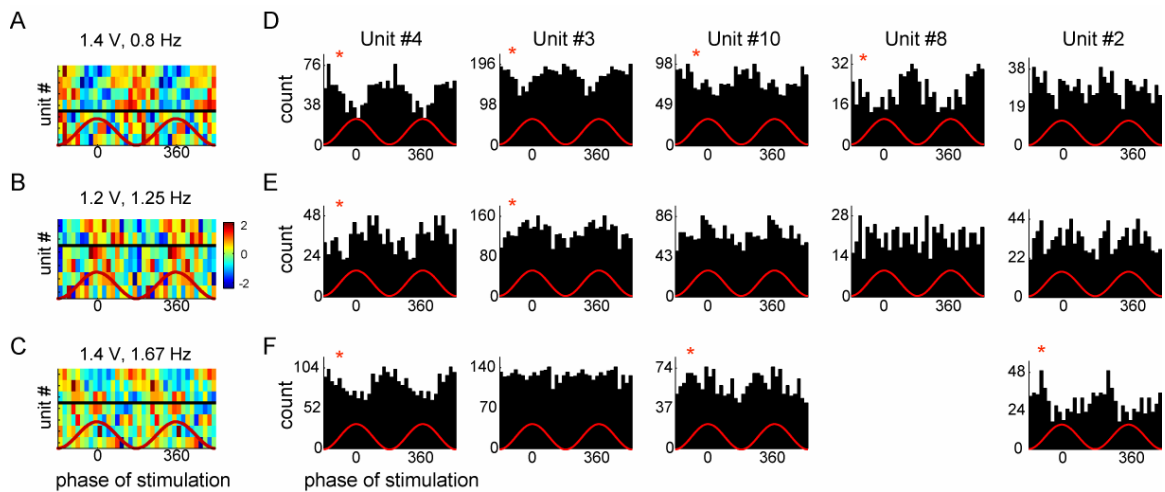
Figure 3.12. **Effects of stimulation-frequency on phase-modulation.** A,B,C. Summary plots showing spike phase histograms of simultaneously recorded units for the similar intensity (1.4 V for A and C; and 1.2 V for B) different frequency stimulations, applied through 2 stimulating poles (Chapter 2, Fig. 2.2Aa). Each row corresponds to a unit, color-coded for standardized firing rate (mean subtracted from instantaneous rate and divided by the standard deviation). Units are ordered depending on their significance of phase-modulation. The unit with the smallest P-value is at the top. *Black lines* separate significantly modulated units (P<0.01, Kuiper's test against uniformity) from non-modulated ones. *Red sinusoid*, the reference stimulation signal. Units were recorded in mPFC (AP 2.8mm, ML 0.5 mm from bregma and spanning in between 2.7-2.85 mm depth). D,E,F. Spike phase histograms of 5 example units. Same recording as in (*A,B,C*). *Red star,* significant phase-modulation (P<0.01, Kuiper's test). Note the different entrainment profiles of the same cell for different frequency stimulations.

3.4.4. Bimodality of phase-modulation

A subset of the modulated neurons displayed two prominent peaks in the phase histograms (Fig 3.13; Fig. 3.4B; Fig. 3.5A). These multiple peaks indicate

that some neurons increased their firing at more than one, typically 2, phases of

the stimulation.
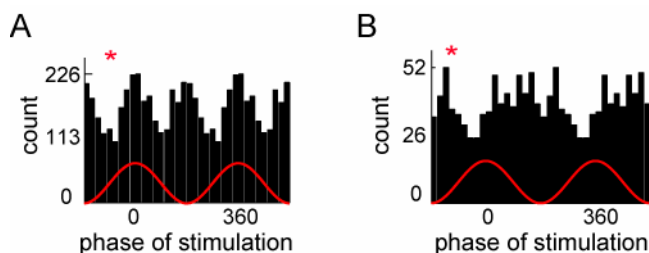
Figure 3.13. **Bimodal unit entrainment.** A,B. Representative single units with bimodal phase-modulation. Both are significantly entrained by stimulation (P<0.01, Kuiper's test). A. Prefrontal cortical unit. Stimulation, 1.2 V, 1.25 Hz. B. Somatosensory cortical unit. Stimulation, 0.1 mA, 0.8 Hz. Note the multiple bumps associated with increased firing for a given cycle (trough – to – trough) of stimulation.

The number of units with bimodal phase preference varied across

experiments (%3 - %6; Table 3.1). Despite the positive trend between the

intensity and the bimodal phase preference, the difference between weak and

strong intensity groups was not significant (p=0.08, unpaired T-test).

Stimulation intensity range (V)	# of sessions	Mean of % bimodal entrainment	Median of % bimodal entrainment	SD of % bimodal entrainment	Range of % bimodal entrainment
0.12 – 1.2	10	11.96	8.12	± 8.65	2.86 – 28.57
1.2 – 2.8	10	30.21	26.79	± 18.95	7.69 – 61.54

Table 3.1. **Summary of the significantly phase-modulated units with a bimodal (or multimodal) phase preference.** Stimulation sessions that yielded phase-modulation were divided into 2 categories based on the intensity. Lower and upper borders are given in the first column. From third to sixth columns summarize the mean percentage of significantly modulated units (P<0.01, Kuiper's test) with a non-unimodal profile across 10 stimulation sessions. All sessions were conducted with 2-pole configuration (Chapter 2, Fig. 2.2.Aa-c). Note the variability across experiments.

In these experiments, stimulating electrodes were placed bilaterally (Fig.

2.2Aa-c). The phase-opposition in the two hemispheres could have driven

neurons receiving ipsilateral and contralateral inputs at multiple phases of the stimulation. Alternatively, the double-phase entrainment can also be explained by the combination of the direct and indirect (i.e., synaptically mediated) effects on the same neuron. Multiple other mechanisms can also give rise to double-phase entrainment (see Chapter 5).

3.4.5. Field-effects on firing rate

Effects of field-stimulation on firing rate were investigated in a small subset of experiments where the same stimulation was repeated for multiple trials (>6) so that a sufficient number of spikes was collected. Average firing rate of each unit was calculated for each cycle of the stimulation and for 10 sham cycles, pre and post stimulation.

Figure 3.14 illustrates data from 91 units across 8 experiments (n=6 animals; n=88 units in mPFC, n=3 units in somatosensory cortex). Black lines show mean firing rate across all units for a given stimulation session. In some of the experiments, firing rates decreased during stimulation. In experiments with >10 units (n=4 experiments), the mean firing rates were compared across four conditions: 1) pre vs. post stimulation, 2) pre vs. first 15 cycles of stimulation (early stimulation), 3) first vs. last 15 cycles of stimulation (late stimulation), 4) post vs. late stimulation. In two experiments, the mean firing rates of neurons were significantly different between pre vs. early stimulation, and post vs. late stimulation (P<0.01, unpaired T-test, red stars in Fig 3.14). In one experiment, early and late stimulation periods were also different (P<0.01, unpaired T-test).
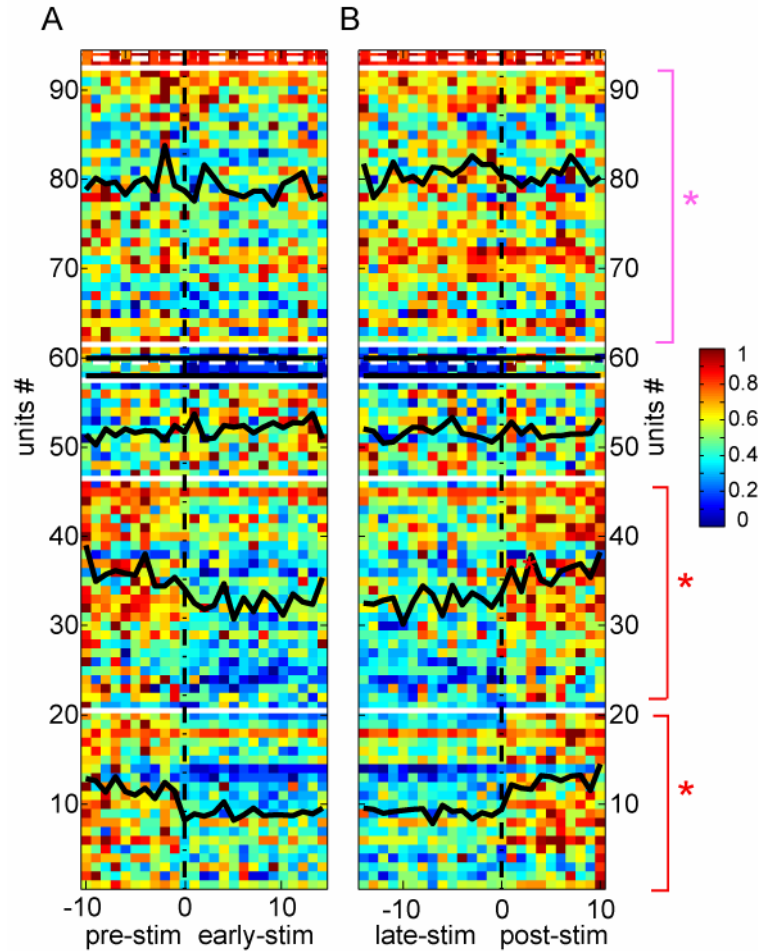
Figure 3.14. **Field-stimulation decreased the mean firing rate in a subset of experiments.** A,B. Stimulation evoked population unit activity from multiple experiments (n=8). A. Pre-stimulation (10 sham cycles) and early-stimulation (15 cycles) period. 0, the onset of the stimulation. B. Late-stimulation (15 cycles) and post-stimulation (10 sham cycles) period. 0, the offset of the stimulation. Each row is a unit, color-coded for normalized firing rate (maximum rate=1). Bins reflect the normalized rates for each cycle of the applied field (peak to peak). White lines separate recordings from different animals (n=6). White dotted lines separate different stimulation sessions recorded from the same animal. Top 2 rows are 2 different sessions from the intracellular-recording-only experiment from one animal. *Black lines*, session averages of normalized firing rates. *Red line and star,* significant difference between pre vs. early stimulation, and post vs. late stimulation (P<0.01, unpaired T-test). *Magenta line and star*, significant difference between early vs. late stimulation (P<0.01, unpaired T-test). Note that the effects on individual cells varied within and between experiments.

These results should be viewed with caution, however. The noise elimination

procedure we used for eliminating potential high frequency components of

stimulus artifacts could have systematically eliminated spikes during stimulation.

While artificially reducing spikes may not affect phase entrainment estimation of neurons, the procedure may have exerted an undetectable effect on firing rate. Further experiments would help to clarify how electric fields affect firing rates.

The time course of stimulation-induced effects was further investigated in a subset of experiments that had a significant difference (n=3 animals) in mean firing rates across pre vs. early, pre vs. post, post vs. late stimulation conditions. The evolution of the effects could not be observed at a cycle-by-cycle level (Fig. 3.15). However, the decrease in the firing rate could be observed, at least in some of the units (Unit #32 vs. Unit #2 in Fig. 3.15B).
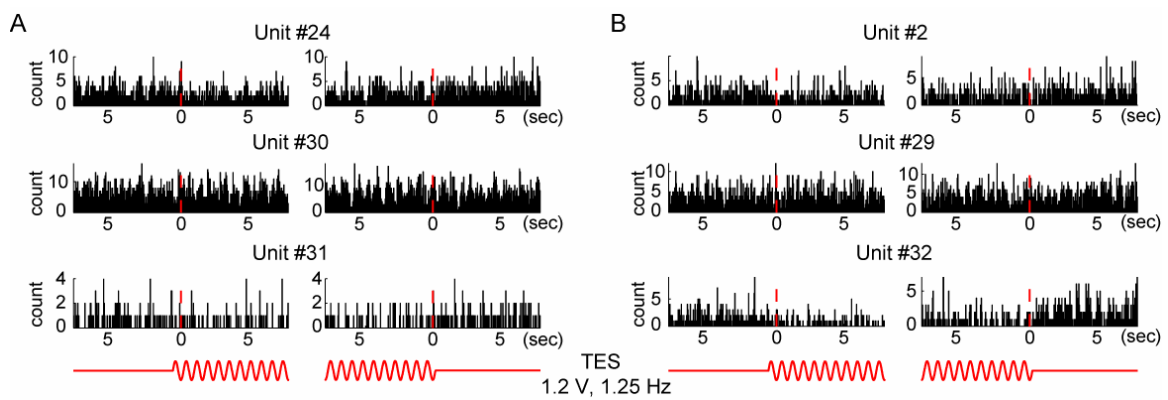
Figure 3.15**. Field-effects on firing rate were variable across units.** A,B. Spiking activity from 3 units, referenced to the onset and offset of the stimulation. Same stimulation (1.2 V, 1.25 Hz) applied in different experiments. A. 2-pole configuration (Chapter 2, Fig. 2.2Aa). From top to bottom: physiologically identified putative inhibitory cell in mPFC, morphologically identified putative excitatory cell in somatosensory cortex, and multiunit in mPFC. B. 2-pole configuration (Fig. 2.2Ab). From top to bottom: single unit in mPFC, morphologically identified putative excitatory cell in somatosensory cortex, multiunit in mPFC.

3.4.6. Stimulation-induced electric fields

The magnitude of *volume-conducted* electric fields was estimated in post-mortem recordings (n=10 experiments). Prior to sacrifice, the approximate

threshold current needed to entrain at least a few of the recorded neurons was determined. Next, brain activity was abolished by administration of a lethal dose of anesthetic.

For the example shown in Figure 3.16, the activity was recorded from the somatosensory cortex and the CA1 subregion of the hippocampus (AP 3.5 mm, ML 2.5 mm from bregma, and 2.3 mm deep from the dura; the orange location in Fig. 3.16A). The minimal stimulation intensity required to reliably entrain neurons was estimated to be 0.12 mA (peak-to-peak). The entrainment of neurons was later confirmed by statistical assessment conducted off-line.

After abolition of brain activity, the peak-to-peak amplitude of the stimulation-induced potential was consecutively measured at multiple antero-posterior locations (Fig. 3.16A,B). The amplitude of the intracortical potential varied almost 3-fold in the range of 0.4 - 1.4 mV depending on the distance from the stimulating electrodes, with the largest fields present in the axis of the shortest distance between the electrodes, i.e., the axis of the induced dipole. On the other hand, the magnitude of the recorded local field remained relatively constant across different cortical layers, indicating that the induced fields near the midline of the brain were comparable in the hippocampus and the overlying neocortex. This was probably due to the relatively large spatial homogeneity of the field obtained by using the grid electrodes that spanned 2.5 x 4 mm surface area. At the recording site where stimulation induced neuronal entrainment was observed in the living animal (Fig. 3.16C, D), the volume conducted potential was around 1.3 mV and decreased rapidly with distance in both anterior and posterior directions

(compare red dot values/positions with black and magenta values/positions in

Fig. 3.16A, B).
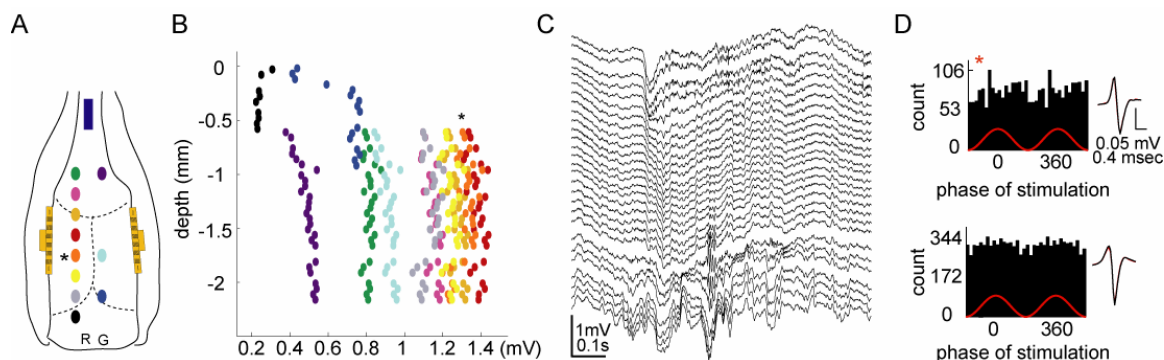
Figure 3.16. **Effective magnitude of the applied field.** A. Locations of the penetration sites for measuring the volume-conducted local potentials (0.8 Hz; 3-pole configuration). Star, the anatomical location of the recording shown in *(C,D)*. B. Locally measured voltage between each active recording site, indicated by the color code in *(A)*. *R*, the reference electrode. *G*, ground. Depth measurements were carried out with a 32-site single-shank probe, with recording sites at 50 μm from each other. The probe was moved in the antero-posterior axis after each measurement. Stimulation was at 0.8 Hz frequency, 0.12 mA peak-to-peak intensity. C. Short epoch of simultaneously recorded LFP from deep layers of the neocortex and the underlying hippocampus; orange site in *(A)*. Top recording sites correspond to layer 5. Sites at the bottom are at CA1 region of the hippocampus. Note ripple-related reversal of sharp wave in the CA1 stratum radiatum. D. Spike-phase histograms for 2 units recorded in layer 5 (top) and CA1 (bottom). *Red star*, significant modulation (P-value <0.01, Kuiper's test). Insets, averaged filtered unit waveforms. *Black*, during prestimulation epochs. *Red*, during stimulation. Note that waveforms overlap completely. Measurements in B were carried out after the rat was injected with a lethal dose of anesthetic, using the same intensity stimulation, which entrained the unit in *(D)*.

To estimate the minimum voltage gradient necessary to bias neuronal firing,

voltage measurements were also made in the medio-lateral direction, i.e., in

parallel with the field-induced current flow. As in the previous experiment, the

induced potentials were comparable at different depths (compares same color

dots in Fig. 3.17C. In this experiment, 0.8 V stimulation induced a potential

difference of ~0.4 mV between site 1 and 3. Since the distance between these

shanks was 0.4 mm, the voltage gradient in the medio-lateral plane was ~1 mV/mm. Other experiments yielded similar values.
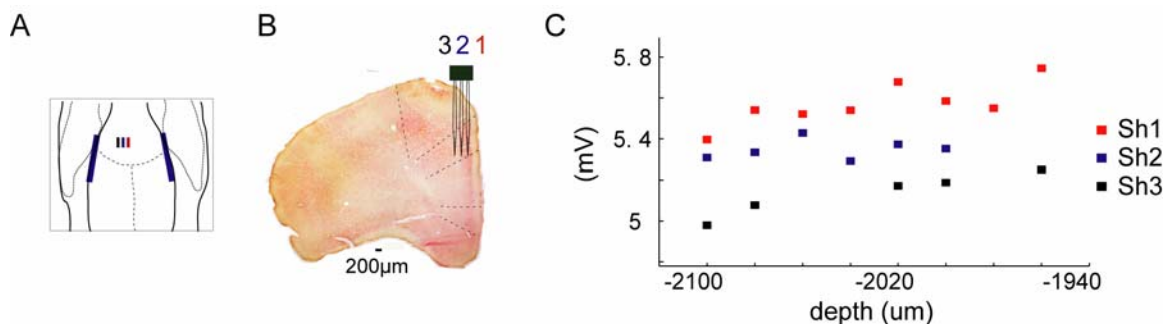
Figure 3.17. **Field-stimulation induced ~1 mV/mm electric fields in recording locations.** Estimation of the electric field generated in the extracellular space. A,B. Placement of three-shank probe parallel to the main current flow induced by stimulation electrodes. C. Postmortem voltage measurements at all probe sites. Stimulation was at 1.25 Hz, 1.2 V peak-to-peak intensity. In the same animal, 1.6 V stimulation had significantly phase-modulated 8% of units (n=13 units). Note approximately 400 µV difference between shank 1 and shank 3 (Saunders and Jefferys, 2002) at all depths. Inter-shank distance: 200 µm.

3.5. Discussion:

The main objective of these experiments was to find suitable electrode configurations and stimulation parameters, which could be used to affect cortical activity without current spread to the temporal muscles or other tissue. After extensive modifications and refinements, an effective stimulation protocol was achieved and neocortical neurons could be reliably phase-modulated regardless of the cell type and the differences in their dendritic orientation.

Urethane and ketamine-xylazine anesthesia provided a stable and robustly synchronized baseline activity in a frequency range of 1-1.5 Hz. The combined effects of these two forces, intrinsic and applied slow oscillations, were

demonstrated by the distribution of the transmembrane voltage in intracellular experiments (Fig. 3.6 and Fig. 3.7). UP and DOWN states that were induced by the intrinsic slow oscillations were still present but their onsets and offsets were biased by the phase of the stimulation signal.

Sub- and supra-threshold (spiking) entrainment was stimulation-intensity dependent. As the intensity increased, overall entrainment became more pronounced; more cells got entrained and the preferred phase(s) became more similar across neurons.

It should be noted that there was a considerable amount of variability in unit entrainment. This variability was not unexpected since even the same cell type can respond differently to the same electric field in well-controlled in vitro experiments (Chan and Nicholson, 1986). The major source of variability in our results could be attributed to the interaction between the ongoing (spontaneous) activity and the field-induced polarization, itself.

Some of the units had bimodal phase preference, i.e., their activity increased at two different phases of the stimulation. Such double-phase locking could have been introduced by the bilateral electrode configuration, leading to out-of phase activation of ipsilateral and contralateral inputs. Many other factors could have contributed to the multi-modal entrainment, some of which are discussed in Chapter 5.

Postmortem recordings demonstrated that the induced voltage gradients that were effective in entraining neurons were ~ 1 mV/mm (Fig. 3.17). Such fields are considered 'weak-to-medium' in intensity and they may or may not induce

membrane polarization sufficient to drive or to suppress spiking activity in neurons in vitro (Bindman et al., 1964b; Jefferys, 1995; Radman et al., 2007). Our results demonstrate that such weak fields were effective to entrain unit activity in vivo, likely due to the coincidence of network induced subthreshold activation and the additional polarization induced by the external field.

In experiments where stimulation was applied through bilaterally placed wire or screw electrodes (~10 mm apart depending on the size of the animal), direct-field induced polarization was not likely to be 'strong' at all recording locations. However, neurons nearby the stimulating electrodes could have been directly entrained by the stimulation and they could have transmitted these effects to their synaptic partners. Thus, unit entrainment possibly reflected the combination of both polysynaptically mediated and direct field-induced effects, at least in a subset of neurons.

In summary, the experiments presented here 1) led to the development of an efficient stimulation technique and protocol, and 2) showed that ongoing neural activity in the intact brain could be reliably entrained by applied electric fields. The next question was whether these finding could be extended into the naturally sleeping animals.

Chapter 4: Effects of transcranial electric stimulation (TES) on neuronal activity in behaving animals

4.1. Summary

Our study in anesthetized animals demonstrated that the activity of cortical neurons could be phase-biased by externally applied electric fields. Relatively-synchronous neocortical activity induced by anesthesia had provided a background activity that temporally matched with the stimulation. We followed up on the same question in a more physiological setting and asked whether electric fields have similar effects in naturally sleeping animals.

Extracellular unit activity was recorded in multiple cortical regions in 3 animals using the field-stimulation technique modified for chronic application. The results from the freely moving animals extended those from the acute experiments: intact neuronal activity could be phase-modulated by TES in an intensity-dependent manner. Neocortical and hippocampal regions were both entrained in a way suggesting that at least some of the cells were directly polarized by the induced fields. In addition, the comparison of the same-TES application during sleep and exploration revealed that the ongoing behavioral state of the animal was critical in shaping the TES-induced effects. Finally, TES-application did not induce any side-effects that were observable at the behavioral level. Overall, TES was effective in biasing the timing of neuronal activity in behaving animals.

4.2. Background and significance

In our second project, we investigated whether field-induced cortical entrainment as observed in anesthetized animals, could also be achieved in sleeping animals. We performed recordings in chronically implanted rats and monitored neocortical and hippocampal unit activity under the influence of slowly oscillating TES across different behavioral states.

For the purpose of understanding TES-induced effects, recording from behaving animals provided three major strengths. The most critical one was the ability to monitor the activity across naturally occurring different behavioral states, e.g., sleep vs. wake. Another advantage of chronic recording was the ability to collect data from multiple experiments on the same animal. The use of the same recording electrodes and stimulation parameters eliminated many of the experimental variability which may have confounded comparisons across different stimulation protocols applied in different experiments in our previous study. Finally, using TES in chronically implanted animals allowed us to closely monitor the animal and detect any potential undesirable side-effects.

Another addition to this study was the more extensive use of hippocampal recordings. Previous research had shown that neocortical slow oscillations can only weakly affect hippocampal firing patterns (Sirota et al., 2003; Battaglia et al., 2004; Sirota and Buzsaki, 2005; Isomura et al., 2006). As shown in the previous chapter, neocortical activity could be entrained by applied fields at slow oscillation frequency. Thus, it was critical to understand whether and how these TES-induced effects would be relayed to the hippocampus.

4.3. Methods

Stimulating electrodes needed modification for chronic usage. To have the closest form to *transcranial* application and to provide stability across multiple days, a 200-µm bifilar wire was spiraled to form a circular shape electrode (~3 mm in diameter) and 3 of such electrodes were placed onto the skull (see Chapter 2, Fig. 2.2Ae). The stimulation parameters, i.e., the duration, the frequency, and the repetition rate of TES trains, remained the same as before. The intensity parameter was adjusted according to the aim of the experiment.

In most sessions, the stimulation was applied in 3-pole configuration yielding in-phase activation of two hemispheres. Recordings were performed when the animal was sleeping or resting in its home-cage, except for the experiments in which TES-induced effects were compared across sleeping vs. exploration. Exploration sessions were performed in a novel environment, either an open maze or a circular track, for random food search.

For the 1st and 2nd animals, the cortical activity was ceased by administering a lethal dose of anesthetic, and the volume-conducted potential of TES was recorded postmortem. In the 2nd and 3rd animals, a small intensity current (2 µA for 10 sec) was passed through the electrodes at the end of the experiments to aid histological verification of the recording sites. Recording (Chapter 2, Fig. 2.1B), data acquisition and analysis were performed as described in Chapter 2.

4.4. Results

Extracellular recordings were obtained from 3 animals in 77 stimulation
sessions (n=169 units in total; n=136 units in neocortex from superficial to deep
layers (0.4 - 2 mm from the surface of the brain), n=33 units in hippocampus). All
recordings, unless stated otherwise, were performed while the animals were
naturally sleeping or immobile resting in their home cages. Occasional waking
interrupted the sleep as the animal moved around, groomed, ate and drank.
During those periods, recording and stimulation were temporarily stopped.
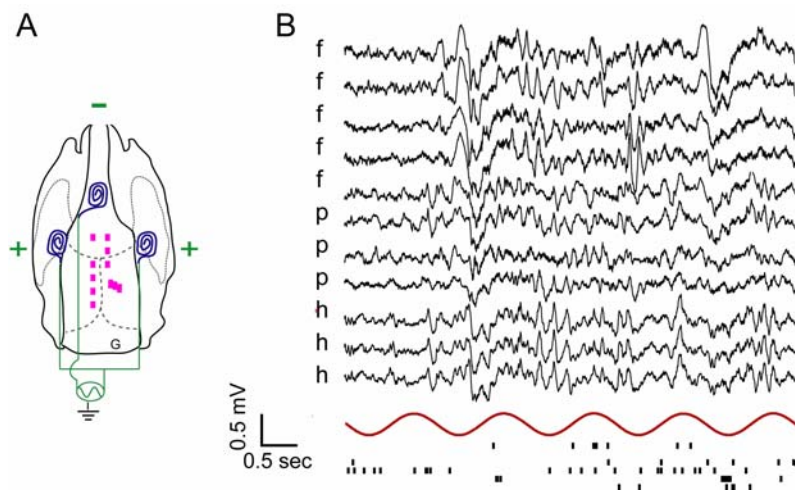
Figure 4.1. **Neocortical slow oscillation was the major background activity during
sleep.** A. Placement of stimulating and recording electrodes from rat #1. B. Activity
during TES while the animal was sleeping. LFP traces (<1250 Hz) were recorded
through single wires across different recording locations. Raw LFP; TES-induced volume
conducted current was not removed. TES, 1.25 Hz, 3-pole configuration. *f*, frontal
recording locations. *p*, posterior recording locations. *h*, posterior recording locations over
the hippocampus. All neocortical electrodes (f, p) were fixed at 1.2 mm from the cortical
surface. Hippocampus-targeting (movable) electrodes were positioned in the infra-
granular layers of the overlaying neocortex at the time of recording (1.2 – 2 mm from the
cortical surface). *Red sinusoid*, TES. *Dots,* extracellularly recorded spikes. Note that the
largest amplitude slow waves were recorded from the frontal electrodes.

During sleep, the most prominent neocortical activity was slow oscillation

providing a comparable baseline to TES oscillating at 1.25 Hz. Figure 4.1

illustrates the activity recorded during natural SWS and in the presence of TES.

The slow wave activity was particularly robust at the frontal recording sites.

4.4.1. TES-induced phase-modulation

Figure 4.2 demonstrates unit firing recorded during TES. Visual inspection

reveals that spikes of apparently different neurons were intermittently associated

with similar phase of TES stimulation.
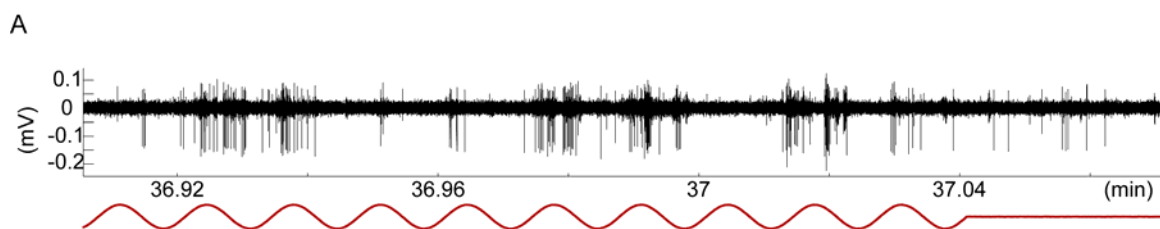
Figure 4.2 **Entrainment of unit firing by TES**. A. Short segment of filtered (1-5 kHz) unit trace during stimulation. TES, 4.8 V (peak-to-peak) amplitude, 1.25 Hz frequency, 3-pole configuration. The recording was performed using a multi-shank silicon probe at AP -3.9 mm, ML 1 mm from bregma, and 3.15 mm from the cortical surface, in rat #3. Note the entrainment of seemingly different units across consecutive cycles of TES.

Similar to the results of acute experiments, TES reliably phase-modulated a

fraction of neurons depending on the intensity of the stimulation (8%, n=12 units

for low intensity TES (0.4 V peak-to-peak); 33%, n=12 units for medium intensity

TES (1.6 V); and 82%, n=11 units for high intensity TES (2.8 V); Fig. 4.3).

Intensity-dependence of phase-modulation was investigated across multiple

stimulation sessions performed in three implanted animals. The results supported

previous findings in anesthetized rats (Chapter 3). Weak intensity stimulation

affected only a few neurons, while increasing stimulus intensity recruited an

increasingly larger fraction of the population. With strong TES, the effects

became more similar across multiple regions and a larger fraction of the recorded

neurons was significantly phase-biased by the TES forced field (Fig. 4.3B).
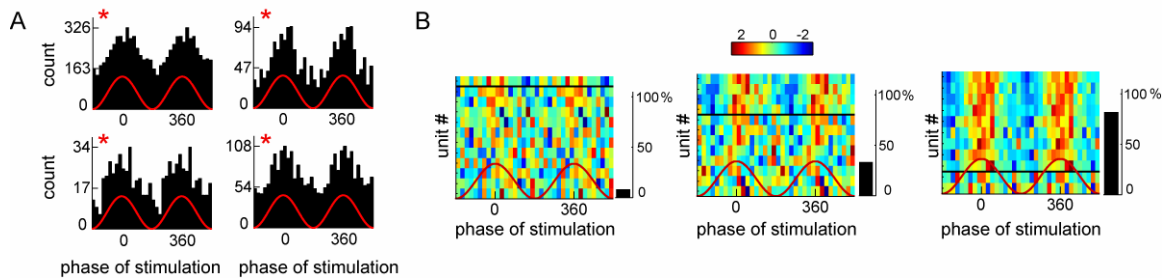
Figure 4.3. **TES-induced phase-modulation of unit firing.** A. TES-induced phase-locked discharge of four example single units. TES, 1.25 Hz, 2.8 V (peak-to-peak), 3-pole configuration (Chapter 2, Fig. 2.1Ba; Fig. 2.2Ae). Averages of >500 stimulation cycles. *Red star*, significant phase-modulation (P<0.01, Kuiper's test). B. TES intensity-dependence of unit entrainment. Each row represents color-coded, normalized discharge probability of a unit (single or multiunit) as a function of TES-phase. TES, 1.25 Hz, applied at weak, medium, and strong intensities (0.4 V, 1.6 V, 2.8 V, respectively); and recorded in rat #1. Units are ordered by the significance of their phase entrainment (P-value, Kuiper's test); the unit with the smallest P-value is at the top. *Black lines* separate the significantly modulated units (P<0.01) from the non-modulated ones. Right-side bars, percentage of significantly modulated units. Recordings were performed using single wires implanted at multiple locations in infragranular layer of the neocortex (9 wires at 1.2 mm, 4 wires spanning in between 1.2-1.9 mm from the cortical surface). The neuronal population at leftmost plot (0.4 V) was recorded on a different day.

Figure 4.4A displays results from all TES sessions where ≥ 5 units were

recorded. As the intensity increased, the number of significantly phase-

modulated units also increased. For a more condensed group display, stimulation

sessions were divided into 5 TES-intensity categories (Fig 4.4B). The mean

percentage of significantly entrained units across experiments was 7% for low

intensity TES (<0.4 V peak-to-peak, n=4 experiments) which increased up to

29% for medium intensity TES (1.6 ≤ TES < 2.4 V, n=4). The mean fraction of

significantly TES modulated neurons increased monotonically with stimulation

intensity. Statistical evaluation of low and high intensity TES combined for all

sessions (<1.2 V, n=5; and ≥1.2 V, n=5), revealed a significant difference in

mean-percent entrained neurons (p<0.05, one-way ANOVA). The data points

from one experiment in rat #2 were not included in this analysis because this

session was a clear outlier during which no entrainment could be elicited

regardless of the stimulus intensity.
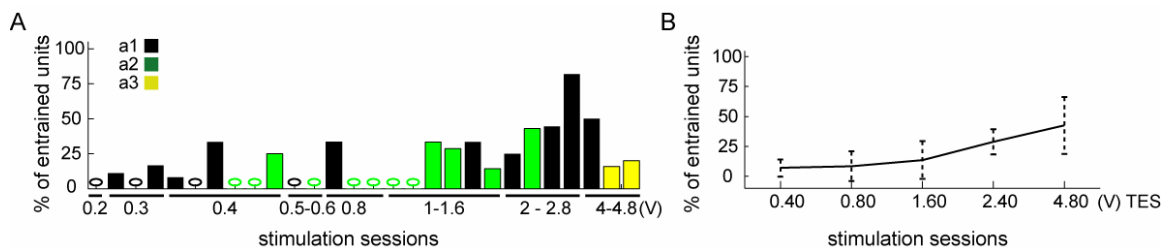
Figure 4.4. **TES-intensity dependent modulation of unit activity.** A. Percentage of significantly modulated units (P<0.01, Kuiper's test). Each bar represents a single stimulation session. TES, 1.25 Hz. *Black*, rat #1. *Green*, rat #2. *Yellow*, rat #3 (Fig 2.1Ba,Bb,Bc, respectively). Only sessions during which the activity from > 5 units was recorded, were included. The lowest intensity tested was 0.2 V. Intensities < 1.6 V were not tested for the 3rd animal; and intensities < 4 V were not included due to the criterion for minimum number of units. B. Mean percentage of significantly entrained units in 5 intensity groups. Upper boundaries of the intensity-groups are shown in x-axis. Lower boundary of each group was the upper boundary of the previous group. For the 0.4 V group, lower boundary was 0.2 V. *Dashed lines*, ± 1 standard deviation.

Figure 4.4A also illustrates some degree of variability across stimulation

intensities, and across animals. Although the size and placement of the

stimulation electrodes were the same, the variability across animals could be due

to various uncontrolled factors, such as the thickness and resistance of the skull.

More recent data from our laboratory indicates that skull thickness and resistance indeed inversely correlates with effective TES intensity (Berenyi et al., 2010).
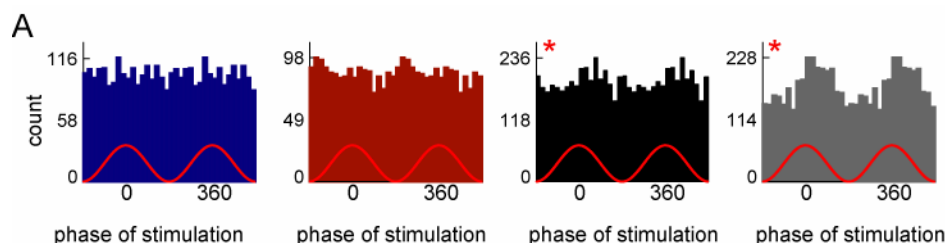
Figure 4.5. **Excitatory and inhibitory neurons had similar response patterns to TES**. A. Phase histograms of 4 simultaneously recorded units in neocortex (0.5-1.5 mm depth) in rat #3 (Chapter 2, Fig. 2.1Bc). *Blue,* putative excitatory cell. *Red*, putative inhibitory cell. *Black,* unidentified single unit. *Gray*, multiunit. *Red star*, significant modulation (P<0.01, Kuiper's test). TES, 1.25 Hz, 4.2 V, 3-pole configuration (Fig 2.2Ae). In this session, n=2 excitatory cells and n=2 inhibitory cells were identified in addition to n=15 unidentified single units and n=6 multiunit clusters. Overall, 16% of units were significantly entrained.

In experiments with well-isolated single unit clusters, we attempted to identify monosynaptically connected pairs as excitatory and inhibitory cells (Chapter 2). Monosynaptic connections among single units were investigated in 10 sessions, where the activity from >2 isolated-single units was recorded (n=89 single units). In our database, only a few cells had statistically putative monosynaptic connections (n=12 excitatory and n=11 inhibitory cells). The small number of physiologically identified neurons precluded statistical judgment of the potential differences in TES-entrainment of principal cells and interneurons. Figure 4.5 shows data from a single experiment. Viewing all neurons individually, and combined with the findings in acute experiments (Chapter 3, Fig. 3.9), we can only tentatively conclude that both populations of neurons were similarly affected by TES.

The geometry of the induced-field was varied by changing the polarity of the stimulator outputs. As expected, in response to such a manipulation, the phase preference of units was completely reversed (Fig. 4.6).
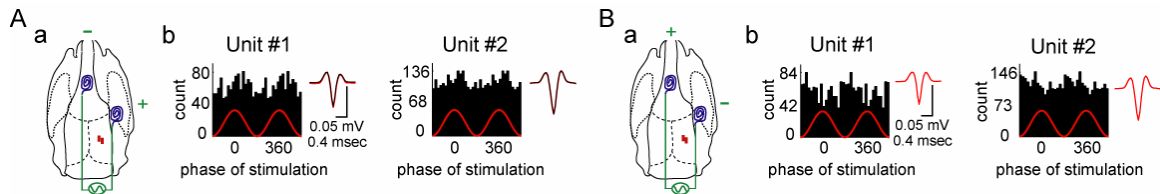
Figure 4.6. **Neuronal entrainment depends on the geometry of the induced-field**. Unit responses to TES at 1.25 Hz, 3.4 V. Sessions were different only in the polarity of the stimulating electrodes. Aa,Ba. TES configurations. Ab,Bb. Spike phase histograms of 2 simultaneously recorded multiunits. Recording was in hippocampal formation in rat #3 (at 3.7-4.5 mm from the cortical surface; Chapter 2, Fig. 2.1Bc). Units were significantly entrained (P<0.01, Kuiper's test) for both TES sessions. Note that reversing the output of the stimulator induced a 180° phase shift in unit entrainment.

i. Stronger entrainment of multiunits

Multiunits constituted a considerable fraction of our data (n=75 multiunits vs. n=94 single units; n=17 recording days; n=3 animals). TES-induced phase-modulation was more pronounced in multiunits compared to single units. The comparison of significant phase-modulation between multiunits and single cells revealed that 1) both of these factors were critical to affect TES-induced phase-modulation (two-way ANOVA; cell-type, P<0.05; intensity, P<0.001; interaction, P<0.01); 2) there was a significant interaction between the stimulation intensity and the cell type (multiunit vs. single unit; Fig. 4.7).
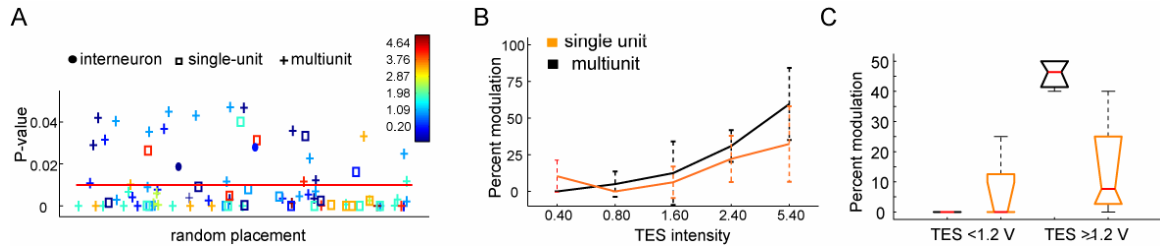
Figure 4.7. **Phase-modulation was more pronounced in multiunits**. A. Distribution of significance of phase-modulation as a function of TES-intensity (n=3 animals; n=67 stimulation sessions, n=35 multiunits, n=14 single units). Note that the same unit may appear more than once for different intensity stimulation protocols. P-values <0.05 are plotted. *Plus-sign*, multiunits. *Square*, single units. *Filled-circle*, interneurons. Note that none of the 12 excitatory cells had P-values <0.05. Colors indicate TES intensity in volts (V). B. Mean percentage of significantly entrained multi- and single units in 5 intensity groups (n=20 sessions with >5 units). Note that the fraction of significantly entrained units were computed relative to the number of single-and multiunits in each session. Upper boundaries of the intensity-groups are shown in x-axis. Lower boundary of each group was the upper boundary of the previous group. For the 0.4 V group, lower boundary was 0.2 V. *Dashed lines*, ± 1 standard deviation. C. Multiunit and single unit entrainment for low and high intensity TES (n=3 animals; n=20 sessions with >5 units). *Orange*, single units. *Black*, multiunits. TES intensity and cell-type were both critical variables to affect unit modulation (P<0.001, two-way ANOVA).

Stronger entrainment of multiunits could be explained by the increased likelihood of having at least a fraction of spikes of to be entrained per given cycle. Figure 4.2 demonstrates multiunit activity recorded during TES. The trace illustrates different cells that would be lumped into a *single multiunit* cluster. For a given stimulation cycle, not all but *some* of the spikes of *seemingly different neurons* were entrained by the stimulation.

ii. Bimodal phase-modulation

Similar to the results obtained in anesthetized animals, several significantly modulated neurons had two prominent peaks at different phases of TES. The percent of bimodally entrained neurons was somewhat higher with stronger

stimulus intensities (Table 4.1). Despite the positive trend, the differences among groups were not statistically significant (one-way ANOVA).

Such double responses were not only present for multiunits but also for the well-isolated single neurons (n=22 stimulation sessions; n=7 single neurons and n=15 multiunits that were significantly phase-modulated with a bimodal phase preference). In case of multiunits, one potential explanation is that two or more neurons with different phase preferences were lumped together as a multiunit. However, this explanation does not explain the bimodality observed in single neurons. Therefore, it's more likely that the double-peak phase histograms reflect a combination of the direct effect of TES and multi-synaptically mediated drive of neuron(s) from more distant, directly entrained cells.

TES intensity range (V)	# of sessions	Mean of % bimodal entrainment	Median of % bimodal entrainment	SD of % bimodal entrainment	Range of % bimodal entrainment
0.3 – 1.2	3	20.4	16.7	± 9.4	11.1 – 33.3
1.2 – 2.4	3	21.4	25	± 5.1	14.3 – 25
2.4 – 4.8	5	27.7	25	± 19.2	6.7 – 54.5

Table 4.1. **Summary of the significantly phase-modulated units with a bimodal (or multimodal) phase preference.** Stimulation sessions that yielded phase-modulation were divided into 3 categories based on intensity. Lower and upper borders are given in the first column. The second column, number of stimulation sessions. From third to sixth columns, summary statistics for significantly modulated units with a bimodal entrainment profile. Note that the fraction of units with bimodal entrainment seemingly increased as TES intensity increased. All sessions were conducted with 3-pole stimulation configuration (Chapter 2, Fig. 2.2Ae). Only sessions with > 5 units were included.

iii. Entrainment across multiple cortical areas

In 3-pole stimulation configuration, TES-induced effects were similar across both hemispheres (Fig. 4.8, n=1 session, n=7 units recorded in left hemisphere

using tetrodes, n=18 units recorded in right hemisphere using a 4-shank silicon probe).
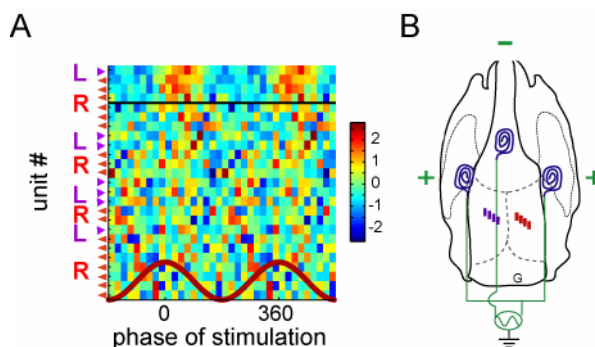
Figure 4.8. **Synchronous entrainment of units in both hemispheres.** A. Summary plot showing spike phase histograms of simultaneously recorded units in neocortex (0.5-1.5 mm from the cortical surface). Each row corresponds to a unit, color-coded for standardized firing rate. Units are ordered according to the significance of their phase-modulation; unit with the smallest P-value is at the top. *Black line*, separates significantly entrained units (P-value <0.01, Kuiper's test) from non-modulated ones. TES, 4.2 V, 1.25 Hz. *Purple arrowhead (L),* units (n=7) recorded in the left hemisphere using tetrodes. *Red arrowhead (R),* units (n=18) recorded in the right hemisphere using a multiple-shank silicon probe. B. Placement of recording and stimulating electrodes. *Red*, shanks of the silicon probe. *Purple*, tetrodes. *G*, ground.

Widespread and potentially direct effects of TES were visible when recordings from the neocortex and the hippocampus were compared. As shown in Figure 4.9B, TES induced entrainment occurred in comparable fractions of neurons in the deep layers of the neocortex (16%) and the hippocampal CA1 region (29%). In contrast, during slow oscillations of natural sleep, almost all neocortical neurons were phase-locked to the UP state of the oscillation but only a moderate number of CA1/subicular cells were affected, supporting previous observations (Fig. 4.9C; Isomura et al., 2006).
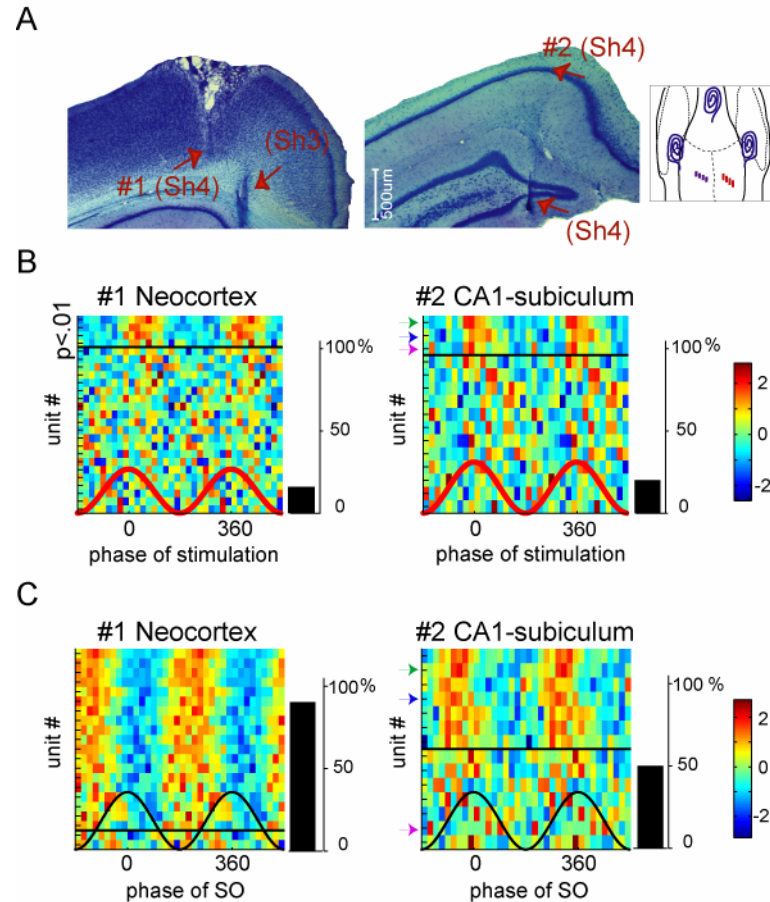
Figure 4.9. **TES entrained neurons in multiple cortical areas.** A. Histologically verified tracks of a 4-shank silicon probe. Tracks of the two most lateral probe shanks are shown in the neocortex (left, sh4 and sh3) and the deep recording sites in the hippocampus (right, sh4). The silicon probe was moved deeper after each recording session. Probe recordings were made at 2 different recording depths (*red arrows*): in the deep layers of the neocortex (#1) and hippocampal CA1-subiculum area (#2). Right inset: locations of the stimulating electrodes, silicon probe (*red*) and tetrodes (*purple*). B. TES entrainment of neurons in 2 recording sessions from the same rat. Each row corresponds to a unit, color-coded for standardized firing rate. Units are sorted by their P-values (Kuiper's test); the unit with the smallest P-value is at the top. *Black lines*, separate the significantly modulated units (P<0.01) from non-modulated ones. Side bars, percent of neurons significantly modulated. TES, 1.25 Hz, 3-pole configuration. Left to right, 4.2 V, 4.8 V, peak-to-peak intensity, respectively. The fraction of TES-entrained neurons might be overestimated since neurons firing at a low rate might not have been detected properly by clustering algorithms. Same color scale for both plots. *Colored arrowheads*, show the identity of the neurons that were entrained by TES. C. Network-controlled phase-locking of neuronal activity to slow oscillations during natural sleep (illustrated by black line) in the absence of TES. *SO*, slow oscillation. Same units as in *B* but ordered according to the significance of their phase-modulation (P-values, Rayleigh test). Same color scale for both plots. Note the strong phase-locking of neocortical neurons to slow oscillation (Steriade et al., 1993c), and moderate entrainment of CA1-subicular cells (Isomura et al., 2006). LFP recordings were performed in the Layer 5/6 of the contralateral neocortex.

The entrained neurons in the hippocampus / subiculum were phase-locked to later phases of the slow oscillation than the neocortical cells (Fig. 4.9C; Isomura et al., 2006). On the other hand, TES-entrained hippocampal neurons were locked to slightly earlier phases of TES than the neocortical cells. These findings support the hypothesis that at least a fraction of hippocampal neurons were directly affected by TES rather than indirectly influenced by TES-triggered neocortical neurons through multisynaptic actions.

4.4.2. TES-induced electric fields

Postmortem recordings were performed in order to measure the extracellular potential created by TES which was effective to drive cells in vivo. TES of 3.2 V (peak-to-peak) intensity that entrained more than half of the neurons, induced 2.5-5 mV of volume conducted extracellular potential at the recording locations (rat #1, Fig. 4.10A).

Similarly, 4 V intensity stimulation elicited 1 - 4 mV volume conducted potential in the other animal (rat #2, Fig 4.10B). The voltage gradients created by the same stimulation were ~1.5 mV/mm in the medio-lateral direction when TES was applied through bilaterally placed electrodes (Fig. 4.10C). Although weak, such a voltage gradient could be effective to induce membrane polarization, directly.
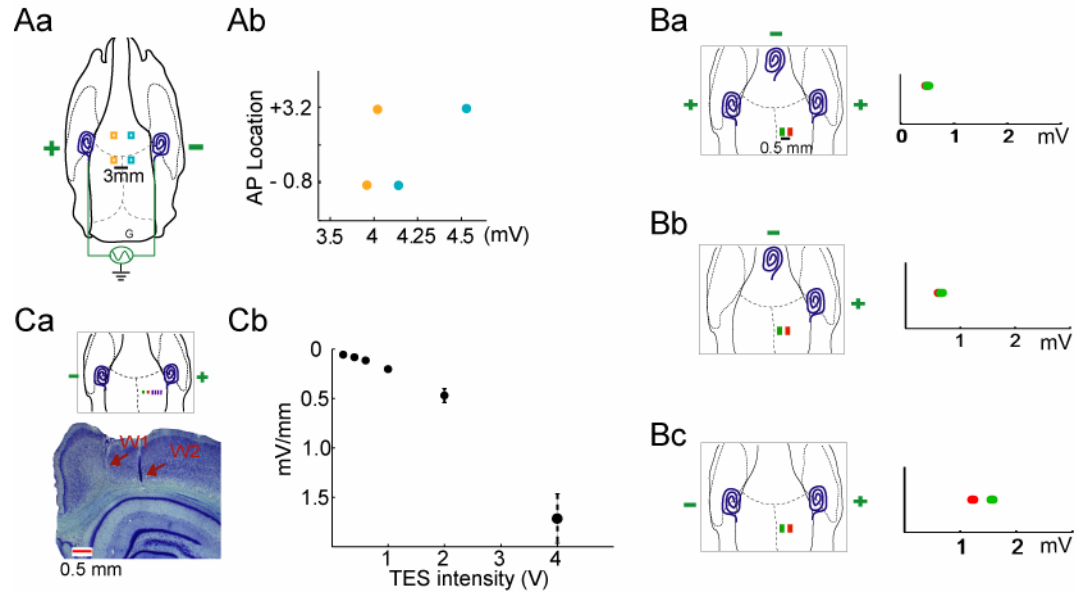
Figure 4.10. **The magnitude of TES-induced voltage gradient.** Postmortem voltage measurements from rat #1(*A*) and rat #2 (*B,C*). Aa. Placement of 4 recording wires and stimulating electrodes. The medio-lateral distance between recording electrodes was ~3 mm. *G*, ground. Ab. Volume-conducted potential at recording sites. The voltage differences measured between anterior and posterior pairs of electrodes were ~0.5 mV and 0.2 mV, respectively. TES, 3.2 V (peak-to-peak) intensity, 1.25 Hz frequency, 2-pole configuration. Induced electric field was 0.12 mV/mm (± 0.07 mV/mm). Ba,b,c. Placement and postmortem voltage measurements from 2 recording wires, 0.5 mm apart in medio-lateral axis, for 3 stimulation-configurations. TES, 4 V, 1.25 Hz. The tracks of the recording electrodes are shown in (*C*). Note that the largest voltage gradient (~0.9 mV/mm) was induced with the stimulus configuration, which generated relatively parallel fields to the recording sites (*Bc*). C. Voltage gradient measured for the stimulation configuration shown in (*B*). Ca. Placement of recording and stimulating electrodes (top). Histological verification of the tracks of single wires (bottom). Cb. Mean (1 ± standard deviation) voltage gradient as a function of TES intensity. Measurements were done across all recording electrodes, shown. *Pink*, single wires. *Purple*, tetrodes. Note that 4 V TES induced ~1.5 mV/mm of voltage gradient.

4.4.3. Stability of phase-modulation

Repeated long trains of TES generated stable phase-modulation over time. Figure 4.11 illustrates unit entrainment from an example experiment in which significantly entrained units (82%, n=11 units) displayed similar entrainment profiles across trials of the same protocol. Sham TES-signal was constructed for

stimulation-free periods between stimulation trials. As expected, the phase-modulation was specific to the stimulation period. The entrainment developed rapidly after the stimulation onset; and disappeared quickly after the offset.
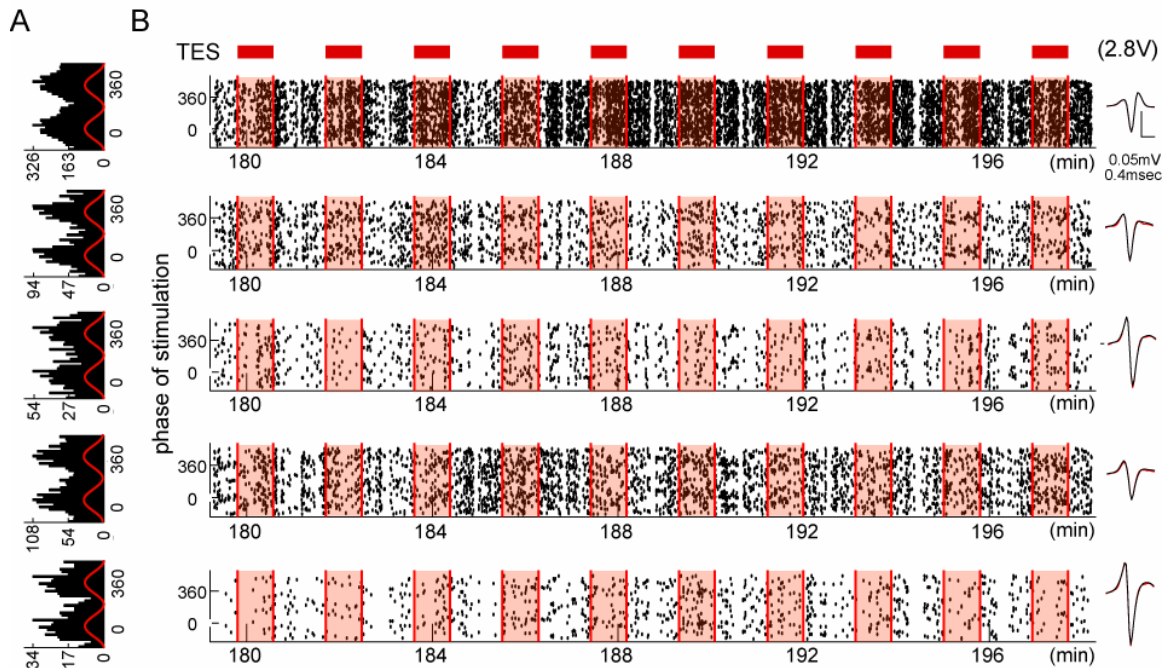
Figure 4.11. **Stability of unit entrainment by TES**. Five simultaneously recorded units from the 1st chronically implanted animal (Chapter 2, Fig. 2.1Ba). TES, 2.8 V (peak-to-peak), 1.25 Hz. A. TES phase histograms for the entire session. B. Each dot represents a spike, as a function of stimulus phase (ordinate) during 10 successive, one-minute long stimulation trials (red bars) with one minute resting (stimulation-free) intervals. Sham-stimulation signal is interpolated for pre and post-stimulation periods (the middle where the interpolated pre and post-stimulation signals converge, was excluded). Note the stability of TES entrainment over multiple trials. *Right column*, average filtered unit waveforms recorded during stimulation-free periods (*black*) and during TES (*red*). Note that waveforms were stable across TES and TES-free periods; so traces overlap.

In addition to consistent responses, more complex responses, e.g., suppression; rebound activity, etc., were also observed across individual trials. However, these interesting features could not be studied since they were not consistent across trials.

4.4.4. TES-induced effects on firing rate

TES-induced phase-modulation was not coupled with a firing rate change

(Fig. 4.12, Fig. 4.13). Figure 4.12 summarizes data from 184 putative single and

multiple units recorded in 18 sessions from 3 chronically implanted rats.
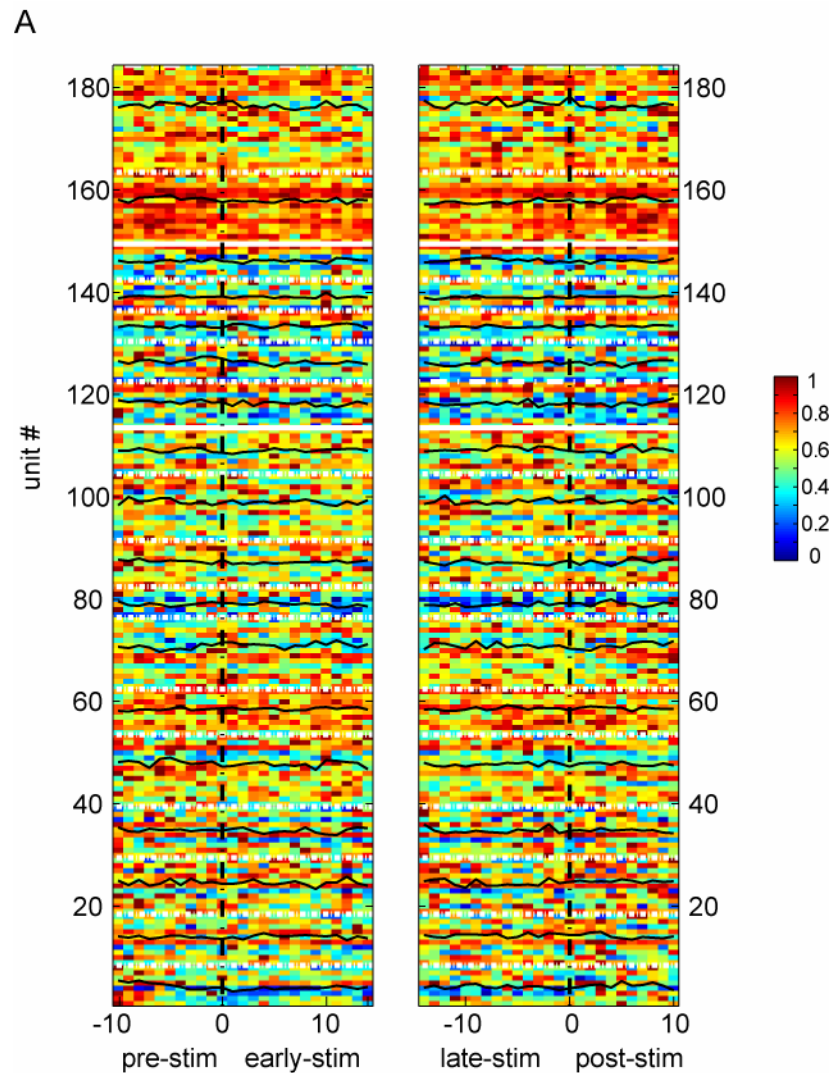
Figure 4.12. **TES did not affect firing rate.** TES evoked unit activity in multiple experiments (n=18 sessions, n=92 units, Chapter 2, Fig. 2.1Ba-c). A. Onsets (*left*, 0 cycle) and offsets (*right*, 0 cycle) are shown separately. Each row is a unit, color-coded for normalized firing rate (maximum rate=1). Bins reflect the normalized rates for each cycle of TES (one period (peak to peak). Pre and post epochs are sham cycles. Note that same unit might appear more than once for different stimulation sessions. *White lines,* separate rats. *White dotted lines,* separate sessions. *Black lines*, session averages of normalized firing rates.

Despite slight variation in the firing rates of some of the neurons, neither of the following comparisons yielded a significant difference across groups: i) pre vs. early-stimulation (first 15 cycles of stimulation); ii) late (last 15 cycles of stimulation) vs. post-stimulation; iii) post vs. pre-stimulation; iv) early vs. late-stimulation (Fig. 4.12).

Figure 4.13 illustrates spiking activity from 3 example units evaluated for the beginning and ending of the stimulation. Except slight phasic changes, TES did not induce a robust effect on spike count of neurons. These are important observations because they demonstrate that the phasic modulation of firing activity was accompanied by an overall balanced firing rate integrated over the duration of the TES cycle.
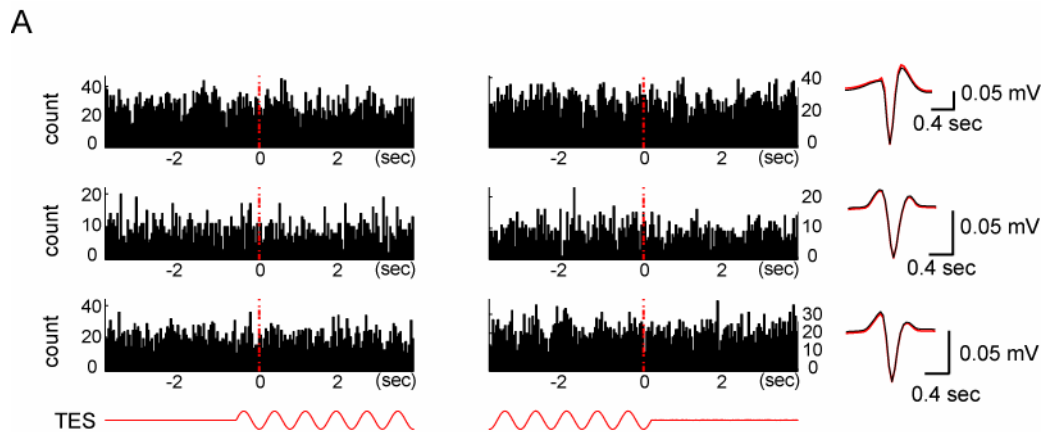
Figure 4.13. **Modulation of firing rate by TES.** A. Averaged TES phase onset (left) and offset (right) triggered histograms of unit activity. TES, 4.8 V, 1.25 Hz, 3-pole configuration (Chapter 2, Fig. 2.2Ae). *Red dotted lines*, troughs of the first and the last cycles. Insets, average filtered unit waveforms recorded during stimulation-free periods (*black*) and during TES (*red*). Unit at top is a single unit; the others are multiunits.

4.4.5. Interaction of TES with behavioral state

Intracellular experiments performed in the anesthetized rat had demonstrated that network-imposed effects and TES forced stimulation can exert a combined

effect on single neurons. The effects of background neural activity on TES-

induced entrainment were further evaluated in chronic experiments by applying

same stimulation parameters across two different behavioral states of the animal.
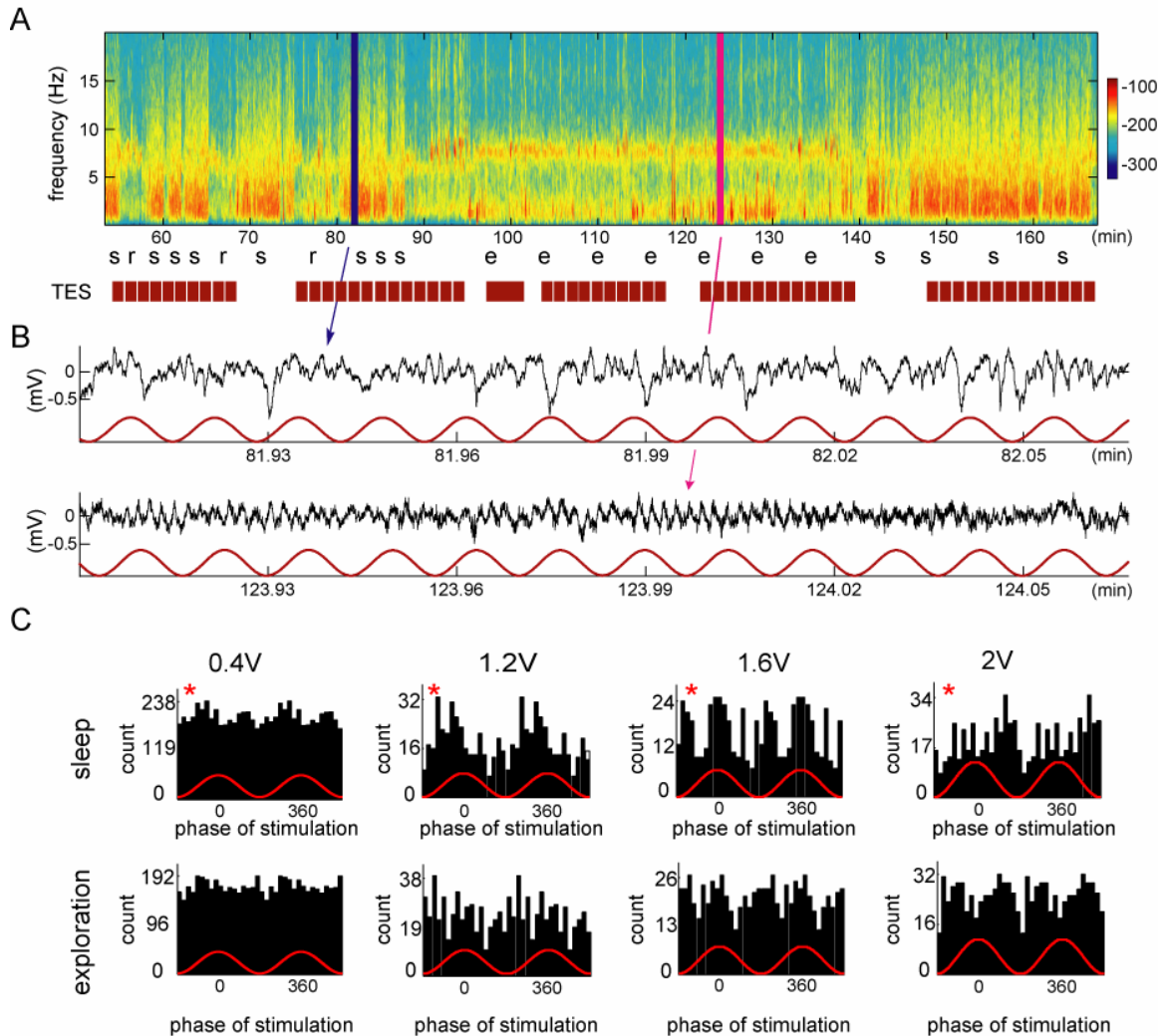
Figure 4.14. **Network state-dependence of TES entrainment**. A. Spectrogram of power in LFP (<1250 Hz) signal from the CA1 pyramidal layer (~2 mm from cortical surface). Sleep related (alternation between SWS and REM epochs) and exploration-associated activity (dominant 8 Hz theta oscillation) are distinguishable. Letters indicate state of vigilance defined by manual scoring. *s*, SWS. *r*, REM. *e*, exploration. *Red boxes*, TES. The color-scale, the power in each frequency band of the time spectrum (arbitrary units). B. Zoomed epochs taken from (*A). Blue* and *magenta* lines illustrate state-dependent LFP activity. TES, 1.25 Hz, 1.2 V, 3-pole configuration (Fig 2.2Ae). C. Spike-phase histograms of example units during sleep (top row) and exploration (bottom row). *Red star*, significant phase-modulation (P<0.01, Kuiper's test). Note that as the intensity increased, the spiking activity became much more sensitive for TES-phase, even during exploration. However, same units were entrained better during sleep than exploration.

As Fig. 4.14A, B illustrates, these behavioral states were well-defined by characteristically different LFP patterns. Slow oscillation was the dominant neocortical activity (Steriade et al., 1993c) during SWS, interspersed with short REM epochs associated with bouts of hippocampal theta oscillations. On the other hand, in the ambulating rat, ~8 Hz theta oscillation of hippocampal origin was the dominant activity (Vanderwolf, 1969; Sirota and Buzsaki, 2005)

At the intensities tested, none of the neurons were affected by TES in the exploring animal, while at least a fraction of the neurons was significantly entrained during sleep (n=2 units, for 0.4 V TES; n=4 units for 1.2 V, 1.6 V and 2 V TES sessions; Fig. 4.15C). Distributions of phase modulated units across behavioral states were significantly different for medium-to-high intensity TES (Fig. 4.15; P<0.05 for 1.2 and 2 V TES and P≤0.005 for 1.6 V TES, Chi-Square Test). This finding suggests that TES was more effective in a state where the intrinsic pattern and TES forced pattern were similar; perhaps due to the transient entrainment of the slow oscillation of sleep.
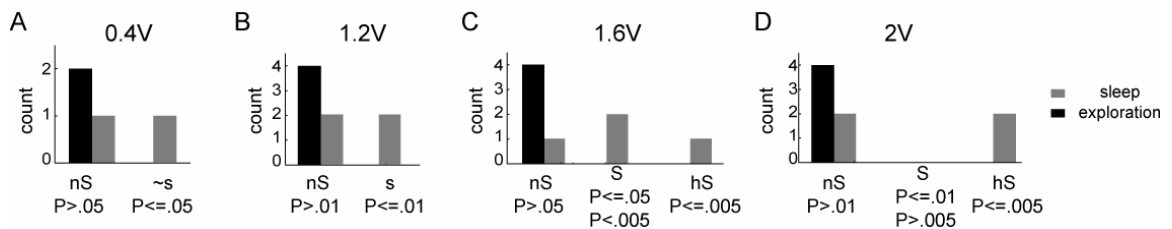
Figure 4.15. **TES-entrainment across different network states**. Frequency histograms showing phase-modulation of multiunits for different intensity stimulation. TES, 1.25 Hz, 3-pole configuration (Chapter 2, Fig. 2.2Ae). Recording from the Infragranular layer of neocortex. *Gray*, sleep. *Black,* exploration. *nS*, not modulated (P>0.01, Kuiper's test). *S*, significantly modulated either according to P<0.05 or P<0.01. *hS*, highly significantly modulated (P≤0.005). Only 2 categories were compared in (*A)* and (*D*). Note that *S* and *hS* categories increased with increasing TES intensity in the sleeping animal but not during exploration.

4.4.6. Lack of disruptive behavioral side-effects

The behavior of the animal was monitored throughout the chronic experiments. Stimulation onset or offset did not elicit any noticeable behavior in the animal. When stimulation was presented during sleep, no behavioral arousal or abrupt change of the EEG state was observed. While these observations do not exclude the possibility that the animals detected or 'felt' TES stimulation, it did not appear aversive or arousing at the intensities used here (≤ 5.4 V).

4.5. Discussion

Modifications to the previous experimental design enabled secure and reliable recordings for a duration of 2-to-5 weeks from each chronically implanted animal. These recordings provided the opportunity to observe TES induced effects in naturally sleeping animals in the absence of any pharmacological intervention. Most of the results confirmed the findings obtained from the acute experiments.

TES induced reliable phase-modulation regardless of the anatomical location. The intensity and the geometry of the induced field were critical in shaping unit entrainment. For significantly entrained units, multiple repetitions of the same stimulation elicited stable phase-modulation across trials. Phase-modulation ceased almost immediately after the offset of the stimulation.

The ongoing brain activity was essential in shaping the effects of the stimulation. When the same intensity TES was applied; the cortical recruitment was much higher during natural sleep. This was probably because neurons were already tuned to an activity mode that matched with the temporal characteristic of

the stimulation. Neural activity in the actively exploring rat was completely different from the temporal characteristics of the stimulation. As a result neurons could not be recruited by the external force. As higher intensities were applied, the competition biased towards the artificial force and the effects of TES started to become more visible. However, the overall entrainment was more effective in the sleeping animal.

One aspect that could not be addressed in anesthetized recordings was the potential side effects of the stimulation. Monitoring of the behavior of the animal revealed the absence of any noticeable disruptions.

Separate lines of evidence suggested that direct field-induced polarization was the dominant mediator for the entrainment of recorded neurons: 1) Hippocampal neurons were entrained by TES; but not by intrinsic slow oscillations. It is likely that hippocampal entrainment was mostly due to field-induced direct polarization rather than transsynaptic recruitment. 2) Phase-modulation emerged and disappeared relatively quickly. 3) Bimodal entrainment of, at least, single cells could be explained by differential polarization of different neural compartments.

In short, our findings suggest that TES could reliably entrain unit firing in behaving animals depending on the temporal characteristics of the background activity and the stimulation.

Chapter 5: Discussion

5.1. Overview

Controllable and reliable manipulation of brain activity through non-invasive methods is one of the major quests in neuroscience. TES has that potential for diffusely affecting neuronal activity in widespread areas of the brain.

Electrical stimulation of neuronal elements has a wide range of applications. Current applied by a small sized electrode can activate axon bundles, a local population of neuronal somata and dendrites, or under special conditions, a single cell, directly. Depending on the strength of the focal stimulation, neurons in more distant regions of the brain can be activated antidromically through their axons or anterogradely by mono- or multisynaptic connections (Histed et al., 2009; Fritsch and Hitzig, 2009; 1870). The goal of focal electric stimulation, under most conditions, is to drive specific pathways or to identify neuronal groups with specific projections (Tepper and Groves, 1990). However, under many experimental and clinical conditions, it is more desirable to affect large numbers of neurons distributed over large areas without the need to identify the exact neuronal populations affected by the stimulation. TES can meet these requirements.

Field-induced membrane polarization, either through electrical coupling between neighboring neural elements or through extracellular current flow, constitutes a common form of non-synaptic neural transmission (Bindman et al., 1964b; Taylor and Dudek, 1982; Jefferys and Haas, 1982; Chan et al., 1988). Whether intrinsically generated by the neurons themselves or externally induced,

electric fields work through the same mechanism (Bishop and O'leary, 1950; Bindman et al., 1964a; Rosenthal and Wulfsohn, 1970; Frohlich et al., 2008).

TES has a convenient and simple application for temporary or long-term modulation of neural activity for therapeutic use (Rosenthal, 1972a; Fregni et al., 2006; Boggio et al., 2008; Nitsche et al., 2009). However, the application of TES in human subjects is currently limited due to the lack of understanding of the mechanisms and the extent of field-induced effects.

Recent studies (Marshall et al., 2004; 2006; Kirov et al., 2009) examining the behavioral consequences of induced fields in humans rekindled interest in the usefulness of TES for manipulating brain activity and highlighted the importance of understanding how electric fields interact with and affect intact neural activity.

The primary goal of my dissertation research was to better understand the mechanism underlying electric-field induced effects. To accomplish this aim, I studied the single unit activity in response to field stimulation in anesthetized and naturally sleeping animals.

Consistent with previous studies (Francis et al., 2003; Bikson et al., 2004; Radman et al., 2007; Frohlich et al., 2008), we found that relatively weak electric fields, applied through the skull could powerfully affect neurons in widespread cortical areas. The induced effects were brought about largely by an interaction between TES-induced field and ongoing network activities of the intact brain. The major form of modulation was the temporal bias introduced by certain phases of the stimulation. The effects were dependent on background neural activity and

certain features of the stimulation, i.e., stimulation intensity, the geometry of the induced-field, etc.

5.2. In vivo application of TES

5.2.1. Technical considerations

Prior to our study, TES combined with large-scale unit recording in chronically implanted animals, had not yet been attempted. In the absence of previous expertise, a significant portion of my efforts was devoted to the development of proper techniques. I used anesthetized rats to find the optimal parameters of stimulation. While these acute experiments enabled the examination of many electrode configurations, the duration of the experiments (4 to 6 hours) limited the testing of various stimulation parameters in the same animal. Thus, once the optimal TES application (spiraled bifilar wires placed on the skull) was determined, we extended the experiments to behaving animals. Chronic recordings (with a fixed stimulation set-up) provided the opportunity of comparing various stimulation features recorded in the same animal. The principal finding of our experiments, 'the reliable and effective entrainment of neurons by TES', was consistent across these diverse experimental conditions.

Constant voltage stimulation was used for the majority of the experiments for practical reasons. In a subset of experiments, constant current stimulation was used to measure the currents flowing between the electrodes. The use of constant current stimulation is a more common practice since 1) the amount of current flowing to the tissue is constant and 2) the intensity is directly comparable

across studies. However, chronic situation with stable resistance - impedance between the non-polarizing electrodes (and using AC stimulation) eliminated any difference between the uses of constant current and constant voltage stimulation.

Capacitive effects of our stimulation were estimated to be minor since the stimulation frequency was always ~1 Hz (Gabriel et al., 1996). Numerical simulations of a purely resistive model of the brain were consistent with our experimental findings indicating a clear match between the theory and the experiments (Ozen et al., 2008). Therefore, capacitive effects of the stimulation could be safely disregarded.

The imposed electrical field was volume conducted to the intrinsic brain activity. Thus, the separation of two sources from the combined LFP recording was technically challenging. Although we attempted to subtract the added field and 'clean' the recorded LFP (see Chapter 2), we remained only partially satisfied by the reliability of these off-line methods. Since our main goal was to identify TES-field effects on spiking activity, we focused our analysis solely on unit activity.

5.2.2. Factors related to unit modulation

Unit activity was monitored through complementary techniques: intracellular recordings and large-scale extracellular recordings using wire electrodes and silicon probes. Single wires and tetrodes were used for simultaneous recordings in multiple locations; high-density silicon probes were used for recordings from large neuronal ensembles in a relatively small volume of tissue.

Intracellular recordings were performed in a small subset of experiments in order to assess the field-induced changes on the membrane potential. Analysis of subthreshold activity was particularly useful to demonstrate the interaction between TES-induced and slow oscillations-induced effects. UP and DOWN states were consistently observed throughout the experiments, as a demonstration of the persisting control of the intrinsic network on the recorded neurons. At the same time, the probability that the membrane potential would be in either UP or DOWN state was reliably biased by the applied field in a stimulus intensity-dependent manner, demonstrating the temporary control of the external field on neuronal excitability. These findings were in support of previous in vitro studies using low-to-medium intensity electric fields to polarize neurons (Taylor and Dudek, 1982; Jefferys and Haas, 1982).

Examining the impact of applied fields on the activity of extracellularly recorded neurons with large spikes is straightforward. Indeed, we obtained clearly separated units generating large amplitude spikes in both acute and chronic experiments, and showed that their activity was phase-locked to the applied fields. In order to include smaller amplitude single units and multiunit activity (these latter two classes were dominant in most experiments), all clusters were tested for potential contamination of high-frequency artifacts of the stimulation. All spikes were screened and the ones included in the analyses had to meet our strict spike-quality criteria (see Chapter 2), followed by a visual inspection of waveform stability for the duration of the recording. Due to these strict criteria, this process inevitably eliminated an unknown number of real

spikes for smaller amplitude clusters. On the other hand, it ensured the exclusion of false-positive errors in unit entrainment.

TES-induced decreases in the firing rate of a subset of recorded units can be explained by the elimination of 'real spikes'. However, this observation can also reflect a physiological condition, such as inhibition induced by TES-activated inhibitory interneurons or a biased, stronger hyperpolarizing effect of TES. However, TES-induced decreases in firing rates were rarely observed. The presence and the proportion of 'suppressed' units varied strongly across experiments. Irrespective of the potential rate change in a minority of neurons, our results demonstrate that the primary effect of TES was the phase-modulation of the discharge probability of neurons by the balanced polarizing effects of the forced field. This interpretation is supported by recent experiments showing that the LFP spike component of 'spike-and-wave' epileptic patterns can be alternatively increased and decreased by TES, depending on the phase of the applied field (Berenyi et al., 2010).

As opposed to the unimodal entrainment induced by intrinsic slow oscillations, TES induced a bimodal phase-modulation in some of the neurons. Such multiple peaks were mostly observed in response to high-intensity TES, independent of the stimulation configuration and the unit-type (multiunit vs. single unit). Potential reasons include but are not limited to 1) competing phases of depolarization introduced by TES and the intrinsic slow-oscillations; 2) converging inputs from neurons with different entrainment profiles; 3) alternating polarization of different compartments of the same neuron; 4) ipsilateral and contralateral inputs

converging onto a single cell (for the case of bilateral stimulation configuration);
5) different phase-preferences of individual neurons combined into a multiunit.
Any combination of these sources can explain non-unimodal phase preferences.
However, the most likely explanation is the combination of direct and indirect
(transcallosal, multisynaptic) effects acting on the same neuron, since high
intensity TES recruited many of the neurons into a bimodal-phase-modulation.

Isolation of units into single unit clusters requires a sufficient number of
relatively large amplitude spikes. Thus, relying on only single unit data would
have meant discarding units with smaller amplitude spikes and low firing rates.
Since the entrainment did not differ depending on the cell types, spikes of not-so-
well isolated units were also included in the analysis. Pooling spikes from
different neurons into a multiunit cluster increased the likelihood of having phase-
modulation for any given cycle of TES. Accordingly, multiunits were entrained
more easily by TES-induced phase-modulation.

5.2.3. Stimulating at the slow oscillation frequency

The frequency of the stimulation was kept in the range of neocortical slow
oscillation frequency (0.8 -1.7 Hz) for the following reasons: 1) This type of
stimulation has been previously shown to modulate neural activity in healthy
humans (Marshall et al., 2006) but the impact of TES on brain activity could not
be directly assessed. 2) This is the dominant frequency of slow oscillations
observed across large areas of the neocortex during SWS (Steriade et al.,
1993c; Achermann and Borbely, 1997; Steriade, 2001; Ros et al., 2009).

Therefore, an external stimulation, temporally mimicking this intrinsic rhythm, would be effective to recruit large populations of cortical neurons (Sanchez-Vives and McCormick, 2000; Shu et al., 2003). 3) Intrinsic slow oscillations also occur under anesthesia. Thus, we could use and compare acute and chronic recordings / stimulations during relatively similar brain activity (Marshall et al., 2006; Frohlich et al., 2008).

Our results demonstrated a wide-spread unit entrainment in anesthetized and in sleeping animals. Furthermore, the entrainment was stronger during sleep than behavioral exploration. In other words, the impact of intrinsic slow oscillations on unit activity was not only present but also it was critical to shape the external-field effects.

5.2.4. Focus on hippocampal entrainment

In addition to the 'unspecific' targeting across wide regions of the neocortex, the hippocampal formation was particularly targeted due to its distinct activities during intrinsic slow oscillations. In line with previous studies, robust neocortical synchrony during SWS and under anesthesia was only partially relayed to the hippocampus (Siapas and Wilson, 1998; Battaglia et al., 2004; Isomura et al., 2006; Hahn et al., 2007). However, TES mimicking the neocortical slow oscillation could entrain the activity of hippocampal cells. The functional implications of introducing such an effect on hippocampal activity are discussed in subsequent sections (see section 5.3.2).

5.2.5. Stimulation-related factors

i. Stimulation intensity

There was a positive relationship between the stimulation intensity and the fraction of significantly phase-modulated units. This relationship was observed in individual experiments both under anesthesia and during sleep, as well as in the group data. A larger range of stimulation intensities, applied to each animal in each session, would have been ideal for the demonstration of intensity and phase-modulation relationship. However, this was not possible due to time constraints. Nevertheless, a monotonic relationship between the intensity and the unit modulation could be observed in our data. Across all experiments, TES of ~1.2 V (peak-to-peak) intensity elicited a reliable entrainment in 20 – 25 % of units.

It should be noted that the percentages reported above are likely to be overestimates since the majority of neurons present in the recorded brain volume are either virtually silent or fire at a rate too low to be identified with our clustering methods (Fujisawa et al., 2008). In other words, the clustering method inevitably favors the selection of active neurons. To establish the true percentage of TES affected neurons will require unbiased methods of neuronal sampling.

Postmortem measurements demonstrated that electric fields of 1 mV/mm were sufficient to affect the excitability of at least some neurons. This magnitude is comparable to the magnitudes measured in vitro (Francis et al., 2003; Deans et al., 2007; Radman et al., 2007) and to the estimated fields used in human studies (Marshall et al., 2006; Kirov et al., 2009).

TES, as low as 0.2 - 0.4 V, applied to the surface of the skull by our coil-shaped electrodes, was sufficient to bias the discharges of a few cortical neurons. Given a 50 to 100 kΩ resistance between the surface of the skull and the recording site in the brain (our measurements), the present findings suggest that as low as 2-5 µA current flow through brain tissue is sufficient to affect neuronal discharges.

ii. Current flow and dendritic layout

Due to in vivo application, the geometry of the induced fields in our experiments deviated from the well-arranged electric fields used in vitro studies. However, in several individual experiments, we could demonstrate the importance of the direction of the current flow on unit entrainment (Lippold et al., 1961; Bindman et al., 1964b; Jefferys, 1981; Rossini et al., 1985). By altering the direction of the current flow, the preferred phase of the entrainment was changed and/or different sets of neurons were affected by the applied field.

Another key parameter known to shape TES-induced effects is the dendritic layout of the cells (Jefferys, 1981; Chan and Nicholson, 1986). While it is likely that in our in vivo experiments, the relationship between neuronal morphology and the unit entrainment was also a significant factor, this issue could not be directly addressed. In addition, the crude comparisons across somatosensory and prefrontal cells did not reveal any difference in phase-modulation. However, the bimodal phase-modulation can be attributed to the depolarization of opposite arbors of the dendrites by alternating fields, causing the same neuron to

discharge at both phases of the stimulation (Jefferys, 1981; Chan and Nicholson, 1986; Radman et al., 2009).

5.2.6. Stimulation-independent factors

i. Neuronal properties

In principle, applied fields can preferentially discharge neurons at their preferred resonant frequency. Most neocortical neurons possess a resonant frequency in the range of 1-6 Hz at the resting membrane potential (Hutcheon and Yarom, 2000). Thus, slowly oscillating (~1.25 Hz) TES-induced current flow was potentially a favorable factor for many neocortical neurons. In addition to single neurons, cortical networks also show resonance, and such network-level mechanism might be especially effective during SWS (Curro Dossi et al., 1992; Destexhe et al., 1996). However, the frequency band used in our current study, 0.7-1.7 Hz, did not cover a sufficiently broad frequency range to identify specific resonance effects; thus the effects of resonance properties on TES-induced entrainment remain to be tested.

An initial goal of our project was to identify at least a fraction of the recorded units as inhibitory and excitatory and examine whether TES affects these two neuronal classes differentially (Purpura and McMurtry, 1965; Chan and Nicholson, 1986; Radman et al., 2009; Anastassiou et al., 2010). Simultaneous recordings of multiple cells provided the opportunity of classifying neurons as putative excitatory or inhibitory cells based on monosynaptic connections among isolated cell pairs. In some sessions, several neurons in both classes could be

identified; and we could show that both putative inhibitory and excitatory neurons were affected by TES. However, the number of these physiologically identified neurons varied across experiments, and very few cells could be identified for the majority of the recordings. Thus, only tentatively, we can suggest that TES effects did not depend on the transmitter content of the neuron.

ii. Morphological properties

The neocortex along with the CA1 and CA3 fields of the hippocampus are perfect examples of organized dipoles (Nunez and Srinivasan, 2006) that can amplify the spiking-induced electric fields created by individual neurons (Ylinen et al., 1995). Thus, the laminar organization of the neocortex and hippocampus could have amplified TES-induced fields, especially when multiple cells fired in-phase, leading to a stronger level of entrainment. Future studies of the brain regions without such an organization, e.g., basal ganglia, amygdala, basal forebrain, etc., would demonstrate the importance of 'laminar organization' on TES-induced effects.

5.2.7. Mechanisms of field-induced effects

Phase-modulation of neuronal activity can be caused by two different mechanisms: 1) If the applied field in the vicinity of the recorded cells is too low; it has no direct impact on the firing activity of the monitored neurons. However, other unrecorded neurons in the immediate vicinity of the stimulating electrodes can still be phase-locked to the stimulation; and the recorded cells can be

modulated through mono- or multisynaptic connections formed by these affected cells. We refer to this mechanism as '*indirect*' or '*synaptically mediated*' TES-effects. 2) The alternative mechanism, '*direct*' effects of TES, entails the case when the applied fields, directly, polarize the recorded neurons. This effect does not necessarily imply that TES alone is capable of discharging the neurons. It only implies that the induced field in the vicinity of neurons is critical in combination with the network-related effects. Our results suggest the involvement of both mechanisms.

Certainly, unrecorded neurons in the vicinity of the stimulating electrodes were more strongly affected by TES than neurons at more distant sites, since the current density was higher around the stimulating electrodes than at a distance (Ozen et al., 2008). However, several observations argue against the exclusive role of such indirect, synaptically-mediated effects. TES induced current density, even in the tissue directly under the stimulating electrodes, is relatively low due to the strongly diffusing and shunting effects of the skull, dura, pia, vessels and cerebrospinal fluid. In contrast to focal intracortical stimulation, which could effectively trigger slow oscillations in the entire neocortex (Vyazovskiy et al., 2009), we have never observed consistent entrainment of the LFP slow oscillation at the stimulus intensities tested. This suggests that TES led to low intensity currents spread across a large area.

Furthermore, approximately the same proportion of neocortical and hippocampal neurons was affected by TES in contrast to the segregation of hippocampal - neocortical modulations by intrinsic slow oscillations neurons

(Isomura et al., 2006). The bimodal phase preference of some of the neurons can also be interpreted as evidence supporting the presence of direct field-induced effects. The alternation of the virtual cathodal field could have differentially affected neural processes with distinct orientations, such as the apical and basal dendrites of the same neuron (Ranck, 1975; Radman et al., 2009). Finally, the immediate onset and offset of the TES effects as well as their stability across repeated stimulation trials further support the notion of direct effects since synaptically mediated entrainments are typically characterized by short-term depression or potentiation.

Overall, these findings indicate that in addition to polysynaptically evoked effects, TES can directly affect neurons in a large volume of the cortex even with the relatively small size electrodes and low stimulus intensities used in our study.

5.2.8. Importance of background neural activity

Biological noise is an inevitable part of neural operation. The membrane noise level of neocortical cells in vitro fluctuates between 0.2 - 0.5 mV (Jacobson et al., 2005). The physiological noise is even higher in vivo where large numbers of neurons are typically close to the spiking threshold. Network oscillations are particularly effective in (periodically) bringing neurons close to the threshold so that the smallest of inputs (synaptic or field-mediated) can discharge them (Wiesenfeld and Moss, 1995; Gluckman et al., 1998; Buzsaki and Draguhn, 2004; Saunders and Jefferys, 2007). Accordingly, unit entrainment in our data reflected the combination of both network- and TES-induced effects.

The same intensity TES exerted a differential effect on neuronal discharges during behavioral exploration and sleep. Several related mechanisms could explain the stronger effects observed during sleep. 1) The magnitude of membrane voltage fluctuations in individual neurons is larger during sleep than in the wake state (Steriade et al., 1993c). Therefore, while weak TES was only rarely effective in discharging a neuron in the exploring animal, the coincidence of TES-induced depolarization with near-threshold (UP states) membrane potential might have discharged the cell more easily during SWS. Note that under this mechanism, cortical slow oscillations did not have to be entrained by TES. It is sufficient that UP states occasionally coincided with the TES-mediated weak depolarization. 2) TES intermittently and partially entrained cortical slow oscillations. Such transient entrainment of the network may not be obvious at the LFP level. 3) Similarly, directly stimulated unrecorded neurons in the vicinity of the stimulating electrodes could have led to the partial entrainment of the slow oscillation. If such phase-bias had spread to the area of the recorded neurons, then the polysynaptically-mediated effects could have amplified the direct effects of TES.

5.2.9. Side effects of TES

In chronically implanted animals, behavior was monitored for potential side effects of TES application. Pain was the primary concern since TES could have activated nociceptors in the dura mater under the stimulating electrodes. However, the stimulation intensities used for the entrainment of neurons did not

elicit any observable behavioral effects: discomfort, distress, disruption of sleep or ongoing behavior. In fact, TES did not even induce any noticeable arousal effect on the EEG activity during sleep. Only at much stronger intensities (>6 V), twitches of the temporal muscles were observed and such stimulations aroused the rat instantaneously. These earlier experiments were not included in my dissertation. In other words, TES-induced phase-modulation was not coupled with stimulation of sensory or pain receptors.

5.3. Implications and implementations of results

5.3.1. Understanding endogenous electric fields

Intrinsic brain activity generates extracellular electric fields of substantial magnitude (Purpura and Malliani, 1966; Jefferys and Haas, 1982; Kamondi et al., 1998; Henze et al., 2000). The functional role of these endogenous fields is unclear (Buzsaki and Draguhn, 2004; Frohlich et al., 2009; Anastassiou et al., 2010). On one hand, the synchronous activity of multiples of cells creates the extracellular field. On the other hand, the induced field affects back the activity of the very same cells creating it.

Experimental application of electric fields can facilitate our understanding of endogenous fields. However, intrinsically generated fields are often spatially heterogeneous (Anastassiou et al., 2010) and thus they substantially differ from the spatially homogeneous fields, induced experimentally (Jefferys and Haas, 1982; Chan and Nicholson, 1986; Chan et al., 1988; Radman et al., 2007). Spatial heterogeneity polarizes different compartments of the cells differently.

Anastassiou et al (2010) demonstrated that hippocampal theta oscillations differently affect spike timing for somatic and dendritic regions (3-4° of advancement vs. 14-60° of delay). For higher magnitude fields, such as sharp-waves, the difference becomes even more substantial (36° of delay vs. 72° of advancement; Anastassiou et al., 2010). In other words, endogenous electric fields can lead to far more complicated effects than seen in slice preparations.

In our application, the spatial homogeneity of the applied field was disrupted since it varied depending on the placement of stimulating electrodes. Thus, to a certain degree, our results are close to the effects introduced by intrinsic fields. Some of our findings, such as bimodal phase preference, can be interpreted as representing the intrinsic conditions described above. The use of spatially heterogeneous fields and recordings from different processes of the same cells would facilitate our understanding of how single neurons are affected by local electric fields.

5.3.2. Future research directions

The main contribution of our study was to show that TES could be used for long-term investigations in behaving animals. Beyond this methodological development, some of our findings raised interesting questions that could be pursued in future experiments combining behavioral and electrophysiological methods. Two of such examples are given below:

TES induced wide-spread unit entrainment. Temporal organization in the discharge probability of multiple cells can be interpreted as the source of 'a cell

assembly formation'. TES-synchronizing multiple cells, in a way, disrupted the existing assemblies and forced 'the entrained cells' to form a new assembly. Future work in behaving animals can explain the functional consequences of such TES-induced assembly (de-formation and) formation.

TES fluctuating at a slow frequency entrained hippocampal units. TES-induced hippocampal manipulation can be utilized to investigate neocortical - hippocampal interplay (Siapas and Wilson, 1998; Sirota et al., 2003; Battaglia et al., 2004; Sirota and Buzsaki, 2005). In preparations similar to the ones described here, the effects of TES-induced slow oscillations on hippocampal activities such as ripples can be investigated. Similarly, TES fluctuating at slow oscillation or theta oscillation frequencies can be delivered to enhance or disrupt intrinsic oscillations during sleep or learning and to observe the consequences of such manipulations on memory formation (Lisman and Idiart, 1995; Buzsaki, 1998; Buzsaki, 2002; Hoffman et al., 2007).

5.3.3. Implementing rodent TES application to humans

Our results demonstrate that temporal (and potentially rate) coding of the majority of the neurons could be reliably manipulated by nonfocal electric field stimulation. Moreover, as shown in our and others' studies (Rigonatti et al., 2008), TES-induced effects were relatively quick to develop. Thus, TES could be used to bridge the time until pharmacological treatments become effective.

Although there are major differences between the human and rodent head, it is theoretically possible to achieve successful human applications with minor

modifications. Electric fields can be applied by percutaneous electrodes in acute experiments (Marshall et al., 2006; Kanai et al., 2008b) or by electrodes implanted subcutaneously or into the skull for chronic applications. In both cases, electric fields can affect spiking activity of cortical neurons without intracortical tissue reaction, a typical problem of electrodes placed in the brain parenchyma (van Kuyck et al., 2007; Kanai et al., 2008a). Electrodes implanted into the skull and powered by ultralight, minimal electrical circuits can eliminate stimulation of pain receptors in the skin or in the periosteum. The large brain size and convolution of the cortex can be utilized for more restricted stimulation of specific brain areas by proper design of current delivery. Further experiments in chronically implanted animals would provide more detailed information regarding the benefits and side effects of TES.

5.4. Concluding remarks

The primary aim of my dissertation was to understand how the intact neuronal activity is affected by applied electric fields. Through experiments conducted in anesthetized and behaving animals, I demonstrated that relatively weak electric fields applied through the skull could affect neurons in widespread cortical areas. The induced effects were brought about by an interaction between TES-induced field and ongoing network activities of the intact brain.

The effects of TES on spontaneous network patterns, demonstrated here, may be used to manipulate brain activity for experimental as well as clinical purposes. Both regular and irregular population network activity can easily be

recorded by the readily available techniques (Buzsaki and Draguhn, 2004). In turn, these activities can be used to time the enhancing or suppressing effects of TES on spontaneous or sensory stimulation-evoked neuronal activity. Exploiting the temporal windows of spike timing-dependent plasticity (Levy and Steward, 1983; Markram et al., 1997; Magee and Johnston, 1997; Bi and Poo, 1998), such pairing may be used to increase or decrease the gain between synaptic inputs and spiking output in the intact cortex (King et al., 1999). Similarly, abnormal patterns, such as epileptic spikes or other pathological rhythms can be used to trigger TES with the goal of attenuating or abolishing them (Gluckman et al., 1996; Ghai et al., 2000; Gluckman et al., 2001; Francis et al., 2003).

Overall, TES has a strong potential as a safe and reliable method to manipulate brain activity.

References

1. Achermann P, Borbely AA (1997) Low-frequency (< 1 Hz) oscillations in the human sleep electroencephalogram. Neuroscience 81: 213-222.

2. Amaral DG, Witter MP (1989) The three-dimensional organization of the hippocampal formation: a review of anatomical data. Neuroscience 31: 571-591.

3. Amzica F, Steriade M (1997) The K-complex: its slow (<1-Hz) rhythmicity and relation to delta waves. Neurology 49: 952-959.

4. Anastassiou CA, Montgomery SM, Barahona M, Buzsaki G, Koch C (2010) The effect of spatially inhomogeneous extracellular fields on neurons. J Neurosci 30: 1925-1936.

5. Aserinsky E, Kleitman N (1953) Regularly occurring periods of eye motility, and concomitant phenomena, during sleep. Science 118: 273-274.

6. Baker AP (1970) Brain stem polarization in the treatment of depression. S Afr Med J 44: 473-475.

7. Barker AT, Jalinous R, Freeston IL (1985) Non-invasive magnetic stimulation of human motor cortex. Lancet 1: 1106-1107.

8. Bartho P, Hirase H, Monconduit L, Zugaro M, Harris KD, Buzsaki G (2004) Characterization of neocortical principal cells and interneurons by network interactions and extracellular features. J Neurophysiol 92: 600-608.

9. Battaglia FP, Sutherland GR, McNaughton BL (2004) Hippocampal sharp wave bursts coincide with neocortical "up-state" transitions. Learn Mem 11: 697-704.

10. Berenyi A, Belluscio M, Buzsaki G (2010) Suppressing epileptic spike-and-wave discharges by extracranial alternating current stimulation. Society for Neuroscience Meeting. Abstract.

11. Bi GQ, Poo MM (1998) Synaptic modifications in cultured hippocampal neurons: dependence on spike timing, synaptic strength, and postsynaptic cell type. J Neurosci 18: 10464-10472.

12. Bikson M, Inoue M, Akiyama H, Deans JK, Fox JE, Miyakawa H, Jefferys JG (2004) Effects of uniform extracellular DC electric fields on excitability in rat hippocampal slices in vitro. J Physiol 557: 175-190.

13. Bindman L, Ippold OC, Redfearn J (1964a) The action of brief polarizing currents on the cerebral cortex if the rat (1) during current flow and (2) in the production of long-lasting after effects. J Physiol 172: 369-382.

14. Bindman L, Lippold O, Redfearn J (1964b) Relation between the size and form of potentials evoked by sensory stimulation and the background electrical activity in the cerbral cortex of the rat. J Physiol 171: 1-25.

15. Bishop G, O'leary J (1950) The effects of polarizing currents on cell potentials and their significance in the interpretation of central nervous system activity. Electroencephalogr Clin Neurophysiol 2: 401-416.

16. Boggio PS, Alonso-Alonso M, Mansur CG, Rigonatti SP, Schlaug G, Pascual-Leone A, Fregni F (2006) Hand function improvement with low-frequency repetitive transcranial magnetic stimulation of the unaffected hemisphere in a severe case of stroke. Am J Phys Med Rehabil 85: 927-930.

17. Boggio PS, Rigonatti SP, Ribeiro RB, Myczkowski ML, Nitsche MA, Pascual-Leone A, Fregni F (2008) A randomized, double-blind clinical trial on the efficacy of cortical direct current stimulation for the treatment of major depression. Int J Neuropsychopharmacol 11: 249-254.

18. Bragin A, Csicsvari J, Penttonen M, Buzsaki G (1997) Epileptic afterdischarge in the hippocampal-entorhinal system: current source density and unit studies. Neuroscience 76: 1187-1203.

19. Bragin A, Jando G, Nadasdy Z, Hetke J, Wise K, Buzsaki G (1995) Gamma (40-100 Hz) oscillation in the hippocampus of the behaving rat. J Neurosci 15: 47-60.

20. Brocke J, Irlbacher K, Hauptmann B, Voss M, Brandt SA (2005) Transcranial magnetic and electrical stimulation compared: does TES activate intracortical neuronal circuits? Clin Neurophysiol 116: 2748-2756.

21. Bullock TH, Buzsaki G, McClune MC (1990) Coherence of compound field potentials reveals discontinuities in the CA1-subiculum of the hippocampus in freely-moving rats. Neuroscience 38: 609-619.

22. Buzsaki G (1986) Hippocampal sharp waves: their origin and significance. Brain Res 398: 242-252.

23. Buzsaki G (1996) The hippocampo-neocortical dialogue. Cereb Cortex 6: 81-92.

24. Buzsaki G (1998) Memory consolidation during sleep: a neurophysiological perspective. J Sleep Res 7 Suppl 1: 17-23.

25. Buzsaki G (2002) Theta oscillations in the hippocampus. Neuron 33: 325-340.

26. Buzsaki G, Czopf J, Kondakor I, Kellenyi L (1986) Laminar distribution of hippocampal rhythmic slow activity (RSA) in the behaving rat: current-source density analysis, effects of urethane and atropine. Brain Res 365: 125-137.

27. Buzsaki G, Draguhn A (2004) Neuronal oscillations in cortical networks. Science 304: 1926-1929.

28. Buzsaki G, Horvath Z, Urioste R, Hetke J, Wise K (1992) High-frequency network oscillation in the hippocampus. Science 256: 1025-1027.

29. Buzsaki G, Leung LW, Vanderwolf CH (1983) Cellular bases of hippocampal EEG in the behaving rat. Brain Res 287: 139-171.

30. Chan CY, Hounsgaard J, Nicholson C (1988) Effects of electric fields on transmembrane potential and excitability of turtle cerebellar Purkinje cells in vitro. J Physiol 402: 751-771.

31. Chan CY, Nicholson C (1986) Modulation by applied electric fields of Purkinje and stellate cell activity in the isolated turtle cerebellum. J Physiol 371: 89-114.

32. Contreras D, Timofeev I, Steriade M (1996) Mechanisms of long-lasting hyperpolarizations underlying slow sleep oscillations in cat corticothalamic networks. J Physiol 494 (Pt 1): 251-264.

33. Creutzfeldt OD, Fromm GH, Kapp H (1962) Influence of transcortical d-c currents on cortical neuronal activity. Exp Neurol 5: 436-452.

34. Crowell B (2007) Fields. In: Simple Nature: An introduction to physics for engineering and physical science students Fullerton: Light and Matter.

35. Csicsvari J, Henze DA, Jamieson B, Harris KD, Sirota A, Bartho P, Wise KD, Buzsaki G (2003) Massively parallel recording of unit and local field potentials with silicon-based electrodes. J Neurophysiol 90: 1314-1323.

36. Dayan P, Abbott L (2001) Model neurons II: Conductance and morphology. In: Theoretical neuroscience Cambridge: MIT.

37. Deans JK, Powell AD, Jefferys JG (2007) Sensitivity of coherent oscillations in rat hippocampus to AC electric fields. J Physiol 583: 555-565.

38. Destexhe A, Bal T, McCormick DA, Sejnowski TJ (1996) Ionic mechanisms underlying synchronized oscillations and propagating waves in a model of ferret thalamic slices. J Neurophysiol 76: 2049-2070.

39. Destexhe A, Contreras D, Steriade M (1999) Spatiotemporal analysis of local field potentials and unit discharges in cat cerebral cortex during natural wake and sleep states. J Neurosci 19: 4595-4608.

40. Dolorfo CL, Amaral DG (1998) Entorhinal cortex of the rat: organization of intrinsic connections. J Comp Neurol 398: 49-82.

41. Curro Dossi R, Nunez A, Steriade M (1992) Electrophysiology of a slow (0.5-4 Hz) intrinsic oscillation of cat thalamocortical neurones in vivo. J Physiol 447: 215-234.

42. Engel AK, Singer W (2001) Temporal binding and the neural correlates of sensory awareness. Trends Cogn Sci 5: 16-25.

43. Fecteau S, Knoch D, Fregni F, Sultani N, Boggio P, Pascual-Leone A (2007) Diminishing risk-taking behavior by modulating activity in the prefrontal cortex: a direct current stimulation study. J Neurosci 27: 12500-12505.

44. Fisher NI (1993) Analysis of a single sample. In: Statistical Analysis of Circular Data Cambridge: University of Cambridge.

45. Fitzgerald PB, Fountain S, Daskalakis ZJ (2006) A comprehensive review of the effects of rTMS on motor cortical excitability and inhibition. Clin Neurophysiol 117: 2584-2596.

46. Francis JT, Gluckman BJ, Schiff SJ (2003) Sensitivity of neurons to weak electric fields. J Neurosci 23: 7255-7261.

47. Fregni F, Boggio PS, Mansur CG, Wagner T, Ferreira MJ, Lima MC, Rigonatti SP, Marcolin MA, Freedman SD, Nitsche MA, Pascual-Leone A (2005a) Transcranial direct current stimulation of the unaffected hemisphere in stroke patients. Neuroreport 16: 1551-1555.

48. Fregni F, Boggio PS, Nitsche M, Bermpohl F, Antal A, Feredoes E, Marcolin MA, Rigonatti SP, Silva MT, Paulus W, Pascual-Leone A (2005b) Anodal transcranial direct current stimulation of prefrontal cortex enhances working memory. Exp Brain Res 166: 23-30.

49. Fregni F, Boggio PS, Valle AC, Rocha RR, Duarte J, Ferreira MJ, Wagner T, Fecteau S, Rigonatti SP, Riberto M, Freedman SD, Pascual-Leone A (2006) A sham-controlled trial of a 5-day course of repetitive transcranial magnetic stimulation of the unaffected hemisphere in stroke patients. Stroke 37: 2115-2122.

50. Fritsch G, Hitzig E (2009) International Classics in Epilepsy and Behavior:1870. Electric excitability of the cerebrum (Über die ektrische Erregbarkeit des Grosshirns). Epilepsy and Behavior 15: 123-130.

51. Frohlich, Sundberg, McCormick, D (2008) Does the field potential influence normal network activity? Society for Neuroscience Meeting 41.18. Abstract.

52. Frohlich, Sundberg, McCormick, D (2009) Local field potential guides neocortical network activity. Society for Neuroscience Meeting 722.15. Abstract.

53. Fujisawa S, Amarasingham A, Harrison MT, Buzsaki G (2008) Behavior-dependent short-term assembly dynamics in the medial prefrontal cortex. Nat Neurosci 11: 823-833.

54. Fujisawa S, Matsuki N, Ikegaya Y (2004) Chronometric readout from a memory trace: gamma-frequency field stimulation recruits timed recurrent activity in the rat CA3 network. J Physiol 561: 123-131.

55. Gabriel S, Lau RW, Gabriel C (1996) The dielectric properties of biological tissues: III. Parametric models for the dielectric spectrum of tissues. Phys Med Biol 41: 2271-2293.

56. Galea JM, Celnik P (2009) Brain polarization enhances the formation and retention of motor memories. J Neurophysiol 102: 294-301.

57. Ghai RS, Bikson M, Durand DM (2000) Effects of applied electric fields on low-calcium epileptiform activity in the CA1 region of rat hippocampal slices. J Neurophysiol 84: 274-280.

58. Gilula MF, Barach PR (2004) Cranial electrotherapy stimulation: a safe neuromedical treatment for anxiety, depression, or insomnia. South Med J 97: 1269-1270.

59. Gluckman BJ, Neel EJ, Netoff TI, Ditto WL, Spano ML, Schiff SJ (1996) Electric field suppression of epileptiform activity in hippocampal slices. J Neurophysiol 76: 4202-4205.

60. Gluckman BJ, Nguyen H, Weinstein SL, Schiff SJ (2001) Adaptive electric field control of epileptic seizures. J Neurosci 21: 590-600.

61. Gluckman BJ, So P, Netoff TI, Spano ML, Schiff SJ (1998) Stochastic resonance in mammalian neuronal networks. Chaos 8: 588-598.

62. Gold C, Henze DA, Koch C, Buzsaki G (2006) On the origin of the extracellular action potential waveform: A modeling study. J Neurophysiol 95: 3113-3128.

63. Gray CM, Singer W (1989) Stimulus-specific neuronal oscillations in orientation columns of cat visual cortex. Proc Natl Acad Sci U S A 86: 1698-1702.

64. Haas HL, Jefferys JG (1984) Low-calcium field burst discharges of CA1 pyramidal neurones in rat hippocampal slices. J Physiol 354: 185-201.

65. Hahn TT, Sakmann B, Mehta MR (2007) Differential responses of hippocampal subfields to cortical up-down states. Proc Natl Acad Sci U S A 104: 5169-5174.

66. Haider B, Duque A, Hasenstaub AR, Yu Y, McCormick DA (2007) Enhancement of visual responsiveness by spontaneous local network activity in vivo. J Neurophysiol 97: 4186-4202.

67. Hakkinen V, Eskola H, Yli-Hankala A, Nurmikko T, Kolehmainen S (1995) Which structures are sensitive to painful transcranial electric stimulation? Electromyogr Clin Neurophysiol 35: 377-383.

68. Hallett M (2000) Transcranial magnetic stimulation and the human brain. Nature 406: 147-150.

69. Harris KD, Henze DA, Csicsvari J, Hirase H, Buzsaki G (2000) Accuracy of tetrode spike separation as determined by simultaneous intracellular and extracellular measurements. J Neurophysiol 84: 401-414.

70. Hattori Y, Moriwaki A, Hori Y (1990) Biphasic effects of polarizing current on adenosine-sensitive generation of cyclic AMP in rat cerebral cortex. Neurosci Lett 116: 320-324.

71. Hazan L, Zugaro M, Buzsaki G (2006) Klusters, NeuroScope, NDManager: a free software suite for neurophysiological data processing and visualization. J Neurosci Methods 155: 207-216.

72. Henze DA, Borhegyi Z, Csicsvari J, Mamiya A, Harris KD, Buzsaki G (2000) Intracellular features predicted by extracellular recordings in the hippocampus in vivo. J Neurophysiol 84: 390-400.

73. Henze DA, Buzsaki G (2001) Action potential threshold of hippocampal pyramidal cells in vivo is increased by recent spiking activity. Neuroscience 105: 121-130.

74. Histed MH, Bonin V, Reid RC (2009) Direct activation of sparse, distributed populations of cortical neurons by electrical microstimulation. Neuron 63: 508-522.

75. Hobson JA (2005) Sleep is of the brain, by the brain and for the brain. Nature 437: 1254-1256.

76. Hoffman KL, Battaglia FP, Harris K, MacLean JN, Marshall L, Mehta MR (2007) The upshot of up states in the neocortex: from slow oscillations to memory formation. J Neurosci 27: 11838-11841.

77. Holt GR, Koch C (1999) Electrical interactions via the extracellular potential near cell bodies. J Comput Neurosci 6: 169-184.

78. Hotary KB, Robinson KR (1990) Endogenous electrical currents and the resultant voltage gradients in the chick embryo. Dev Biol 140: 149-160.

79. Huber R, Graf T, Cote KA, Wittmann L, Gallmann E, Matter D, Schuderer J, Kuster N, Borbely AA, Achermann P (2000) Exposure to pulsed high-frequency electromagnetic field during waking affects human sleep EEG. Neuroreport 11: 3321-3325.

80. Huber R, Treyer V, Borbely AA, Schuderer J, Gottselig JM, Landolt HP, Werth E, Berthold T, Kuster N, Buck A, Achermann P (2002) Electromagnetic fields, such as those from mobile phones, alter regional cerebral blood flow and sleep and waking EEG. J Sleep Res 11: 289-295.

81. Huerta PT, Lisman JE (1995) Bidirectional synaptic plasticity induced by a single burst during cholinergic theta oscillation in CA1 in vitro. Neuron 15: 1053-1063.

82. Hummel F, Celnik P, Giraux P, Floel A, Wu WH, Gerloff C, Cohen LG (2005) Effects of non-invasive cortical stimulation on skilled motor function in chronic stroke. Brain 128: 490-499.

83. Hutcheon B, Yarom Y (2000) Resonance, oscillation and the intrinsic frequency preferences of neurons. Trends Neurosci 23: 216-222.

84. Isomura Y, Sirota A, Ozen S, Montgomery S, Mizuseki K, Henze DA, Buzsaki G (2006) Integration and segregation of activity in entorhinal-hippocampal subregions by neocortical slow oscillations. Neuron 52: 871-882.

85. Iyer MB, Mattu U, Grafman J, Lomarev M, Sato S, Wassermann EM (2005) Safety and cognitive effect of frontal DC brain polarization in healthy individuals. Neurology 64: 872-875.

86. Jacobson GA, Diba K, Yaron-Jakoubovitch A, Oz Y, Koch C, Segev I, Yarom Y (2005) Subthreshold voltage noise of rat neocortical pyramidal neurones. J Physiol 564: 145-160.

87. Jefferys JG (1981) Influence of electric fields on the excitability of granule cells in guinea-pig hippocampal slices. J Physiol 319: 143-152.

88. Jefferys JG (1995) Nonsynaptic modulation of neuronal activity in the brain: electric currents and extracellular ions. Physiol Rev 75: 689-723.

89. Jefferys JG, Haas HL (1982) Synchronized bursting of CA1 hippocampal pyramidal cells in the absence of synaptic transmission. Nature 300: 448-450.

90. Kamondi A, Acsady L, Wang XJ, Buzsaki G (1998) Theta oscillations in somata and dendrites of hippocampal pyramidal cells in vivo: activity-dependent phase-precession of action potentials. Hippocampus 8: 244-261.

91. Kanai R, Chaieb L, Antal A, Walsh V, Paulus W (2008a) Frequency-dependent electrical stimulation of the visual cortex. Curr Biol 18: 1839-1843.

92. Kandel E, Schwartz J, Jessell T (1991) Principles of Neural Science. McGraw Hill Companies.

93. Kincses TZ, Antal A, Nitsche MA, Bartfai O, Paulus W (2004) Facilitation of probabilistic classification learning by transcranial direct current stimulation of the prefrontal cortex in the human. Neuropsychologia 42: 113-117.

94. King C, Henze DA, Leinekugel X, Buzsaki G (1999) Hebbian modification of a hippocampal population pattern in the rat. J Physiol 521 Pt 1: 159-167.

95. Kirov R, Weiss C, Siebner HR, Born J, Marshall L (2009) Slow oscillation electrical brain stimulation during waking promotes EEG theta activity and memory encoding. Proc Natl Acad Sci U S A.

96. Kirsch D (2002) The Science Behind Cranial Electrotherapy Stimulation. Alberta, Canada: Medical Scope Publishing Corporation.

97. Koch C (1999) Biophysics of Computation: Information Processing in Single Neurons. New York: Oxford University Press.

98. Lang N, Siebner HR, Ward NS, Lee L, Nitsche MA, Paulus W, Rothwell JC, Lemon RN, Frackowiak RS (2005) How does transcranial DC stimulation of the primary motor cortex alter regional neuronal activity in the human brain? Eur J Neurosci 22: 495-504.

99. Levy WB, Steward O (1983) Temporal contiguity requirements for long-term associative potentiation/depression in the hippocampus. Neuroscience 8: 791-797.

100. Lian J, Bikson M, Sciortino C, Stacey WC, Durand DM (2003) Local suppression of epileptiform activity by electrical stimulation in rat hippocampus in vitro. J Physiol 547: 427-434.

101. Liebetanz D, Nitsche MA, Tergau F, Paulus W (2002) Pharmacological approach to the mechanisms of transcranial DC-stimulation-induced after-effects of human motor cortex excitability. Brain 125: 2238-2247.

102. Lippold OCJ, Redfearn JWT, Winton LJ (1961) The potential level at the surface of the cerebral cortex of the rat and its relation to the cortical activity evoked by sensory stimulation. J Physiol 157: 7-9.

103. Lippold O, Redfearn J (1964) Mental changes resulting from the passage of small direct currents through the human brain. Br J Psychiatry 110: 768-772.

104. Lisman JE, Idiart MA (1995) Storage of 7 +/- 2 short-term memories in oscillatory subcycles. Science 267: 1512-1515.

105. Lopez L, Chan CY, Okada YC, Nicholson C (1991) Multimodal characterization of population responses evoked by applied electric field in vitro: extracellular potential, magnetic evoked field, transmembrane potential, and current-source density analysis. J Neurosci 11: 1998-2010.

106. Luthi A, McCormick DA (1998) Periodicity of thalamic synchronized oscillations: the role of Ca2+-mediated upregulation of Ih. Neuron 20: 553-563.

107. Magee JC, Johnston D (1997) A synaptically controlled, associative signal for Hebbian plasticity in hippocampal neurons. Science 275: 209-213.

108. Markram H, Lubke J, Frotscher M, Sakmann B (1997) Regulation of synaptic efficacy by coincidence of postsynaptic APs and EPSPs. Science 275: 213-215.

109. Marshall L, Helgadottir H, Molle M, Born J (2006) Boosting slow oscillations during sleep potentiates memory. Nature 444: 610-613.

110. Marshall L, Molle M, Hallschmid M, Born J (2004) Transcranial direct current stimulation during sleep improves declarative memory. J Neurosci 24: 9985-9992.

111. Massimini M, Amzica F (2001) Extracellular calcium fluctuations and intracellular potentials in the cortex during the slow sleep oscillation. J Neurophysiol 85: 1346-1350.

112. Massimini M, Huber R, Ferrarelli F, Hill S, Tononi G (2004) The sleep slow oscillation as a traveling wave. J Neurosci 24: 6862-6870.

113. McCormick DA, Bal T (1997) Sleep and arousal: thalamocortical mechanisms. Annu Rev Neurosci 20: 185-215.

114. McCormick DA, Shu Y, Hasenstaub A, Sanchez-Vives M, Badoual M, Bal T (2003) Persistent cortical activity: mechanisms of generation and effects on neuronal excitability. Cereb Cortex 13: 1219-1231.

115. Molle M, Marshall L, Gais S, Born J (2004) Learning increases human electroencephalographic coherence during subsequent slow sleep oscillations. Proc Natl Acad Sci U S A 101: 13963-13968.

116. Mukovski M, Chauvette S, Timofeev I, Volgushev M (2007) Detection of active and silent states in neocortical neurons from the field potential signal during slow-wave sleep. Cereb Cortex 17: 400-414.

117. Nakagawa M, Durand D (1991) Suppression of spontaneous epileptiform activity with applied currents. Brain Res 567: 241-247.

118. Nitsche MA, Boggio PS, Fregni F, Pascual-Leone A (2009) Treatment of depression with transcranial direct current stimulation (tDCS): a review. Exp Neurol 219: 14-19.

119. Nitsche MA, Fricke K, Henschke U, Schlitterlau A, Liebetanz D, Lang N, Henning S, Tergau F, Paulus W (2003a) Pharmacological modulation of cortical excitability shifts induced by transcranial direct current stimulation in humans. J Physiol 553: 293-301.

120. Nitsche MA, Nitsche MS, Klein CC, Tergau F, Rothwell JC, Paulus W (2003b) Level of action of cathodal DC polarisation induced inhibition of the human motor cortex. Clin Neurophysiol 114: 600-604.

121. Nitsche MA, Paulus W (2000) Excitability changes induced in the human motor cortex by weak transcranial direct current stimulation. J Physiol 527 Pt 3: 633-639.

122. Nitsche MA, Schauenburg A, Lang N, Liebetanz D, Exner C, Paulus W, Tergau F (2003c) Facilitation of implicit motor learning by weak transcranial direct current stimulation of the primary motor cortex in the human. J Cogn Neurosci 15: 619-626.

123. Nitsche MA, Seeber A, Frommann K, Klein CC, Rochford C, Nitsche MS, Fricke K, Liebetanz D, Lang N, Antal A, Paulus W, Tergau F (2005) Modulating parameters of excitability during and after transcranial direct current stimulation of the human motor cortex. J Physiol 568: 291-303.

124. Nunez PN, Srinivasan R (2006) Electric Fields of the Brain: The Neurophysics of EEG. Oxford University Press.

125. Ozen S, Sirota A, Anastassiou C, Koch C, Buzsaki, G (2008) Entrainment of the cortical slow oscillation by extracranial weak electric fields. Society for Neuroscience Meeting 435.6. Abstract.

126. Pace-Schott EF, Hobson JA (2002) The neurobiology of sleep: genetics, cellular physiology and subcortical networks. Nat Rev Neurosci 3: 591-605.

127. Park EH, Barreto E, Gluckman BJ, Schiff SJ, So P (2005) A model of the effects of applied electric fields on neuronal synchronization. J Comput Neurosci 19: 53-70.

128. Poreisz C, Boros K, Antal A, Paulus W (2007) Safety aspects of transcranial direct current stimulation concerning healthy subjects and patients. Brain Res Bull 72: 208-214.

129. Purpura DP, Malliani A (1966) Spike generation and propagation initiated in dendrites by transhippocampal polarization. Brain Res 1: 403-406.

130. Purpura DP, McMurtry JG (1965) Intracellular activities and evoked potential changes during polarization of motor cortex. J Neurophysiol 28: 166-185.

131. Radman T, Ramos RL, Brumberg JC, Bikson M (2009) Role of cortical cell type and morphology in subthreshold and suprathreshold uniform electric field stimulation in vitro. Brain Stimulation 2: 215-228.

132. Radman T, Su Y, An JH, Parra LC, Bikson M (2007) Spike timing amplifies the effect of electric fields on neurons: implications for endogenous field effects. J Neurosci 27: 3030-3036.

133. Ranck JB (1975) Which elements are excited in electrical stimulation of mammalian central nervous system: a review. Brain Res 98: 417-440.

134. Ray S, Crone NE, Niebur E, Franaszczuk PJ, Hsiao SS (2008) Neural correlates of high-gamma oscillations (60-200 Hz) in macaque local field potentials and their potential implications in electrocorticography. J Neurosci 28: 11526-11536.

135. Redfearn J, Lippold O, Costain R (1964) A preliminary account of the clinical effects of polarizing the brain in certain psychiatric disorders. Br J Psychiatry 110: 773-785.

136. Rigonatti SP, Boggio PS, Myczkowski ML, Otta E, Fiquer JT, Ribeiro RB, Nitsche MA, Pascual-Leone A, Fregni F (2008) Transcranial direct stimulation and fluoxetine for the treatment of depression. Eur Psychiatry 23: 74-76.

137. Ros H, Sachdev RN, Yu Y, Sestan N, McCormick DA (2009) Neocortical networks entrain neuronal circuits in cerebellar cortex. J Neurosci 29: 10309-10320.

138. Rosanova M, Ulrich D (2005) Pattern-specific associative long-term potentiation induced by a sleep spindle-related spike train. J Neurosci 25: 9398-9405.

139. Rosenthal SH (1972a) Electrosleep therapy. Curr Psychiatr Ther 12: 104-107.

140. Rosenthal SH (1972b) Electrosleep: a double-blind clinical study. Biol Psychiatry 4: 179-185.

141. Rosenthal SH, Calvert LF (1972) Electrosleep: personal subjective experiences. Biol Psychiatry 4: 187-190.

142. Rosenthal SH, Wulfsohn NL (1970) Electrosleep--a clinical trial. Am J Psychiatry 127: 533-534.

143. Rossini PM, Marciani MG, Caramia M, Roma V, Zarola F (1985) Nervous propagation along 'central' motor pathways in intact man: characteristics of motor responses to 'bifocal' and 'unifocal' spine and scalp non-invasive stimulation. Electroencephalogr Clin Neurophysiol 61: 272-286.

144. Sanchez-Vives MV, McCormick DA (2000) Cellular and network mechanisms of rhythmic recurrent activity in neocortex. Nat Neurosci 3: 1027-1034.

145. Saunders RD, Jefferys JG (2002) Weak electric field interactions in the central nervous system. Health Phys 83: 366-375.

146. Saunders RD, Jefferys JG (2007) A neurobiological basis for ELF guidelines. Health Phys 92: 596-603.

147. Scoville WB, Milner B (1957) Loss of recent memory after bilateral hippocampal lesions. J Neurol Neurosurg Psychiatry 20: 11-21.

148. Sejnowski TJ, Destexhe A (2000) Why do we sleep? Brain Res 886: 208-223.

149. Shu Y, Hasenstaub A, McCormick DA (2003) Turning on and off recurrent balanced cortical activity. Nature 423: 288-293.

150. Siapas AG, Wilson MA (1998) Coordinated interactions between hippocampal ripples and cortical spindles during slow-wave sleep. Neuron 21: 1123-1128.

151. Sirota A, Buzsaki G (2005) Interaction between neocortical and hippocampal networks via slow oscillations. Thalamus Relat Syst 3: 245-259.

152. Sirota A, Csicsvari J, Buhl D, Buzsaki G (2003) Communication between neocortex and hippocampus during sleep in rodents. Proc Natl Acad Sci U S A 100: 2065-2069.

153. Sirota A, Montgomery S, Fujisawa S, Isomura Y, Zugaro M, Buzsaki G (2008) Entrainment of neocortical neurons and gamma oscillations by the hippocampal theta rhythm. Neuron 60: 683-697.

154. Snow RW, Dudek FE (1984) Electrical fields directly contribute to action potential synchronization during convulsant-induced epileptiform bursts. Brain Res 323: 114-118.

155. Squire LR (1992) Memory and the hippocampus: a synthesis from findings with rats, monkeys, and humans. Psychol Rev 99: 195-231.

156. Squire LR (2004) Memory systems of the brain: a brief history and current perspective. Neurobiol Learn Mem 82: 171-177.

157. Squire L, Bloom F, McConnell S, Roberts J, Spitzer N, Zigmond M (1999) Fundamental Neuroscience. San Diego: Academic Press.

158. Steriade M (2001) Impact of network activities on neuronal properties in corticothalamic systems. J Neurophysiol 86: 1-39.

159. Steriade M, Amzica F (1998) Coalescence of sleep rhythms and their chronology in corticothalamic networks. Sleep Res Online 1: 1-10.

160. Steriade M, Amzica F, Nunez A (1993a) Cholinergic and noradrenergic modulation of the slow (approximately 0.3 Hz) oscillation in neocortical cells. J Neurophysiol 70: 1385-1400.

161. Steriade M, Contreras D, Curro DR, Nunez A (1993b) The slow (< 1 Hz) oscillation in reticular thalamic and thalamocortical neurons: scenario of sleep rhythm generation in interacting thalamic and neocortical networks. J Neurosci 13: 3284-3299.

162. Steriade M, Nunez A, Amzica F (1993c) A novel slow (< 1 Hz) oscillation of neocortical neurons in vivo: depolarizing and hyperpolarizing components. J Neurosci 13: 3252-3265.

163. Steriade M, Timofeev I (2003) Neuronal plasticity in thalamocortical networks during sleep and waking oscillations. Neuron 37: 563-576.

164. Steriade M, Timofeev I, Grenier F (2001) Natural waking and sleep states: a view from inside neocortical neurons. J Neurophysiol 85: 1969-1985.

165. Stern EA, Kincaid AE, Wilson CJ (1997) Spontaneous subthreshold membrane potential fluctuations and action potential variability of rat corticostriatal and striatal neurons in vivo. J Neurophysiol 77: 1697-1715.

166. Suzuki SS, Smith GK (1988) Spontaneous EEG spikes in the normal hippocampus. III. Relations to evoked potentials. Electroencephalogr Clin Neurophysiol 69: 541-549.

167. Sylantyev S, Savtchenko LP, Niu YP, Ivanov AI, Jensen TP, Kullmann DM, Xiao MY, Rusakov DA (2008) Electric fields due to synaptic currents sharpen excitatory transmission. Science 319: 1845-1849.

168. Tamamaki N, Nojyo Y (1993) Projection of the entorhinal layer II neurons in the rat as revealed by intracellular pressure-injection of neurobiotin. Hippocampus 3: 471-480.

169. Taylor CP, Dudek FE (1982) Synchronous neural afterdischarges in rat hippocampal slices without active chemical synapses. Science 218: 810-812.

170. Taylor CP, Dudek FE (1984) Synchronization without active chemical synapses during hippocampal afterdischarges. J Neurophysiol 52: 143-155.

171. Tepper JM, Groves PM (1990) In vivo electrophysiology of central nervous system terminal autoreceptors. Ann N Y Acad Sci 604: 470-487.

172. Terney D, Chaieb L, Moliadze V, Antal A, Paulus W (2008) Increasing human brain excitability by transcranial high frequency random noise stimulation. J Neurosci 28: 14147-14155.

173. Timofeev I, Grenier F, Bazhenov M, Sejnowski TJ, Steriade M (2000) Origin of slow cortical oscillations in deafferented cortical slabs. Cereb Cortex 10: 1185-1199.

174. Timofeev I, Steriade M (1996) Low-frequency rhythms in the thalamus of intact-cortex and decorticated cats. J Neurophysiol 76: 4152-4168.

175. van Kuyck K, Welkenhuysen M, Arckens L, Sciot F, Nuttin B (2007) Histological Alterations Induced by Electrode Implantation and Electrical Stimulation in the Human Brain: A Review. Neuromodulation 10: 244-261.

176. Vanderwolf CH (1969) Hippocampal electrical activity and voluntary movement in the rat. Electroencephalogr Clin Neurophysiol 26: 407-418.

177. Volgushev M, Chauvette S, Mukovski M, Timofeev I (2006) Precise long-range synchronization of activity and silence in neocortical neurons during slow-wave oscillations [corrected]. J Neurosci 26: 5665-5672.

178. Vyazovskiy VV, Faraguna U, Cirelli C, Tononi G (2009) Triggering slow waves during NREM sleep in the rat by intracortical electrical stimulation: effects of sleep/wake history and background activity. J Neurophysiol 101: 1921-1931.

179. Walsh V, Cowey A (2000) Transcranial magnetic stimulation and cognitive neuroscience. Nat Rev Neurosci 1: 73-79.

180. Webster BR, Celnik PA, Cohen LG (2006) Noninvasive brain stimulation in stroke rehabilitation. NeuroRx 3: 474-481.

181. Wiesenfeld K, Moss F (1995) Stochastic resonance and the benefits of noise: from ice ages to crayfish and squids. Nature 373: 33-36.

182. Winson J (1974) Patterns of hippocampal theta rhythm in the freely moving rat. Electroencephalogr Clin Neurophysiol 36: 291-301.

183. Ylinen A, Bragin A, Nadasdy Z, Jando G, Szabo I, Sik A, Buzsaki G (1995) Sharp wave-associated high-frequency oscillation (200 Hz) in the intact hippocampus: network and intracellular mechanisms. J Neurosci 15: 30-46.

ŞİMAL ÖZEN

Date of Birth and Place: Jan 27' 1981, Izmit - Turkey
Prior education:
    1999-2003: B.A. in Business Administration, Bogazici University, Istanbul - Turkey
    1994-1999: Kabatas High School, Istanbul - Turkey
Peer reviewed articles:
    Ozen S, Sirota A, Belluscio MA, Anastassiou CA, Stark E, Koch C and Buzsaki G. Transcranial electric stimulation entrains cortical neuronal populations in rats. (in revision).
    Isomura Y, Sirota A, *Ozen S*, Montgomery S, Mizuseki K, Henze DA and Buzsaki G. Integration and segregation of activity in entorhinal-hippocampal subregions by neocortical slow oscillations. Neuron, 52(5):871-82, 2006.
Poster presentations:
    Ozen S, Sirota AM, Anastassiou C, Belluscio M, Koch C and Buzsaki G. Entrainment of cortical activity by applied electric fields. SfN (192.8), 2009.
    Ozen S, Sirota AM, Anastassiou C, Belluscio M, Koch C and Buzsaki G. Entrainment of the cortical slow oscillation by extracranial weak electric fields. SfN (435.6), 2008.
    Sullivan DW, *Ozen S* and Buzsaki G. Juxtacellular recording and labeling in the hippocampal dentate gyrus of freely moving rats. SfN (435.2), 2008.
    Ozen S, Sirota A, and Buzsaki G. Effects of weak electrical fields on single cell and network activity in-vivo. ICONX (P035), 2008.
    Ozen S, Sirota A, and Buzsaki G. Effects of weak electrical fields on single cell and network activity in-vivo. SfN (742.15), 2007.
    Sirota AM, Isomura Y, *Ozen S*, Henze D and Buzsaki G. Integration and segregation of activity in neocortex and hippocampus by slow oscillations. SfN (635.7), 2006.
    Ozen S, Goz D, Gurler D, Yapici N, Aksoy A, Kumru G and Canbeyli R. Effects of medial septal lesion on behavioral despair and learning in female Wistar rats. National Congress of Neuroscience (117), Turkey, 2003.
    Kumru G, Baran B, Acik A, Ozcelik S, *Ozen S*, Aksoy A and Canbeyli R. Effects of behavioral despair on navigational learning. National Congress of Neuroscience (122), Turkey, 2003.
    Yapici N, Aksoy A, Goz D, Gurler D, *Ozen S*, Aksel EB and Canbeyli R. Effects of anesthetic dose ketamine injection on the behavior of female wistar rats. Neurobiology Winter School held by Ege University, Turkey, 2003.
Oral presentations:
    Aksoy G., Gadjiyev C., Ozen S., Sefer N., Yasa Y. and Canbeyli R. Effects of exposure to tone presentation on behavioral despair of female Wistar rats during Forced Swim Test, National Congress of Psychology (B31), Turkey, 2002.
Scholarship and Grants:
    EBBS Travel Fellowship, Ararat Memory Meeting, 2010.
    INS Minisymposium, Best Poster Presentation Award, 2009.
    TDLC Travel Award, 2009.
    IBRO Young scientist Travel Award, 2008.
    TASSA Young scholar Travel Grant, 2007.
Honors and Achievements:
    Placed in the top 0.1% in the National Student Placement Examination, held by The Higher Education Council of Turkey, 1998.
    1st place in the National Essay Competition, held by the Ataturk Association,1997.
    1st place in the Regional Essay Competition, held by the Metropolitan Municipality, 1997.
    1st place in the Regional Short Essay Competition, held by the TSI, 1997.
    2nd place in the National Short Essay Competition, held by Turkish Cultural Foundation,1995.
Extracurricular activities :
    2007-2009: Anusara Yoga Teacher Training.
    2007-present: Staff at the Grants and the Writing Departments of the MASP, a non-profit cultural organization.
    1999-2003: Member of the Managerial Board of Bogazici University Mountaineering Club.
Hobbies: Fiction writing, yoga, hiking & backpacking